IPP-Report

Max-Planck-Institut für Plasmaphysik

Luis F. Menchero; Hugh P. Summers

Ab initio study of the Stark effect in neutral hydrogen

IPP 10/49
Mai, 2013

ADAS-EU IPP-MPG

Luis Fernández Menchero[1,2] and Hugh P. Summers[1]

[1]ADAS-EU, Department of Physics, University of Strathclyde,
John Anderson Building, 107 Rottenrow East, Glasgow G4 0NG, United Kingdom
[2]Max Planck Institute for Plasma Physics, EURATOM Association,
Boltzmannstr. 2, 85748 Garching, Germany

Ab initio study of the Stark effect in neutral hydrogen

5th May 2013

Ab initio study of the Stark effect in neutral hydrogen

Luis Fernández Menchero[1,2] and Hugh P. Summers[1]

[1]ADAS-EU, Department of Physics, University of Strathclyde,
John Anderson Building, 107 Rottenrow East, Glasgow G4 0NG, United Kingdom
[2]Max Planck Institute for Plasma Physics, EURATOM Association,
Boltzmannstr. 2, 85748 Garching, Germany

Abstract: *The report focuses in the theoretical study of the effect of a constant electric field on the neutral hydrogen atom, also known as Stark effect. The electric field breacks the spherical symmetry, so the angular momentum is no more conserved, the quantum number l is lost and the wave functions should be labelled in terms of the approximate quantum number $\tilde{k}$.*

The properties of the system makes that perturbation theory is not applicable, so an ab initio *method should be used. In present work we apply the complex coordinate rotation method to spread the resonances from the continious background and determine their energies, widths and wave functions. They are calculated in terms of a variational method, expanding the solution as a linear combination of a basis set of functions.*

The wave functions calculated will be used as ground functions in the Motion Stark Effect routine o the Atomic Data and Analysis Spectra (ADAS) code, ADAS305, which predicts the splitting of the D_α *line of Deuterium in its Stark multiplet.*

Contents

Chapter 1

Introduction

The effect of a constant electric field on the hydrogen atom, also known as the Stark effect [1], has been the subject of study for many years. The problem of finding the positions and widths of the resonances has been carried out by several methods, for example semiclassically [2, 3], using different approximations to get the energies [4, 5, 6, 7, 8] and semiempirical methods to get the widths [6, 9]. The recent work by Lin [10] used an *ab initio* quantum treatment, diagonalising the Hamiltonian in spherical coordinates and expanding the wave functions in Laguerre-mesh polynomials. Lin obtained the solutions in the usual spherical quantum number representation $|n\,l\,m\rangle$, but used a technique to simplify the Hamiltonian based on projection over a subspace defined by a compound of the l quantum number. This allowed him to go to high n and still obtain accurate results. The technique was also used by Maquet [11]. Experimental studies of the Stark effect include Stebbings [12] and Littman [13].

In the present work we solve the Stark Hamiltonian directly in its natural parabolic coordinates [14, 15], thereby obtaining the wave functions labelled with the parabolic quantum numbers $|n\,k\,m\rangle$. We do not make a projection but work with the whole Hilbert space of the Stark Hamiltonian. The technique of complex coordinate rotation [16] is used to distinguish the resonances from the continuum states. The wave functions are expanded in a basis set of Laguerre-mesh polynomials.

When a neutral atom moves across a magnetic field it feels a Lorentz electric field $\vec{F} = \vec{v} \times \vec{B}$, which splits the atomic lines of the atom's spectrum into their Stark multiplet components, the so-called Motion Stark Effect (MSE). This situation takes place in many places, for example, when fast neutrals coming from the solar wind cross the Earth's magnetic field, but the primary field of concern for the present work is in magnetic confinement fusion devices. Neutral beam sources, designed to heat the plasma, inject high energy neutral hydrogen and occasionally neutral helium isotopes. The energies range from $\sim$ 70keV with positive ion sources (such as used at the EFDA-JET Facility) to ($\sim$ 1MeV) with negative ion sources (such as those planned for ITER). Excitation of the beam atoms in the plasma before ionisation leads to spectral emission whose analysis is called Beam eMission Spectroscopy (BMS). Most commonly BMS measures the (D_α) emission of deuterium along multiple lines-of-sight intersecting the beam path. The Stark-split, polarised emission yields important measurements such as internal magnetic fields and current profiles as well as the neutral hydrogen source rates in the plasma for charge exchange spectroscopy of impurities. Proper interpretation of MSE and BMS spectra requires high precision not only of transition energies, but also of all the rate parameters and coefficients supporting the collisional-radiative population models [17] which predict the detailed emission. There is a substantial literature of such models for the various modern fusion devices such as ASDEX Upgrade and Wendelstein 7-X [18], MAST [19], JET [20, 21, 22], TEXTOR [23, 24] and LHD [25, 26]. The MSE spectroscopy capability is also in development to measure the q-profiles and current profiles in ITER [27].

In order for the plasma to reach the temperatures required to allow the fusion of two elements, the tokamak uses a number of methods for heating, including ohmic heating (from the large toroidal current of the tokamak design), radio waves heating for the ions at the cyclotron resonance frequency (ICRH), microwave heating for the electrons at its cyclotron resonance frequency too (ECRH), and Neutral Beam Injection (NBI). All the heating systems have also other important secondary functions, as diagnostics or control, it is the diagnostic capabilities of the neutral beam injection method with which this report is concerned here. The principle is straightforward, an energetic neutral atom, which because of its neutrality can pass through the plasma confining field, is injected into the plasma. After it reaches a certain distance, generally within the core of the plasma region, the neutral atoms ionize and thereafter disperse their

kinetic energy among the plasma ions; thus heating the plasma. At ASDEX-Upgrade or JET, the primary function of the neutral beams is for heating purposes, and therefore the injected species is deuterium atoms, and ultimately will be a mixture of deuterium and tritium at ITER. For ASDEX-Upgrade the injected atom energies are of the order of 25−30 keV/amu to penetrate sufficiently into the core of the plasma (depending on the density and size of the plasma), for JET about 50 keV/amu. The requirements for ITER are much more demanding. At a recent science meeting at EFDA-JET the capabilities being put in place during the JET EP2 and the requirements for ITER were summarised by Ciric [28] and Mc Adams [29].

1.1 Neutral Beam Characteristics

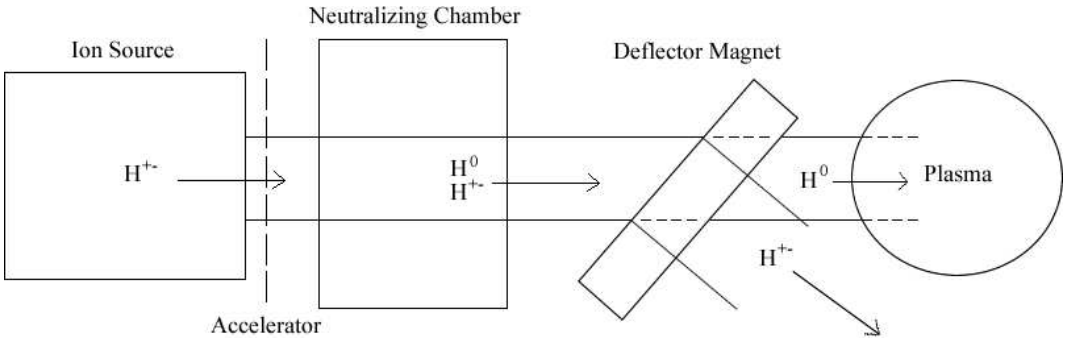

Figure 1.1: Neutral Beam principle for positive and negative ion sources. Here, H is used to denote the deuterium and tritium atoms typically used in JET and ITER.

For magnetic confinement fusion, there are two types of neutral beam which accelerate either positive or negative preionized hydrogen isotope ions. When the energies of the beam are required to be greater than 60 keV/amu, the neutralization of positive ions before its injection becomes inefficient and negative ion sources are preferred. In the case of ITER, where the neutral heating beam energies are required to be of the order 1 MeV, the negative ion sources will be put into action. However, for JET and other current machines, positive ions sources are used for heating. The first stage of the neutral beam is a discharge (low temperature plasma), the discharge will contain species e, H, H^+, H_2^+, H_3^+ and H^-. The abundance of each species is optimised through temperature and density to favour the configuration being used. In particular for positive ion acceleration, the presence of the species H^+, H_2^+, H_3^+ is of greatest concern, while for negative ion acceleration it is the H^- concentration, formed by vibrational excitation of H_2 followed by the dissociative attachment reaction

$$\begin{aligned} e^- + H_2(v^*) &\rightarrow H_2(v'^*) + e^- \\ e^- + H_2(v^*) &\rightarrow H_2^- \rightarrow H^- + H^+, \end{aligned} \tag{1.1}$$

which must be optimised. Cesium is used to aid this process as the minimum energy required to release its electrons is very low so these electrons can then bind to the H to form H^-. If there is a negative voltage applied across the discharge, the positive ions will be accelerated into a neutralising chamber and there will be a backstream of electrons. Conversely, a positive voltage will accelerate the negative species in the direction of the neutralising chamber and create a backstream of positive ions. The backstream of electrons are relatively easy to decelerate however the positive ions may cause a large amount of sputtering through collision with the source. There are therefore a number of different design features associated with the negative and positive ion sources.

The neutralization stage then establishes the key neutral beam populations which matter for plasma heating and diagnostic studies. Positive species then undergo Charge eXchange Recombination (CXR) reactions with a molecular hydrogen gas cloud which neutralise the ion. The neutralising reactions can be written as

$$\begin{aligned} H^+(E) + H &\rightarrow H(E) + X \\ H_2^+(E) + H &\rightarrow H(E/2) + X \\ H_3^+(E) + H &\rightarrow H(E/3) + X, \end{aligned} \tag{1.2}$$

where E is the energy of the accelerated positive ions and X is defined as any other charged or slow reactants. Therefore, there are now three energy fractions of H which enter the plasma. Negative ion neutralization is by stripping

reactions such as

$$H^-(E) + H_2 \rightarrow H(E) + H_2 + e\,, \tag{1.3}$$

and only a single energy component is present in the final neutral beam. However, only a certain fraction of the ionic species will be neutralised through these processes. An electromagnet must be put in place to deflect these residual fast ions to a cooled ion dump that can withstand heavy ion bombardment. It is also important to ensure the purity of the neutral beam by stopping any slow moving particles from the neutralising gas cloud from diffusing into the plasma. This is achieved through using powerful vacuum pumping technology. A basic schematic for the neutral beam is outlined in figure 1.1.

1.1.1 ASDEX Upgrade Positive Preionized Ion Neutral Injection

The ASDEX Upgrade (AUG) Neutral Beam Injection (NBI) System uses Positive Ion Neutral Injectors (PINIs). There are four Neutral Injection Boxes (NIBs) which are both equipped with up to four PINIs (Stäbler *et al.* [30]) An outline of this arrangement can be seen in figure 1.2.

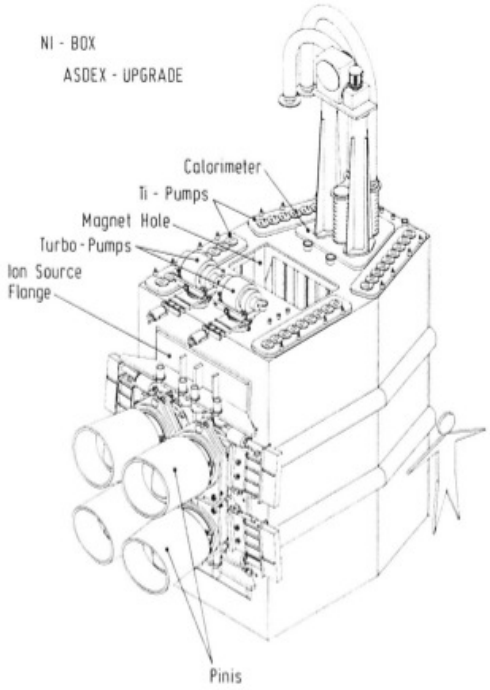

Figure 1.2: An illustration of a ASDEX Upgrade Neutral Injection Box.

These PINIs are able to provide a heating power of up to 6 MW for a hydrogen beam and 9 MW for a deuterium one with a pulse length up to 10 s. The preionized atoms are accelerated at a voltage up to 55 kV for hydrogen and 65 kV for deuterium, this leads to an adequate penetration of about 0.5 m and keeps the efficiency of the system at a tolerable level. Multiplying for the toroidal magnetic field of about 4 T we obtain a Lorentz electric field up to $1.3 \cdot 10^7$ V/m for hydrogen and up to $1.0 \cdot 10^7$ V/m for deuterium.

An overview about the heating, refuelling and current drive capabilities of the Neutral Beam Injectors in ASDEX Upgrade can be found in [31, 32].

1.1.2 JET Positive Preionized Ion Neutral Injection

The JET Tokamak uses also PINIs for heating through neutral beam injection. Jet has two NIBs which are both equipped with up to eight PINIs (Duesing *et al.* [33]). Within the NIB the PINIs are arranged in two vertical banks of four, with each set of four then split into two pairs sharing the same deflecting magnet.

In JET the PINIs require a penetration up to the core of the plasma, about 3 m, which requires kinetic energies of the order of 100 keV. During the year 2009 the EP1 system configuration of neutral beams was replace for the new EP2, this new system achieved a heating power of 34 MW and longest NBI pulse length of 20 s. With the power suplies of the EP2 system the ions are accelerated with a voltage of 130 kV and a current intensity of 130 A.

1.1.3 ITER Negative Preionized Ion Neutral Injection

ITER will require neutral beams with a greater energy and thus penetration (ITER $R \approx 6$ m) due to its larger radius and higher density. Therefore, the NBI System in ITER will use a negative ion source. It can be seen from figure 1.3 that the energies of the beam must be of the order 1 MeV for efficient heating of the ITER plasma.

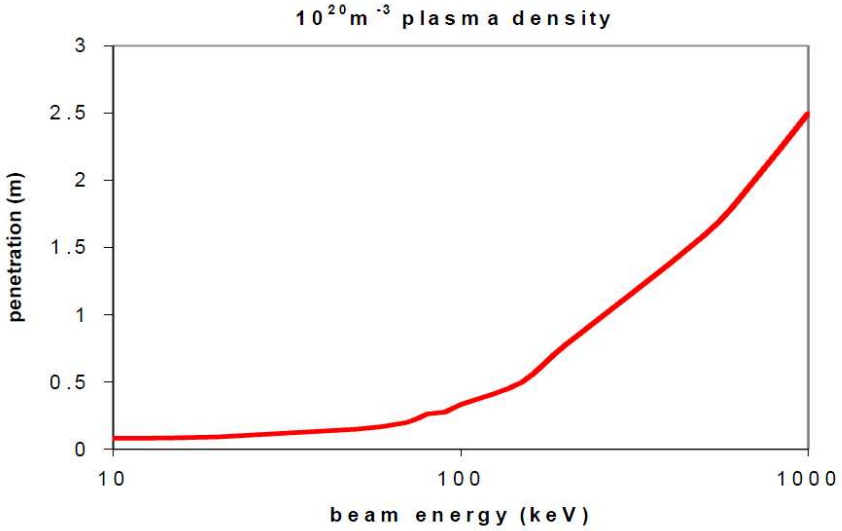

Figure 1.3: A graph showing the penetration distance of a neutral beam for various energies. Image Credit: Mc Adams (2010) [29].

Due to the large diagnostic capabilities of the neutral beams, ITER will have two types of beam in operation: one beam will be solely for heating and will inject neutral deuterium, these beam energies must be greater than 1000 keV; the other beam will be purely for diagnostic use and will inject neutral hydrogen, for it the energies being used will be of the order 100 keV. Therefore, as ITER will be relying heavily on the accuracy and reliability of beam spectroscopy to monitor key plasma parameters, it is important that attention is turned to diagnosis of the beam emission.

1.2 Beam Emission and Spectroscopy

When the beam enters the plasma, the neutral atoms have collisions with the ions and electrons in the plasma and interact with magnetic and electric fields present in the plasma. These interactions with the field and plasma species cause the neutral atoms to become excited and ionised. As the excited beam atoms relax back down to their ground state, they emit radiation. This composite of processes leads to three principal effects: CXR spectroscopy, Beam eMission Spectroscopy (BMS) and Beam Stopping (BS). CXR is how the beam causes the plasma ions to radiate, BMS is the emission of the beam atoms themselves and BS is the effective loss rate of atoms from the beam caused by ionisation or charge exchange with plasma ions.

As the beam leaves the NBI and enters the plasma, it firstly passes through the narrow Scrape Off Layer (SOL). This layer is formed through the small amount of residual plasma separating the edge of the plasma (often referred to as the separatrix) and the tokamak vessel. It is a low density region at relatively low temperatures. As this layer is very narrow, the beam atoms pass straight through with little effect on the population structure of the neutral atoms.

Emission from the beam in this region is negligible compared with emission of thermal neutral deuterium always present in the outer regions of the plasma near the vessel wall (Mc Neil, 1989 [34]). As the beam enters the confined core plasma, the density of the electrons increases by a factor of ten and temperature of the electron and plasma ions rise dramatically to large values ($\simeq$ 3000 keV in the JET tokamak). Now, there is almost no thermal deuterium as it has been ionised and recycled by the plasma. The principal emission driven by the beam is firstly that from full ionised plasma impurity ions following charge exchange reactions between the fully ionised plasma species (both hydrogen nuclei and impurities) and the neutral beam atoms.

Understanding this spectrum is of great diagnostic benefit and is projected to be used as a direct measure of fusion "ash" in the new generation tokamak, ITER. Von Hellermann *et al.* [35] provide accurate data which can be used to model this CX emission. Secondly there is the emission from the beam atoms themselves. Particularly the Balmer series emission in the visible spectral region is evident and characteristically displaced from the natural wavelengths due to Doppler effect (of the fast moving beam atoms with respect to the spectrometer line-of-sight). Generally, the D_α lines are compared with computer simulated spectra which relies on key parameters within the plasma. The CX and BM spectra can be used to find the ion temperature (Kallne *et al.* [36], plasma rotation, impurity concentrations (Boileau *et al.* [37]), internal magnetic and electric fields (Mandl *et al.* [22]) and if the polarisation of the emission is studied one may also determine the magnetic field pitch angle and therefore produce a current density profile [38]. The graph shown in figure 1.4 shows a visible spectrum in the vicinity of H_α. It shows the very broad CXR emission approximately centered on the natural wavelength. This is broad due to the Doppler Effect because of the fact the plasma species are at very high temperatures. The three complex Doppler shifted components are the beam emission and are due to the three fractional energy components of the neutral beam (from the positive ion source). The narrow lines at the natural position are emission of thermal (not beam) hydrogen and deuterium at the edge of the plasma in the vicinity of the scrape-off-layer. They are sharper as they are at lower temperatures than the core plasma species. All these emission are determined theoretically by modelling the collisional, radiative and recombination processes between the neutral beam atoms and the plasma ions and electrons.

The distance at which the neutral beam atoms become fully ionised is determined by a value known as the "stopping coefficient". The beam attenuation length is of great importance. If the beam travels too far it may cause significant damage to the opposite plasma wall and if it does not travel far enough into the core, the heating will be very inefficient. The fourth year report of Henderson [39], discussed in detail the various atomic processes used in calculating this stopping coefficient. In particular, it paid close attention to the population structure of each principal and orbital angular moment quantum shell of the beam atoms in a statistical sense from the balance of atomic processes.

The aim of this report, is to further the studies and discussions of the previous report into the field of BMS combined with a more careful approach to the effects of the magnetic and induced Lorentz field on the emission spectrum. When the beam atoms are travelling through the plasma at a speed, v, they are subject to a large Lorentz electric field perpendicular to the direction of propagation and the magnetic field, this disturbs the atomic level structure of the beam hydrogen atoms causing splitting up of the H_α emission into Stark components as seen in figure 1.4 and modifies the population structure as discussed below.

1.3 Motional Stark Effect

As described earlier, the hydrogen beam atom in a fusion plasma experiences a magnetic field $\vec{B}$ of intensity $\sim 3\,\mathrm{T}$ and because of its velocity $\vec{v}$ across the magnetic field a large Lorentz electric field $\vec{v}\times\vec{B}$ of $\sim 100\,\mathrm{kV/cm}$. In this typical set up, the magnetic field is negligible compared to the Lorentz electric field. Therefore, the neutral beam atoms are perturbed according to the first order disturbance (linear in electric field) of the energy eigenstates, this is known as the Motional Stark Effect. If the speed of the neutral beam atoms was reduced to zero, then there would only be the magnetic field acting on the atoms, this would again cause a first order disturbance (linear in magnetic field) on the energy eigenstates which is known as the Paschen-Back Effect. With a non-hydrogenic atom, the Stark effect would normally be quadratic and the magnetic field disturbance still linear but much weaker, called the Zeeman effect. These differences occur because of the energy level separations of the isolated, field-free, atoms, isolated hydrogen atom levels have an accidental degeneracy of the l-shells of the same n-shell which is not present in non-hydrogenic atoms and ions.

In a detailed study of the following sections, it will become evident that the effects of the electric and magnetic field disturbances must be examined for different magnitudes of field. This will include ranges where the field disturbances

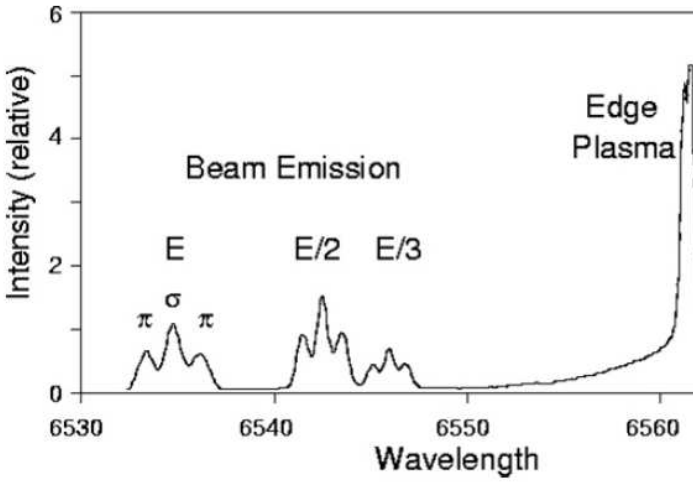

Figure 1.4: A graph showing the visible spectrum, near the D_α line, observed during a neutral beam pulse into a magnetically confined plasma. The three Doppler shifted components are the beam emission due to the three fractional energy components of the neutral beam. The thermal hydrogen and deuterium at the edge of the plasma cause the two spiked features at longer wavelengths. The broad feature in the vicinity of these narrow spikes is due to the CXR emission of the plasma species. Image credit: Von Hellermann *et al.* [35]

can be treated purely as perturbation on the isolated atom states and where the field disturbances are the dominant process in the determination of energy eigenstates. The induced Lorentz field is always perpendicular to the magnetic field. For a pure magnetic field disturbance the angular momentum about the field direction is a constant of motion with the m quantum number assigned. For the pure Lorentz field case, the angular momentum about the field direction is again a constant of the motion with the m quantum number assigned, but this is perpendicular to the magnetic field. Therefore, when the electric and magnetic fields are comparable, there is not an angular momentum component which is a constant of the motion and so there is no well defined m quantum number. When solving for the pure electric field case, the Schrödinger equation can be solved in parabolic coordinates with a new constant of motion (the Runge-Lenz vector) which leads to a new quantum number, defined as k. However, now the usual orbital quantum number l arising from the squared angular momentum operator is no longer a constant of motion. Therefore, there is a lot of confusion as to what labelling convention to use on the atomic states as the fields are explored. Usual quantum numbers are no longer exact and their breakdown must be examined carefully. The computer codes, used in the following sections give correct solutions, but the interpretation in terms of usual quantum numbers, polarisation etc. is not immediate or necessarily possible.

These effects of exploring the different field perturbations are illustrated in figure 1.5. The evolution of the H_α multiplet can be seen as the beam speed is decreased. One can immediately see the characteristic fifteen (although only nine of which are visible) allowed transitions associated with the Stark effect initially begin to transform into the

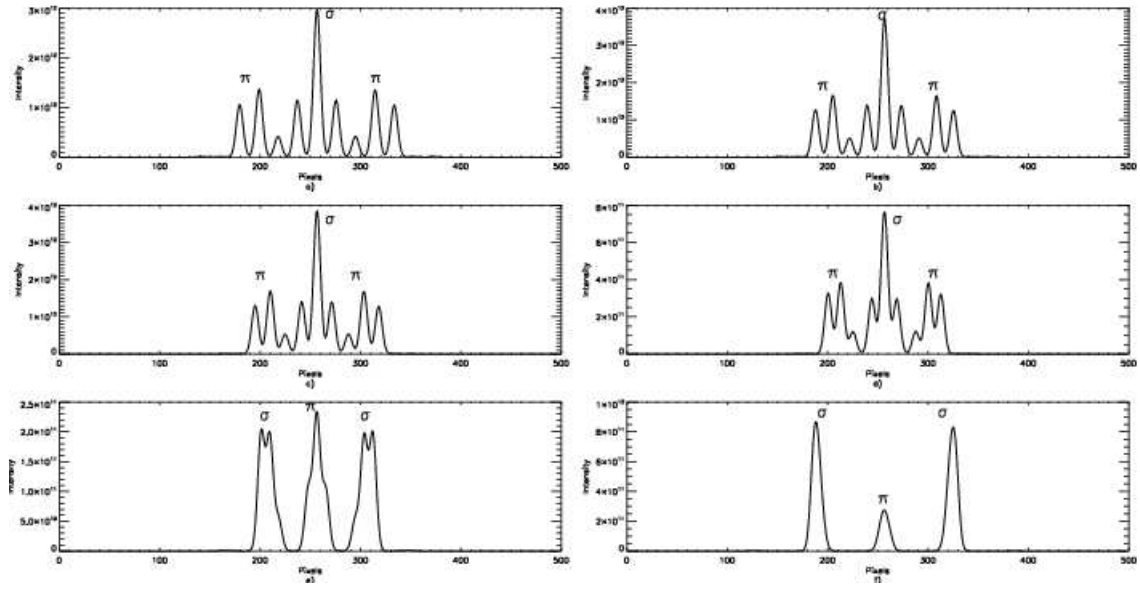

Figure 1.5: A magnetic field of 1.4 T and beam energy of 0.24 MeV/amu is present in a) then as we move through to f) the effects of changing the beam energy down to 100 eV/amu and increasing the magnetic field to 40 T in six steps are shown. The π and σ indicate the two types of polarisation. Although these magnetic and electric fields are not so relevant to a fusion reactor, they have been chosen to exaggerate the evolution of moving from one field to another. Graphs were obtained from the ADAS routine, ADAS305.

characteristic three main transition lines of the Paschen-Back effect. However, an important feature of this evolution is the polarisation, indicated by π and σ. It is clear that as you move from one regime to another, the two polarisations interchange. Although this may not produce any problems in a computer calculation, it can cause confusion when comparing experimental data to the simulated emission spectra.

When dealing with the field values at JET, there is a further independent non-orthogonal electric field which must also be considered. First order perturbation theory in the non-relativistic isolated atom Hamiltonian may be used to calculate both the Stark term (with the external field) and the Zeeman or Paschen-Back term.

1.4 Diagnostics

Spectroscopy on JET is key to interpreting what is happening inside the plasma. To do this, extensive studies must be made into energy levels, oscillator strengths and electron-ion, ion-ion and ion-atom cross sections. The two spectral scenarios that occur along the beam path can be used for diagnostic purposes, CXRS allows the light impurities in the plasma to be studied where they would generally be fully ionized. The width and displacement of the charge exchange induced spectral lines give the ion temperature and plasma rotation (Boileau *et al.* , [37]). However, to accurately interpret these spectral lines, one must exclude the "cold effects" of the plasma (that is emission from the cold edge of the plasma not driven by the beams) and the bremsstrahlung background radiation. The cold effects are illustrated by the narrow features of small thermal Doppler temperature, such as of HeII, BeII, HI and DI in the absence of beams and superimposed on the spectral intervals used to analyst the charge exchange emission. In addition, the shape of the spectral line is governed by the variation of CX cross section with energy.

At the beam emission stage, the H_α features become dominant. Again the cold components within the plasma must be considered when dealing with beam emission. The Stark components of the beam emission are resolved into their π and σ polarisations. As the beam atoms are travelling at such high speeds, the dominant excitation reaction is through positive ion impact. The diagnostic potential of the beam emission is huge and Mandl *et al.* (1993) [22] provide a detailed review of each procedure. To summarise, the combined Doppler shifts of the emission can provide detail as to the radial and vertical position of the observation. If the observation volume is directly perpendicular to the observation viewing point, then there should be no Doppler shift present. If the volume is before this point

along the observation line, then there will be a blue shift and likewise if it is after then there will be a red shift. This is advantageous to know because it gives a good indication as to what part of the plasma is being diagnosed. The strength of the Lorentz field acting on the beam can be calculated by working out the spacing between each of the Stark components, the stronger the field, the larger the distance between each of the components. As the Lorentz field is always perpendicular to the magnetic field, if the direction of the magnetic field changes this will also induce a change to the direction of the Lorentz field. This is measured by studying the polarisation patterns of the emission light. Being able to deduce the direction of the magnetic field is essential as this allows measurement of the pitch angle. In addition, Z_{eff} may be derived from the ratio of the Stark to CX feature. However this interpretation requires accurate fundamental cross section knowledge [20].

The main focus of modern fusion plasma diagnosis has focused on polarisation measurements of particular components of the H_α Stark multiplet for magnetic field characteristics. It is rather difficult to initiate this approach on ITER and so fresh attention has been directed at full population and emission modelling of the sort carried out in the ADAS subroutine, ADAS305. Experimental teams in Madison, Wisconsin and at General Atomics, San Diego are collaborating with EFDA-JET on exploring the use of ADAS305 predictive capabilities in their spectral analysis. Therefore, as these codes are in active use, it is important to explore the accuracy to which these generated emission lines match that of the experimental emission lines. For example, in experiment, it is evident that there is a persistent observation of a slight asymmetry between the blue and red shifted Stark components of the H_α Stark multiplet [40, 41]. It is possible that this asymmetry can arise from geometrical observation effects and line-of-sight superpositions for the multiple beams being fired into the tokamak at JET or ASDEX Upgrade. However, there are also possible theoretical reasons lying above perturbation theory.

In chapter 2 we show an overview about the Stark hydrogen atom, which is the hydrogen atom solved in parabolic coordinates, for zero or non-zero field, so the states are oriented through the z axis and the wave functions are labelled in the parabolic quantum numbers $|n\,k\,m\rangle$, as difference of the usual spherical quantum numbers $|n\,l\,m\rangle$ of the Rydberg hydrogen atom. In this chapter it will be also given an overview about the solution for the Stark effect through perturbation theory and why it is not applicable for the problem of neutral hydrogen under a constant electric field. In the chapter 3 it will be detailed the method of the complex coordinate rotation to solve the Stark effect in neutral hydrogen atom as an *ab initio* method beyond perturbation theory, and get exact results for the position of the resonances, the widths and the wave functions. In chapter 4 we will show the results obtained with the complex coordinate rotation method, the energies, widths and wave functions for the neutral hydrogen atom under a constant electric field. In chapter 5 we will focus in applying the calculated wave functions to obtain physical observables, which can be afterwards applied to more practical issues, as the Stark splitting of the Balmer H_α and D_α lines or the Einstein transition coefficients. A summary of these findings will then be put forward in chapter 6. Atomic units are used throughout unless otherwise specified.

Chapter 2

The Stark hydrogen atom

The non-relativistic Hamiltonian of the neutral hydrogen atom under a constant electric field is

$$H = -\frac{1}{2}\nabla^2 - \frac{1}{r} + \vec{F}\cdot\vec{r}, \tag{2.1}$$

where $\vec{F}$ is the electric field vector and we have neglected the isotopic effects, considering the nucleus of mass infinity.

The electric field vector points through a privileged direction, so the problem loses the spherical symmetry. To solve the problem we use the parabolic coordinates [14, 15], choosing the axis z the direction of the field vector:

$$\begin{aligned} \xi &= r + z = r(1 + \cos\theta) \\ \eta &= r - z = r(1 - \cos\theta) \\ \phi &= \tan^{-1}\frac{y}{x}, \end{aligned} \tag{2.2}$$

or alternatively

$$\begin{aligned} x &= \sqrt{\xi\eta}\cos\phi \\ y &= \sqrt{\xi\eta}\sin\phi \\ z &= \frac{\xi - \eta}{2} \\ r &= \frac{\xi + \eta}{2}. \end{aligned} \tag{2.3}$$

The volume element is

$$\int_{R^3} \mathrm{d}V = \int_0^{2\pi}\mathrm{d}\phi\int_0^{\infty}\mathrm{d}\xi\int_0^{\infty}\mathrm{d}\eta\,\frac{1}{4}(\xi + \eta). \tag{2.4}$$

The coordinate surfaces are paraboloids of revolutions for ξ and η and meridian planes for ϕ. This is shown through a 3D graphical picture in figure 2.1. It is seen that those with $\xi = A$ extend to $z = -\infty$ and those with $\eta = A$ extend to $z = \infty$ where A is a positive constant.

The Hamiltonian is written as

$$H = -\frac{2}{\xi+\eta}\frac{\partial}{\partial\xi}\left(\xi\frac{\partial}{\partial\xi}\right) - \frac{2}{\xi+\eta}\frac{\partial}{\partial\eta}\left(\eta\frac{\partial}{\partial\eta}\right) - \frac{1}{2\xi\eta}\frac{\partial^2}{\partial\phi^2} - \frac{2}{\xi+\eta} + \frac{1}{2}F(\xi - \eta). \tag{2.5}$$

An in-depth overview of the solution for the Stark Hamiltonian for zero field can be found in Condon and Shortley [42], Bethe and Salpeter [43] and Gallagher [44]. In these works it is also treated the Stark effect with perturbation theory, obtaining at first order the known solution of the linear Stark effect, nevertheless this solution can not be considered as true as the Stark effect does not fulfil the conditions of perturbation theory.

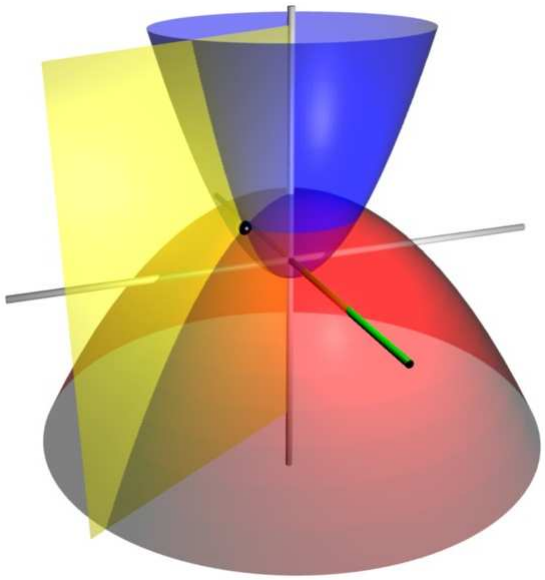

Figure 2.1: Coordinate surfaces of the 3D parabolic coordinates. The red paraboloid corresponds to $\xi = 2$ and the blue paraboloid corresponds to $\eta = 1$ and the yellow half plane corresponds to $\phi = 60^0$. The three surfaces intersect at point P, shown as a small black sphere.

2.1 Solution of the Stark hydrogen atom for zero field

In the case of the zero field, the wave function can be separated as a product of one-variable functions of the parabolic coordinates as

$$\psi(\xi,\eta,\phi) \;=\; \frac{1}{\sqrt{2\pi}}\, u(\xi)\, v(\eta)\, \mathrm{e}^{im\phi}\,, \tag{2.6}$$

which allow us to spread the Schrödinger equation for the separated functions u and v as

$$\begin{aligned}
\frac{\mathrm{d}}{\mathrm{d}\xi}\left(\xi\,\frac{\mathrm{d}u}{\mathrm{d}\xi}\right) + \left(E\,\frac{\xi}{2} \;+\; Z_1 \;-\; \frac{m^2}{4\xi} \;-\; F\,\frac{\xi^2}{4}\right) u \;&=\; 0 \\
\frac{\mathrm{d}}{\mathrm{d}\eta}\left(\eta\,\frac{\mathrm{d}v}{\mathrm{d}\eta}\right) + \left(E\,\frac{\eta}{2} \;+\; Z_2 \;-\; \frac{m^2}{4\eta} \;+\; F\,\frac{\eta^2}{4}\right) v \;&=\; 0\,.
\end{aligned} \tag{2.7}$$

This firstly shows that the magnetic quantum number m is already exact due to the rotation symmetry round the axis z is still conserved. The wave functions are degenerate for $\pm m$. The separation constants, Z_1 and Z_2 are known as the generalised charges, which are related as

$$Z_1 \;+\; Z_2 \;=\; 1\,. \tag{2.8}$$

If the the equations are solved for zero field and bounded states ($E < 0$), then the functions, u and v can be obtained in terms of Laguerre polynomials. This gives

$$\begin{aligned}
u_{n_1 n_2 m}(\xi) \;&=\; N_u\;\sqrt{\epsilon}\,\mathrm{e}^{-\frac{1}{2}\epsilon\xi}\,(\epsilon\xi)^{\frac{|m|}{2}}\,\mathrm{L}_{n_1}^{|m|}(\epsilon\xi) \\
v_{n_1 n_2 m}(\eta) \;&=\; N_v\;\sqrt{\epsilon}\,\mathrm{e}^{-\frac{1}{2}\epsilon\eta}\,(\epsilon\eta)^{\frac{|m|}{2}}\,\mathrm{L}_{n_2}^{|m|}(\epsilon\eta)\,,
\end{aligned} \tag{2.9}$$

where $E = -\frac{1}{2}\epsilon^2$ and

$$\begin{aligned}
n_1 \;&=\; 0, 1, 2, \ldots \\
n_2 \;&=\; 0, 1, 2, \ldots\,,
\end{aligned} \tag{2.10}$$

the two new quantum numbers obtained from the relations in equation 2.9, they are related with the nodes of the Laguerre polynomials and to the original quantum numbers, n and m, through

$$n \;=\; n_1 \;+\; n_2 \;+\; |m| \;+\; 1\,. \tag{2.11}$$

Often, these two new quantum numbers are defined as one quantum number k,

$$k \;=\; n_1 \,-\, n_2\,. \tag{2.12}$$

k is related to the Runge-Lenz vector, which is defined as [45]

$$\vec{K} \;=\; m\,Z\,\mathrm{e}^2\,\hat{r} \;-\; \frac{1}{2}\left(\vec{p}\times\vec{L} \;-\; \vec{L}\times\vec{p}\right). \tag{2.13}$$

Classically, the Runge-Lenz vectors points in the direction along the major axis of the ellipse which describes the trajectory of the classical particle in the Coulomb potential, and its length is equal to the eccentricity of the orbit. The z component of the Runge Lenz vector is expressed in parabolic coordinates as

$$K_z \;=\; \frac{\xi-\eta}{\xi+\eta} \;-\; \frac{2\eta}{\xi+\eta}\,\frac{\partial}{\partial\xi}\left(\xi\,\frac{\partial}{\partial\xi}\right) + \frac{2\xi}{\xi+\eta}\,\frac{\partial}{\partial\eta}\left(\eta\,\frac{\partial}{\partial\eta}\right) + \frac{\xi-\eta}{2\xi\eta}\,\frac{\partial^2}{\partial\phi^2}\,, \tag{2.14}$$

which commutes with the Hamiltonian and the z component of the angular momentum.

In these terms the generalised charges 2.8 result

$$\begin{aligned} Z_{1n_1n_2m} &= \frac{2n_1+|m|+1}{2(n_1+n_2+|m|+1)} \\ Z_{2n_1n_2m} &= \frac{2n_2+|m|+1}{2(n_1+n_2+|m|+1)}\,, \end{aligned} \tag{2.15}$$

and the energy

$$\epsilon_{n_1n_2m} \;=\; \frac{1}{n_1+n_2+|m|+1} \;=\; \frac{1}{n} \tag{2.16}$$

The normalisation constants N_u, N_v result:

$$\begin{aligned} N_u &= \frac{\sqrt[4]{2}}{\sqrt{(n_1+n_2+|m|+1)}}\,\sqrt{\frac{n_1!}{(n_1+|m|)!}} \\ N_v &= \frac{\sqrt[4]{2}}{\sqrt{(n_1+n_2+|m|+1)}}\,\sqrt{\frac{n_2!}{(n_2+|m|)!}}\,, \end{aligned} \tag{2.17}$$

which leads to the expression of the total zero-order wave function as follows:

$$\psi_{n_1n_2m}(\xi,\eta,\varphi) \;=\; \frac{1}{n\sqrt{\pi}}\,\sqrt{\frac{n_1!}{(n_1+|m|)!}}\,\sqrt{\frac{n_2!}{(n_2+|m|)!}}\,\mathrm{e}^{im\varphi}\,\mathrm{e}^{-\frac{1}{2}\epsilon(\xi+\eta)}\,\epsilon^{|m|+1}(\xi\eta)^{\frac{|m|}{2}}\,\mathrm{L}_{n_1}^{|m|}(\epsilon\xi)\,\mathrm{L}_{n_2}^{|m|}(\epsilon\eta) \tag{2.18}$$

This solution makes also diagonal the z component of the Runge-Lenz vector, being its eigenvalues

$$K_z\,|\,n\,k\,m\,\rangle \;=\; \frac{k}{n}\,|\,n\,k\,m\,\rangle\,. \tag{2.19}$$

2.2 Perturbation theory

For a field larger than zero, the last terms of the equations 2.7 can be treated as a perturbation, nevertheless it is not actually correct as the Stark effect does not fulfil the conditions of perturbation theory.

Let be the generic perturbation problem:

$$H \;=\; H_0 \;+\; V\,, \tag{2.20}$$

where the solutions of the ground Hamiltonian H_0 are known

$$H_0\,\phi_k^{(0)} \;=\; \epsilon_k^{(0)}\,\phi_k^{(0)}\,. \tag{2.21}$$

Then the perturbation V that must fulfil the conditions

$$\langle \phi_k \,|\, V \,|\, \phi_k \rangle \;\ll\; \epsilon_k^{(0)} \tag{2.22}$$

and

$$\langle \phi_k \,|\, V \,|\, \phi_l \rangle \;\ll\; \epsilon_k^{(0)} \;-\; \epsilon_l^{(0)} \tag{2.23}$$

for all k and l.

In figure 2.2 it is shown a qualitative diagram, the combined potential Coulomb and constant electric field, the energy of the ground state and its wave function. The supposed perturbation of the constant electric field is a linear term in z, and it is the dominating one asymptotically in comparison with the Coulomb one, which goes like $\frac{1}{r}$, it does not matter how small is the field. A potential which does not tend to zero asymptotically is not a perturbation, so it can not be treated in terms of perturbation theory.

In the other hand, the spectrum of the hydrogen atom under a constant electric field has also a topology absolutely different to the field-free one. The Stark atom has no bounded states, but resonances, and any real number is an eigenvalue of the Stark Hamiltonian, so we have a continuum spectrum which is the hole real line. Inside this continuum spectrum, one can find resonances, which tend to the hydrogen bounded states eigenvalues when the field intensity tends to zero. These resonances have a continuum component, so they have a certain time of live, even the ground state, and their wave functions are not square integrable. It is also shown in diagram 2.2.

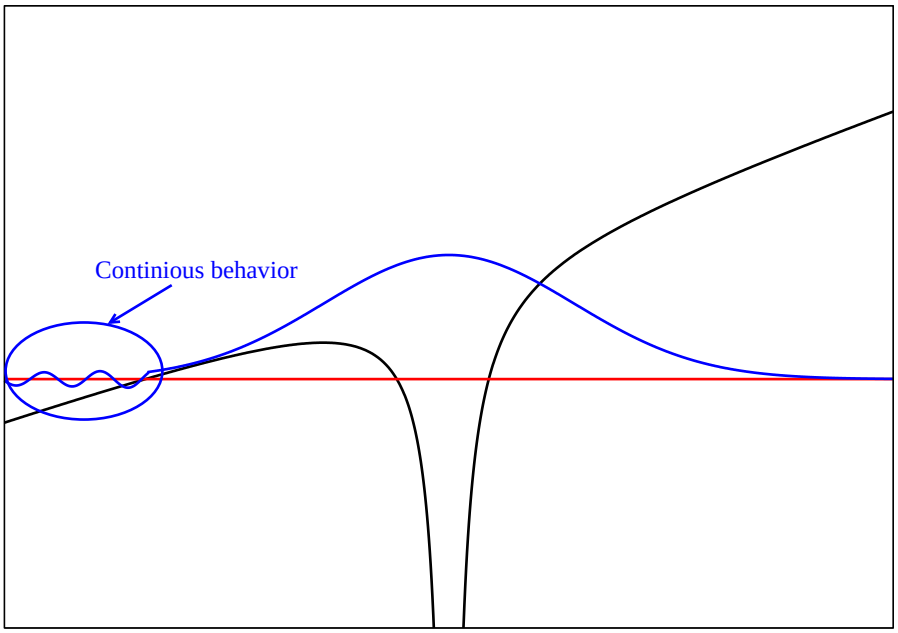

Figure 2.2: Qualitative diagram of the ground state of a one-dimension combined Coulomb and Stark potential

Taking in account that, perturbation theory has critical inconsistencies when it is applied to the problem of a hydrogen atom under a constant electric field which makes its results non trustful.

As an academical work, in [43] the energies for the Stark hydrogen atom are calculated using perturbation theory, the result is up to third order

$$\begin{aligned} E \;=\; & -\frac{1}{2n^2} \;+\; \frac{3}{2} F\, n\, k \;- \\ & \frac{1}{16} F^2 n^4 \left(17\, n^2 \;-\; 3\, k^2 \;-\; 9\, m^2 \;+\; 19\right) \;+ \\ & \frac{3}{32} F^3 n^7 k \left(23\, n^2 \;-\; k^2 \;+\; 11\, m^2 \;+\; 39\right). \end{aligned} \tag{2.24}$$

The expression for the wave functions at higher order perturbation theory is very tedious and requires a great effort to obtain, so an alternative *ab initio* method becomes more valuable to get the energies and wave functions.

2.3 State widths

As shown in the figure 2.2, the states of the Stark hydrogen atom have always asymptotically a part of the wave function above the potential energy, which gives them a behaviour as continuum, so they are no more bounded states but resonances with a width Γ, being $\tau = \frac{1}{\Gamma}$ their lifetime before a tunnel autoionization. These widths can be calculated with perturbation theory at second or higher order and including in the expansion states of the continuum of the zero-order wave functions. The effort required to do so is even larger than using an *ab initio* method, so it is not valuable.

Some works used semiempirical methods to get the widths [6, 9], the expressions for the widths are for energies below the potential barrier

$$\Gamma = \frac{(4R)^{2n_2+m+1}}{n^3 n_2!(n_2+m)!} \exp[y], \tag{2.25}$$

with

$$R = \frac{(-2E)^{\frac{3}{2}}}{F}, \tag{2.26}$$

and

$$y = -\frac{2}{3}R - \frac{1}{4}n^3 F\left(34\,n_2^2 + 34\,n_2\,m + 46\,n_2 + 7\,m^2 + 23\,m + \frac{53}{3}\right). \tag{2.27}$$

This formula is only valid for field strengths

$$F \ll \left[8\,n^3\,(2\,n_2 + m + 1)\right]^{-1}. \tag{2.28}$$

For near the potential barrier, the semiempirical methods obtain:

$$\Gamma = \frac{F\,\log[1+\exp(-2\pi\epsilon)]}{2\,\sqrt{-E}\left[\left(\frac{1}{4} + \frac{\lambda_1}{R}\right)\left(\log 4\,\sqrt{2}\,R - \mathrm{Re}\psi\left(\frac{1}{2} + i\epsilon\right)\right) - 1\right]}, \tag{2.29}$$

with

$$\lambda_1 = n_1 + \frac{1}{2}(m+1) + \frac{1}{4R}(6n_1^2 + 6n_1 m + 6n_1 + m^2 + 3m + 2), \tag{2.30}$$

$$\epsilon = \frac{\sqrt{2}\,\frac{R}{3} - \pi\,(2n_2 + m + 1) + \arg\Gamma\left(\frac{1}{2} + i\epsilon\right)}{\log 4\,\sqrt{2}\,R}, \tag{2.31}$$

and R must be calculated in an implicit way with the auxiliary equation

$$E = -\frac{1}{2}\left(\lambda_1 + \frac{1}{16}R - \frac{\epsilon}{\sqrt{2}}\right)^{-2}. \tag{2.32}$$

The results for the state widths using these semiempirical formulae is not so trustworthy and finally it is worth to use the *ab initio* treatment.

Chapter 3

The complex coordinate rotation method

In present chapter we show in detail how to obtain the energies, widths and wave functions of the Stark hydrogen atom with the *ab initio* method of the complex coordinate rotation (CCR). The method is explained in detail in [46] and [16], the radial coordinate r is rotated in complex plane an angle ϑ

$$r' \;=\; r\,\mathrm{e}^{i\vartheta}\,, \tag{3.1}$$

so the Hamiltonian is transformed as follows:

$$H(\vartheta) \;=\; -\frac{\mathrm{e}^{-2i\vartheta}}{2}\,\nabla^2 \;-\; \frac{\mathrm{e}^{-i\vartheta}}{r} \;+\; \mathrm{e}^{i\vartheta}\,F\,r\,\cos\theta\,. \tag{3.2}$$

The rotated Hamiltonian 3.2 has lost the hermiticity, so its eigenvalues are now complex. The new complex type of the coordinate transform the oscillatory behaviour of the resonances in an exponential decay, making them square integrable. In general there are three types of transformation of the eigenvalues:

- Bounded states remain unchanged.
- Continuum branches are rotated an angle 2ϑ with the real axis, with origin in the threshold energy.
- Resonances are exposed in the complex plane once the rotation angle ϑ is greater then the argument of the complex root of the resonance.

Let the complex energy of the resonance be:

$$E \;=\; E_r \;-\; i\,\frac{\Gamma}{2} \;=\; |E|\,\mathrm{e}^{i\beta}\,, \tag{3.3}$$

where E_r is the position of the resonance and Γ the width. If the rotation angle ϑ is greater than the argument of the resonance β, the resonance becomes visible in the complex plane in a position independent of the rotation angle from this threshold.

We write the Hamiltonian 3.2 in parabolic coordinates:

$$H(\vartheta) \;=\; -\frac{2\,\mathrm{e}^{-2i\vartheta}}{\xi+\eta}\,\frac{\partial}{\partial\xi}\left(\xi\,\frac{\partial}{\partial\xi}\right) \;-\; \frac{2\,\mathrm{e}^{-2i\vartheta}}{\xi+\eta}\,\frac{\partial}{\partial\eta}\left(\eta\,\frac{\partial}{\partial\eta}\right) \;-\; \frac{\mathrm{e}^{-2i\vartheta}}{2\xi\eta}\,\frac{\partial^2}{\partial\varphi^2} \;-\; \frac{2\,\mathrm{e}^{-i\vartheta}}{\xi+\eta} \;+\; \frac{\mathrm{e}^{i\vartheta}}{2}\,F\,(\xi\,-\,\eta)\,, \tag{3.4}$$

and the wave function as an expansion in a basis set separating the variables

$$\Psi(\xi,\eta,\varphi) \;=\; \frac{1}{\sqrt{2\pi}}\,\mathrm{e}^{im\varphi}\,\sum_{k=1}^{N}\sum_{l=1}^{N} c_{klm}\,g_k(\xi)\,g_l(\eta)\,, \tag{3.5}$$

where $\{g_k(x)\}_{k=1}^{N}$ are basis set functions.

Then we can obtain the matrix elements of the Hamiltonian in terms of the proposed basis set as follows:

$$\begin{aligned} H_{klk'l'm}(\vartheta) &= \langle g_k\, g_l \,|\, H(\vartheta) \,|\, g_{k'}\, g_{l'} \rangle \\ &= \int_0^\infty \mathrm{d}\xi \int_0^\infty \mathrm{d}\eta\, \frac{1}{4}\,(\xi + \eta)\, g_k^*(\xi)\, g_l^*(\eta)\, H(\vartheta)\, g_k(\xi)\, g_l(\eta) \\ &= \int_0^\infty \mathrm{d}\xi \int_0^\infty \mathrm{d}\eta\, g_k^*(\xi)\, g_l^*(\eta) \left[-\frac{\mathrm{e}^{-2i\vartheta}}{2} \frac{\partial}{\partial\xi}\left(\xi \frac{\partial}{\partial\xi}\right) - \frac{\mathrm{e}^{-2i\vartheta}}{2} \frac{\partial}{\partial\eta}\left(\eta \frac{\partial}{\partial\eta}\right) \right. \\ &\quad \left. + \frac{\mathrm{e}^{-2i\vartheta}\, m^2}{8}\left(\frac{1}{\xi} + \frac{1}{\eta}\right) - \frac{\mathrm{e}^{-i\vartheta}}{2} + \frac{\mathrm{e}^{i\vartheta}}{8} F\,(\xi^2 - \eta^2) \right] g_k(\xi)\, g_l(\eta)\,, \end{aligned} \tag{3.6}$$

and the overlaps:

$$\begin{aligned} S_{klk'l'm} &= \langle g_k\, g_l \,|\, g_{k'}\, g_{l'} \rangle \\ &= \int_0^\infty \mathrm{d}\xi \int_0^\infty \mathrm{d}\eta\, \frac{1}{4}\,(\xi + \eta)\, g_k^*(\xi)\, g_l^*(\eta)\, g_{k'}(\xi)\, g_{l'}(\eta)\,, \end{aligned} \tag{3.7}$$

where the variable φ has been already integrated. In equation 3.6, the term in m^2 becomes singular in $\xi, \eta = 0$ if the basis functions have not an appropriate behaviour, and it can lead to numerical instabilities, this can be fixed making the transformation

$$g_k(x) = x^{\frac{|m|}{2}}\, f_k(x)\,, \tag{3.8}$$

so the Hamiltonian matrix results in terms of f:

$$\begin{aligned} H_{klk'l'm}(\vartheta) &= \int_0^\infty \mathrm{d}\xi \int_0^\infty \mathrm{d}\eta\, \xi^{|m|}\, \eta^{|m|}\, f_k^*(\xi)\, f_l^*(\eta) \left[-\frac{\mathrm{e}^{-2i\vartheta}}{2} \left(\xi \frac{\mathrm{d}^2 f_{k'}(\xi)}{\mathrm{d}\xi^2} f_{l'}(\eta) + \eta\, f_{k'}(\xi) \frac{\mathrm{d}^2 f_{l'}(\eta)}{\mathrm{d}\eta^2} \right. \right. \\ &\quad \left. + (|m| + 1) \frac{\mathrm{d} f_{k'}(\xi)}{\mathrm{d}\xi} f_{l'}(\eta) + (|m| + 1)\, f_{k'}(\xi) \frac{\mathrm{d} f_{l'}(\eta)}{\mathrm{d}\eta} \right) \\ &\quad \left. + \left(-\frac{\mathrm{e}^{-i\vartheta}}{2} + \frac{\mathrm{e}^{i\vartheta}}{8} F\,(\xi^2 - \eta^2) \right) f_{k'}(\xi)\, f_{l'}(\eta) \right] \end{aligned} \tag{3.9}$$

and the overlaps:

$$S_{klk'l'm} = \int_0^\infty \mathrm{d}\xi \int_0^\infty \mathrm{d}\eta\, \frac{1}{4}\,(\xi + \eta)\, \xi^{|m|}\, \eta^{|m|}\, f_k^*(\xi)\, f_l^*(\eta)\, f_{k'}(\xi)\, f_{l'}(\eta)\,, \tag{3.10}$$

remaining all the terms now regular.

Operating the expression for Hamiltonian and overlap matrixes 3.9 and 3.10 they are simplified splitting the double integrals as follows:

$$H_{klk'l'm}(\vartheta) = -\frac{\mathrm{e}^{-2i\vartheta}}{2}\,(\mathcal{T}_{kk'}\, \mathcal{I}_{ll'} + \mathcal{I}_{kk'}\, \mathcal{T}_{ll'}) - \frac{\mathrm{e}^{-i\vartheta}}{2}\, \mathcal{I}_{kk'}\, \mathcal{I}_{ll'} + \frac{\mathrm{e}^{i\vartheta}}{8} F\,(\mathcal{F}_{kk'}\, \mathcal{I}_{ll'} - \mathcal{I}_{kk'}\, \mathcal{F}_{ll'}) \tag{3.11}$$

and

$$S_{klk'l'm} = \frac{1}{4}\,(\mathcal{S}_{kk'}\, \mathcal{I}_{ll'} + \mathcal{I}_{kk'}\, \mathcal{S}_{ll'}) \tag{3.12}$$

where we have defined the matrix of the single integrals

$$\begin{aligned} \mathcal{T}_{kk'} &= \int_0^\infty \mathrm{d}x\, x^{|m|}\, f_k^*(x) \left[x \frac{\mathrm{d}^2}{\mathrm{d}x^2} + (|m| + 1) \frac{\mathrm{d}}{\mathrm{d}x} \right] f_{k'}(x) \\ \mathcal{I}_{kk'} &= \int_0^\infty \mathrm{d}x\, x^{|m|}\, f_k^*(x)\, f_{k'}(x) \\ \mathcal{F}_{kk'} &= \int_0^\infty \mathrm{d}x\, x^{|m|+2}\, f_k^*(x)\, f_{k'}(x) \\ \mathcal{S}_{kk'} &= \int_0^\infty \mathrm{d}x\, x^{|m|+1}\, f_k^*(x)\, f_{k'}(x)\,. \end{aligned} \tag{3.13}$$

Then we can determine the coefficients of the expansion solving the secular equation

$$(\mathbf{H} - \mathbf{E}\,\mathbf{S})\,\mathbf{C} = 0 \tag{3.14}$$

3.1 The choose of a basis set

In [10] it is used a basis set of Laguerre-mesh functions $\{f_i\}_{i=1}^N$, defined as follows [47]:

$$f_i(x) \;=\; (-1)^i \sqrt{x_i}\, \frac{\mathrm{L}_N(x)\, \mathrm{e}^{-\frac{x}{2}}}{x \,-\, x_i}\,, \tag{3.15}$$

where $\mathrm{L}_N(x)$ is the Laguerre polynomial of grad N, and x_i is its i-th zero. The efficiency and stability of this basis set for hydrogen atom problems was analysed by Vinke and collaborators 1993 in [48].

In Baye and Heenen 1986 [47] it is made the algebra with rigorous proving of the properties of a Lagrange-mesh basis set. The functions must fulfil two properties:

$$f_i(x_j) \;=\; \lambda_i^{-\frac{1}{2}}\, \delta_{ij}\,, \tag{3.16}$$

and

$$\int_a^b \mathrm{d}x\, f_i(x)\, f_j(x) \;=\; \delta_{ij}\,. \tag{3.17}$$

Then the integral of any function can be with a good accuracy approximated by the Gauss quadrature formula

$$\int_a^b \mathrm{d}x\, g(x) \;\approx\; \sum_{i=1}^{N} \lambda_i\, g(x_i)\,. \tag{3.18}$$

This method allows us to calculate the integrals involved in the variational method by a very fast way with quite good accuracy. Anyway in present job we made the full integration of the basis functions using a multistep Simpson formula and not the Gauss quadrature one.

The quotient $\frac{\mathrm{L}_N(x)}{x-x_i}$ has an avoidable singularity in $x = x_i$, and it is a polynomial of grad $N-1$ in the hole complex plane except this singularity. Even when the basis functions are changed just in the point of this avoidable singularity all of them become analytical, this singularity can lead to computational problems in its neighbourhood, which can slow considerably the calculations and even crush them. To avoid this singularity we expand the Laguerre polynomials in its Taylor series centered in it as follows:

$$\mathrm{L}_N(x) \;=\; \sum_{j=0}^{N} \frac{1}{j!}\, \left.\frac{\mathrm{d}^j \mathrm{L}_N(x)}{\mathrm{d}x^j}\right|_{x=x_i} (x \,-\, x_i)^j\,. \tag{3.19}$$

As x_i is by definition a zero of the Laguerre polynomial, the zero order term of 3.19 cancels, we also use the derivative property of the Laguerre polynomials

$$\frac{\mathrm{d}^j}{\mathrm{d}x^j} \mathrm{L}_N^{\alpha}(x) \;=\; (-1)^j\, \mathrm{L}_{N-j}^{\alpha+j}(x)\,. \tag{3.20}$$

We define the Laguerre-mesh polynomials Λ_{Ni} as

$$\Lambda_{Ni}(x) \;=\; (-1)^i \sqrt{x_i}\, \frac{\mathrm{L}_N(x)}{x \,-\, x_i}\,, \tag{3.21}$$

and introducing 3.19 and 3.20 in 3.21 we get a closed expression for $\Lambda_{Ni}(x)$ as follows:

$$\Lambda_{Ni}(x) \;=\; (-1)^i \sqrt{x_i} \sum_{j=0}^{N-1} \frac{(-1)^{j+1}}{(j+1)!}\, \mathrm{L}_{N-j-1}^{j+1}(x_i)\, (x - x_i)^j\,. \tag{3.22}$$

Comparing with the property 3.16 we obtain the value of the weights λ_i as

$$\lambda_i \;=\; \frac{\mathrm{e}^{x_i}}{x_i\, (\mathrm{L}_{N-1}^1(x_i))^2}\,, \tag{3.23}$$

and the property 3.17 can be proved through the properties of the Laguerre generalised polynomials, in the interval $(a, b) \equiv (0, +\infty)$ of the real line.

For calculations, it is useful to know the expressions of the first and second derivatives of $\Lambda_{Ni}(x)$ too, which can be easily calculated from expansion 3.22:

$$\begin{aligned}\Lambda'_{Ni}(x) &= (-1)^{i+1}\,\sqrt{x_i}\left[\frac{\mathrm{L}^1_{N-1}(x)}{x\,-\,x_i}\,+\,\frac{\mathrm{L}_N(x)}{(x\,-\,x_i)^2}\right]\\ &= (-1)^i\,\sqrt{x_i}\sum_{j=0}^{N-2}\frac{(-1)^j\,(j+1)}{(j+2)!}\,\mathrm{L}^{j+2}_{N-j-2}(x_i)\,(x-x_i)^j\,,\end{aligned}\tag{3.24}$$

$$\begin{aligned}\Lambda''_{Ni}(x) &= (-1)^i\,\sqrt{x_i}\left[\frac{\mathrm{L}^2_{N-2}(x)}{x\,-\,x_i}\,+\,2\,\frac{\mathrm{L}^1_{N-1}(x)}{(x\,-\,x_i)^2}\,+\,2\,\frac{\mathrm{L}_N(x)}{(x\,-\,x_i)^3}\right]\\ &= (-1)^i\,\sqrt{x_i}\sum_{j=0}^{N-3}\frac{(-1)^{j+1}\,(j+1)\,(j+2)}{(j+3)!}\,\mathrm{L}^{j+3}_{N-j-3}(x_i)\,(x-x_i)^j\,,\end{aligned}\tag{3.25}$$

so the kinetic term of 3.13 is expressed as

$$\mathcal{T}_{kk'} = \int_0^\infty \mathrm{d}x\,x^{|m|}\,\mathrm{e}^{-x}\,\Lambda_{Nk}(x)\left[x\,\Lambda''_{Nk'}(x)\,+\,(|m|\,+\,1\,-\,x)\,\Lambda'_{Nk'}(x)\,+\,\left(\frac{1}{4}x\,-\,\frac{1}{2}|m|\,-\,\frac{1}{2}\right)\Lambda_{Nk'}(x)\right],\tag{3.26}$$

and the others

$$\begin{aligned}\mathcal{I}_{kk'} &= \int_0^\infty \mathrm{d}x\,x^{|m|}\,\mathrm{e}^{-x}\,\Lambda_{Nk}(x)\,\Lambda_{Nk'}(x)\\ \mathcal{F}_{kk'} &= \int_0^\infty \mathrm{d}x\,x^{|m|+2}\,\mathrm{e}^{-x}\,\Lambda_{Nk}(x)\,\Lambda_{Nk'}(x)\\ \mathcal{S}_{kk'} &= \int_0^\infty \mathrm{d}x\,x^{|m|+1}\,\mathrm{e}^{-x}\,\Lambda_{Nk}(x)\,\Lambda_{Nk'}(x)\end{aligned}\tag{3.27}$$

To calculate the matrix elements it is necessary to get the roots of the Laguerre polynomials as accurate as possible, to do that we took advantage of the property of the roots of the Laguerre polynomials, that all of them are real, positive and of multiplicity one. We made a search on the positive real line starting at zero and increasing the step in 10^{-3} units, when we found two points x_1 and x_2 such as $\mathrm{L}(x_1)\mathrm{L}(x_2) < 0$ then we have a root in between, then we applied a bisection method with precision 10^{-12} and obtained the root. To evaluate the Laguerre polynomial we used the recursive formula

$$\begin{aligned}\mathrm{L}_0(x) &= 1\\ \mathrm{L}_1(x) &= 1\,-\,x\\ N\,\mathrm{L}_N(x) &= (2N\,-\,1\,-\,x)\,\mathrm{L}_{N-1}(x)\,-\,(N\,-\,1)\,\mathrm{L}_{N-2}(x)\,.\end{aligned}\tag{3.28}$$

The calculated roots of the Laguerre polynomials are shown in appendix B.

Now we will check the stability of the calculation respect the accuracy of the roots of the Laguerre polynomials, for that goal we make an error analysis of expression 3.21 of Laguerre-mesh polynomials

$$\delta\Lambda_{Ni} = \left(\sqrt{x_i}\,\frac{|\mathrm{L}_N|}{(x\,-\,x_i)^2}\,+\,\frac{1}{2\,\sqrt{x_i}}\left|\frac{\mathrm{L}_N}{x\,-\,x_i}\right|\right)\delta x_i\,,\tag{3.29}$$

and the expression 3.22 of its Taylor expansion

$$\delta\Lambda_{Ni} = \left(\sqrt{x_i}\sum_{j=0}^{N-2}\frac{(j+1)}{(j+2)!}\,|\mathrm{L}^{j+2}_{N-j-2}(x_i)|\,|x-x_i|^j\,+\,\frac{1}{2\,\sqrt{x_i}}\sum_{j=0}^{N-1}\frac{1}{(j+1)!}\,|\mathrm{L}^{j+1}_{N-j-1}(x_i)|\,|x-x_i|^j\right)\delta x_i\,.\tag{3.30}$$

The error in direct expression 3.21 is proportional to the relation $\frac{1}{(x-x_i)^2}$, so it is large in the neighbourhood of the singularity, and even diverge on it. On the other hand, the error of the Taylor expansion 3.22 is proportional to a power of $(x - x_i)$, it tends to constant in the neighbourhood of the singularity and it blows up as x spreads of it. So we have two complementary regions and to optimise the calculation we choose for the evaluation of the Laguerre-mesh polynomials the direct expression 3.21 in the region far of the singularity $x < x_{i-1}$; $x > x_{i+1}$, and the Taylor expansion 3.22 in its neighbourhood $x_{i-1} \le x \le x_{i+1}$, for the extremes we take as $x_0 = 0$ and $x_{N+1} = 2x_N - x_{N-1}$. For the expressions of the derivatives the argument is equivalent.

3.2 Implementation

The implementation of the complex coordinate rotation method to get the states of the Stark hydrogen atom is spread in two steps: the calculation of the integrals 3.26 and 3.27 and the diagonalisation of the Hamiltonian matrix 3.11.

In the first step we calculate the ground $N \times N$ matrices of the integrals $\mathcal{T}_{kk'}$, $\mathcal{I}_{kk'}$, $\mathcal{F}_{kk'}$ and $\mathcal{S}_{kk'}$ for each value of the magnetic quantum number m, and they are now usable for any value of the field intensity F and the complex rotation angle ϑ, so this step takes a few computation time in comparison with the diagonalisation. In that sense it is valuable to increase the quality of the calculation of the integrals even at a cost of increasing the computation time, so we did not use the Gauss quadrature formula, but a complete numerical integration for each element, using a variable step Simpson formula. This is made by the routine *starkinteg*, it calculates the four ground matrices and stores them in a binary file, prepared to be read by the next routine.

In a second step we build the Hamiltonian and overlap matrices and solve the secular equation to get the eigenvalues and eigenfunctions. This is made by the routine *starkccr*.

Firstly the matrixes $H_{klk'l'}$ and $S_{klk'l'}$ of dimension $N^2 \times N^2$ are built making the tensorial products 3.11 and 3.12 respectively, for a fixed value of the field intensity F and the rotation angle ϑ. Afterwards it is solved the diagonalisation using the computing library Linear Algebra PACKage (LAPACK), we chose the subroutine for solving a secular equation of a general non-Hermitian double precision complex matrix *zggev*.

We solved the eigenvalue problem varying the electric field intensity F from zero to 0.01 a.u. = 5.142×10^9 V/m and for each one the complex rotation angle ϑ between zero and 40^0.

The obtained results are stored as ascii format in a data file called *arch305.dat*. It contains energies, widths and expansion coefficients of the wave functions for each calculated value of the field intensity and for all the resonances. This file will be the starting point of the routine *ADAS305*, which will simulate the MSE spectra making a full collision radiative model of the atoms in the beam.

Chapter 4

Results

We used a basis set of Laguerre-mesh polynomials with $N = 30$, which corresponds to 900 basis functions, thereby obtained acceptably accurate results for all the resonances with principal quantum number $n \leq 5$ and for the values of the magnetic quantum number $m = 0 - 4$. We calculated twenty five values of the field intensity from zero to 0.01 a.u., which corresponds to $5.142 \cdot 10^9$ V/m. The resonances above $n \geq 6$ are strongly mixed with the continuum. To isolate these ones, the basis set should be increased.

We stored all the data in an ascii data file *arch305.dat* of size 33 Mb.

4.1 Energies and state widths for the Stark Hydrogen Atom

Applying the complex coordinate method one has to change the value of the complex rotation angle ϑ in order to distinguish the resonances of the continuum states sea. In figures 4.1 and 4.2 it is showed respectively the real and imaginary part of the obtained roots versus the complex rotation angle, then the behaviour of the roots is appreciated. Most states change their value with the angle, they can be recognised as continuum states, but there are some of them which remain constant since a value of the angle, in terms of the complex coordinate rotation theorem, these states are identified as the resonances. The constant values, when the lines become flat, are related to the energy (real part) and width (imaginary part) of the resonance. Also for these constant values, the wave function of the resonance becomes invariant but phase and square integrable.

Identifying the resonances as in figures 4.1, 4.2 for several values of F and m we get the diagram of energies and widths. In Fig 4.3 we show the identified energies for the shells $n = 2 - 5$ of the hydrogen atom under a constant electric field versus the field intensity. The behaviour for the upper shells $n = 3 - 5$ deviate from the linearity predicted by perturbation theory. In Fig 4.4 the widths for the same shells are shown. The value of the widths increases quite rapidly with the field, so the states become more unstable and the autoionization term should be taken in account in collision radiative models.

4.2 Wave functions

The great advantage of complex coordinate rotation method is that we can obtain the wave functions exactly in terms of the precision of our chosen basis set. With the variational method, the wave functions of the identified states are obtained as a linear combination of the basis functions.

In figures 4.5 – 4.14 the wave functions for several states of the Stark Hydrogen Atom are shown for a value of the electric field intensity of 0.0020 a.u. as a colour map versus the two parabolic coordinates ξ and η. We can obtain

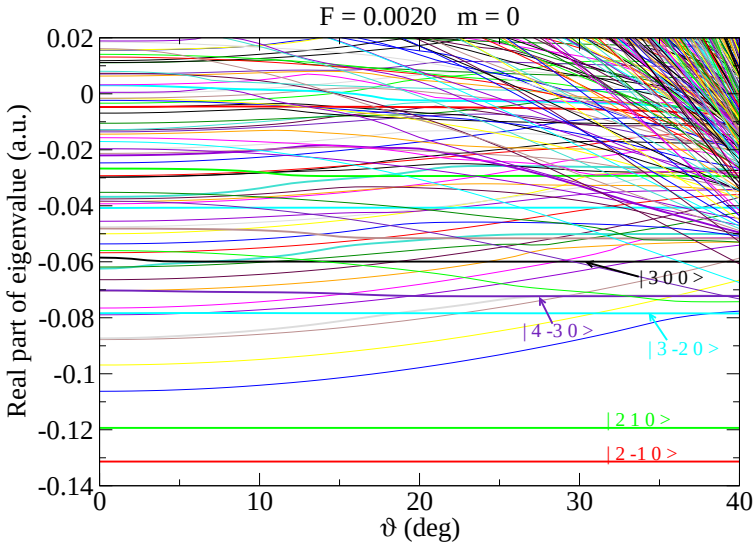

Figure 4.1: Real part of the calculated eigenvalues for the Hydrogen atom under a constant electric field versus the complex coordinate rotation angle.

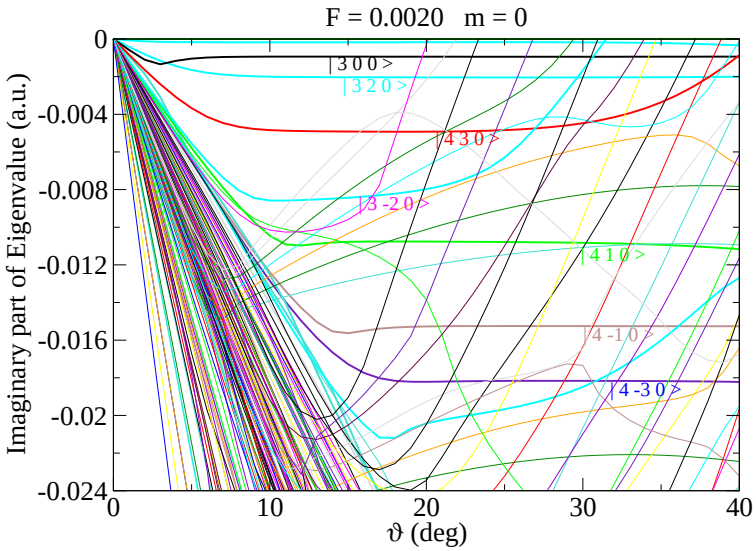

Figure 4.2: Imaginary part of the calculated eigenvalues for the Hydrogen atom under a constant electric field versus the complex coordinate rotation angle.

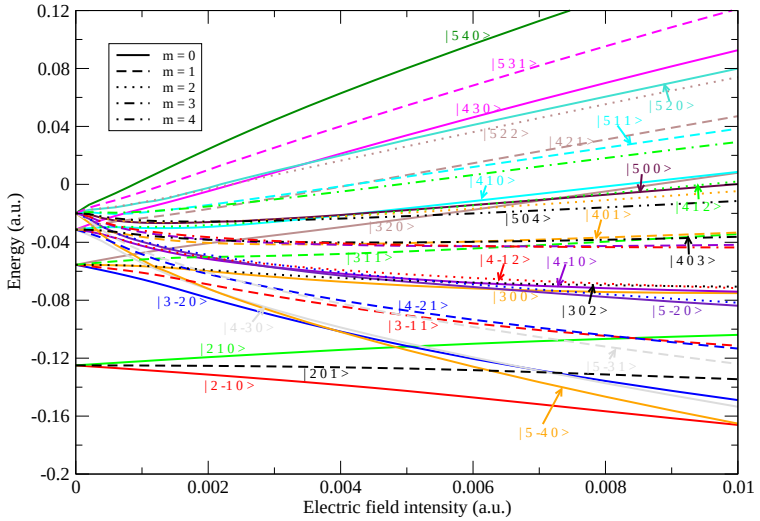

Figure 4.3: Energies of the first resonances of the Hydrogen atom under a constant electric field versus the intensity of such field.

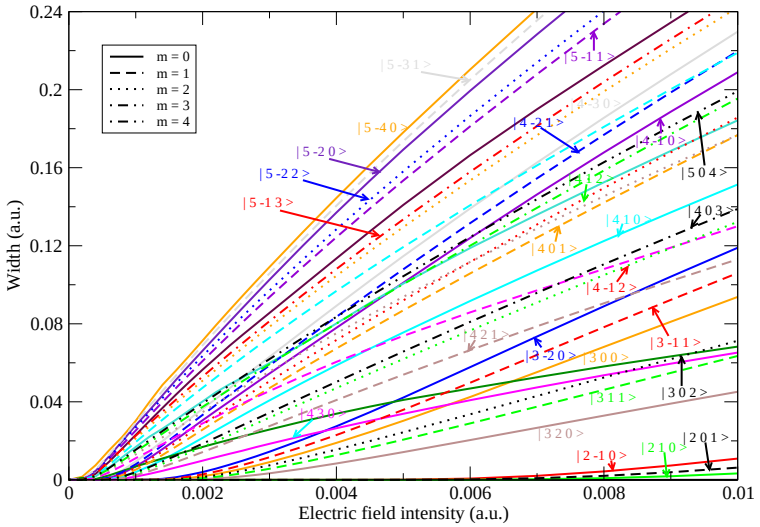

Figure 4.4: State widths of the first resonances of the Hydrogen atom under a constant electric field versus the intensity of such field.

partially integrated wave functions through the integration of them in one of the parabolic variables

$$\begin{aligned} \psi_\xi(\xi) &= \int_0^\infty \mathrm{d}\eta\, \psi(\xi,\eta) \\ \psi_\eta(\eta) &= \int_0^\infty \mathrm{d}\xi\, \psi(\xi,\eta)\,, \end{aligned} \tag{4.1}$$

If we compare the result with the zero field case 2.9, then we can relation the approximated quantum numbers $\tilde{n}_1$, $\tilde{n}_2$ with the minimum of the module of the partially integrated wave functions, which will tend to a node in the limit when the field intensity tends to zero. These wave functions contain the whole information about the system.

A surprising result is that for a constant value of n, the energies increase as k increases, but the widths decrease, so in the same shell states with a higher energy and closer to the ionization limit live longer before ionizing. That can be explained from examination of the wave functions.

Comparing the wave functions for the states $|\,\tilde{n}\,\tilde{k}\,m\rangle$ and $|\,\tilde{n}\;-\tilde{k}\,m\rangle$ we observe that for negative $\tilde{k}$ the partially integrated $|\psi_\eta|^2$ function encloses a larger area beneath it than the other one $|\psi_\xi|^2$. In addition almost the whole probability lies close to $\xi = 0$, so in the case of $\tilde{k} < 0$ the wave function lies on the η axis and $\xi \approx 0$, which corresponds to the negative z semiaxis. In our case $F > 0$, the potential barrier is placed on the negative z axis side with a monotonic increase in the positive z direction. So the main part of the probability lies above the potential barrier for $\tilde{k} < 0$ such that the probability to tunnel through it will be higher. Therefore the widths increase. Just the opposite holds for $\tilde{k} > 0$. In this case the highest probability concentration is in the region $\eta \approx 0$, $\xi > 0$, which corresponds to the positive z semiaxis. Thus with the potential monotonic slope, the main probability for finding the electron is where the potential barrier is wide and the probability to tunnel is much lower. To understand the behaviour of the state widths, it is clear that one has to look not only the energies, but also at the wave functions of the states.

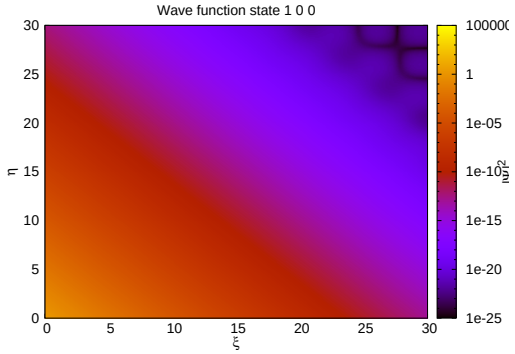

(a) $|\psi_{100}|^2(\xi,\eta)$

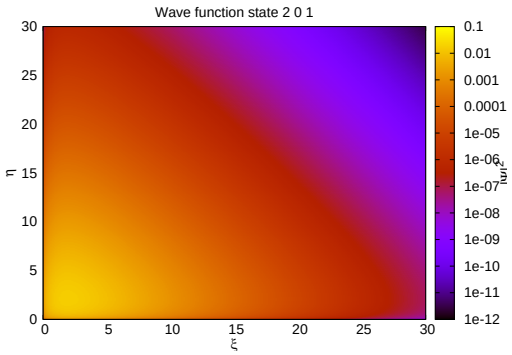

(d) $|\psi_{201}|^2(\xi,\eta)$

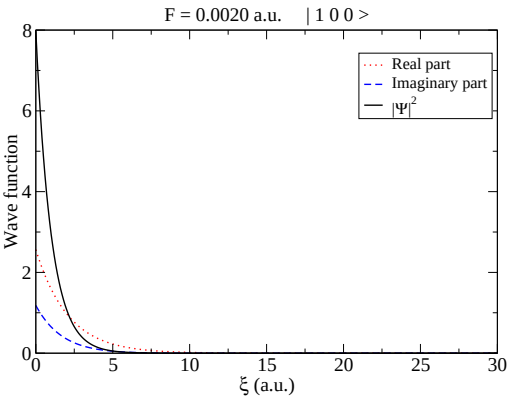

(b) $\psi_{\xi 100}(\xi)$

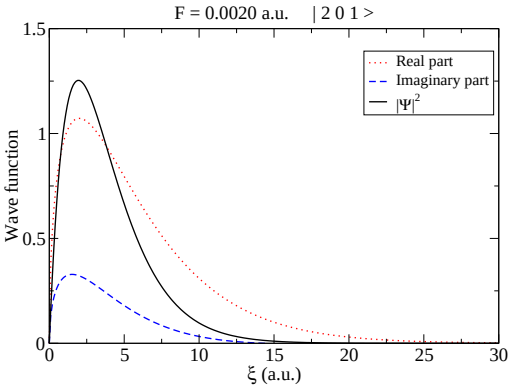

(e) $\psi_{\xi 201}(\xi)$

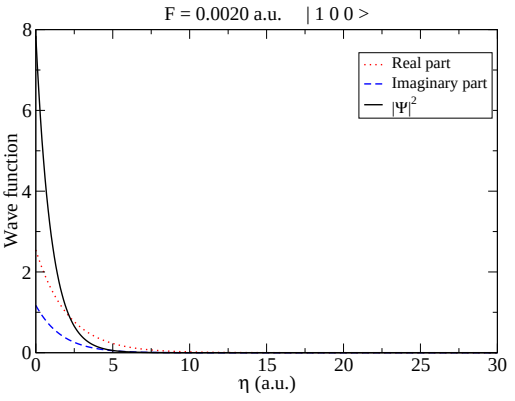

(c) $\psi_{\eta 100}(\eta)$

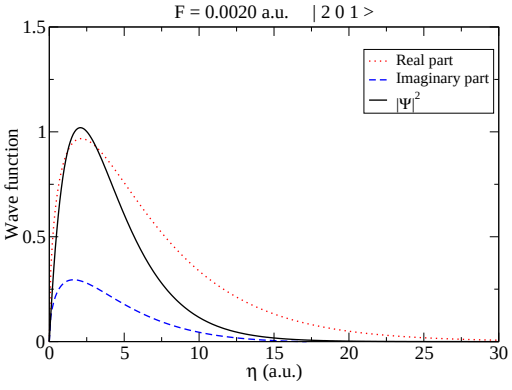

(f) $\psi_{\eta 201}(\eta)$

Figure 4.5: Wave function of the Stark states $|1\,0\,0\rangle$ and $|2\,0\,1\rangle$ for a field intensity of $F = 0.0020$ a.u..

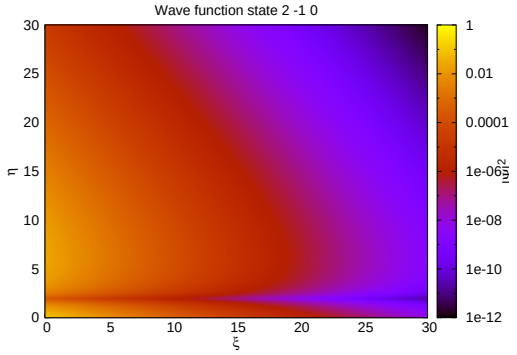

(a) $|\psi_{2-10}|^2(\xi,\eta)$

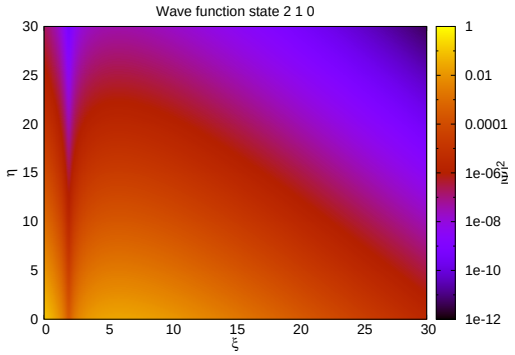

(d) $|\psi_{210}|^2(\xi,\eta)$

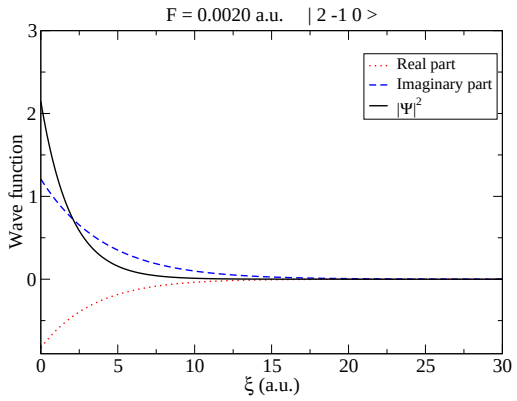

(b) $\psi_{\xi 2-10}(\xi)$

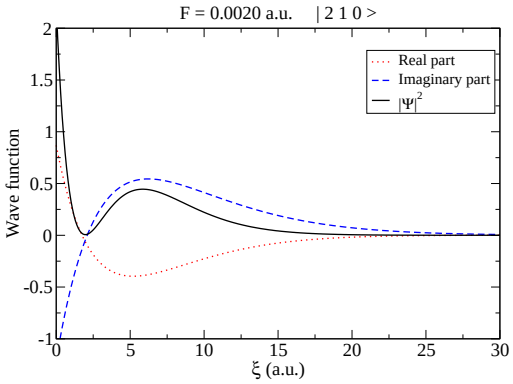

(e) $\psi_{\xi 210}(\xi)$

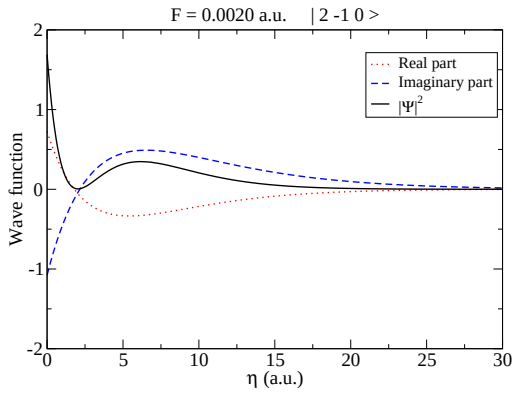

(c) $\psi_{\eta 2-10}(\eta)$

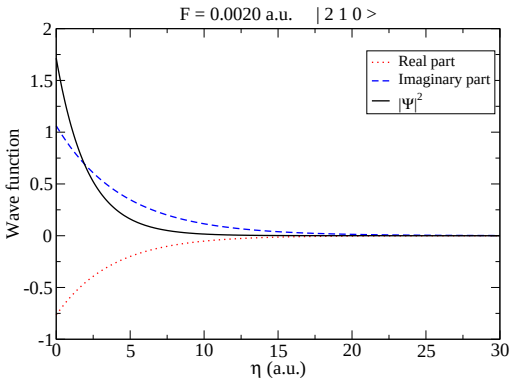

(f) $\psi_{\eta 210}(\eta)$

Figure 4.6: Wave function of the Stark states $|\,2\ -1\,0\,\rangle$ and $|\,2\,1\,0\,\rangle$ for a field intensity of $F = 0.0020$ a.u..

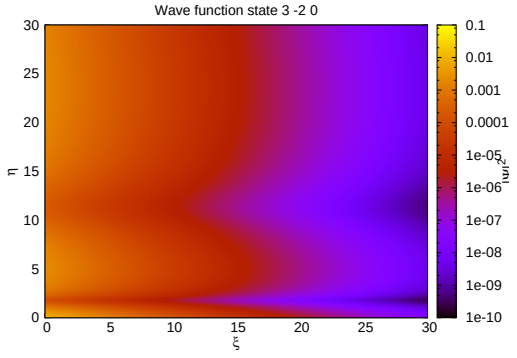

(a) $|\psi_{3-20}|^2(\xi,\eta)$

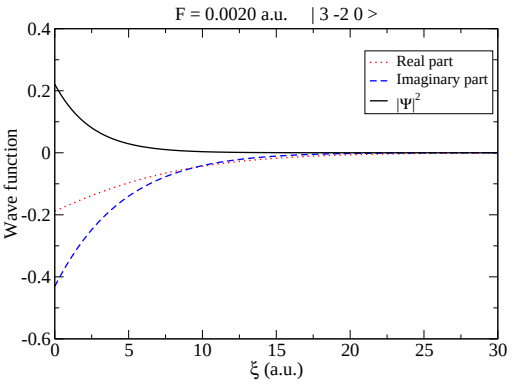

(b) $\psi_{\xi 3-20}(\xi)$

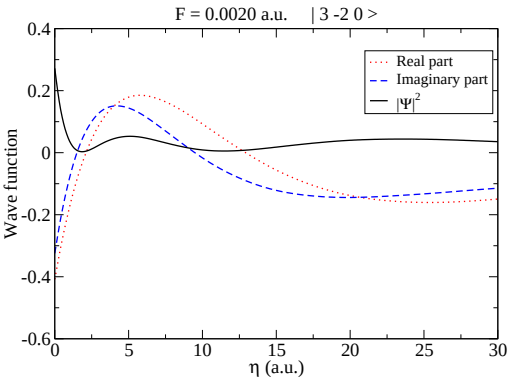

(c) $\psi_{\eta 3-20}(\eta)$

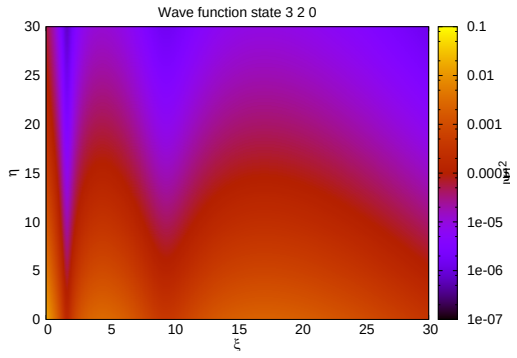

(d) $|\psi_{320}|^2(\xi,\eta)$

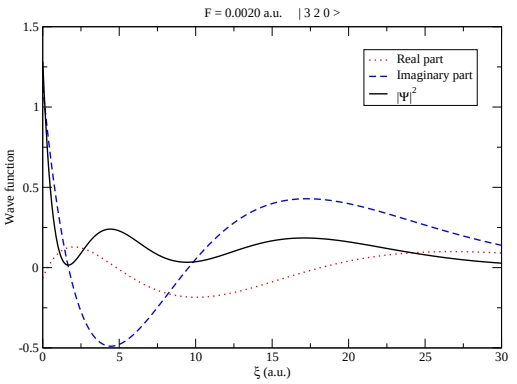

(e) $\psi_{\xi 320}(\xi)$

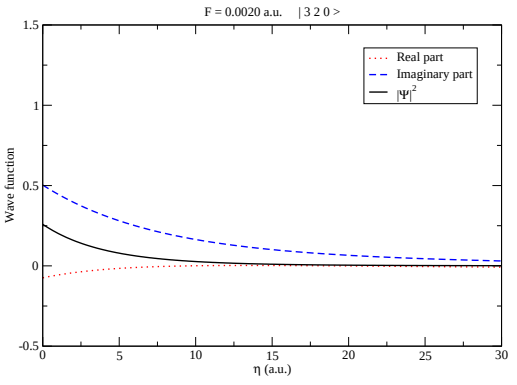

(f) $\psi_{\eta 320}(\eta)$

Figure 4.7: Wave function of the Stark states $|3\ -2\ 0\rangle$ and $|3\ 2\ 0\rangle$ for a field intensity of $F = 0.0020$ a.u..

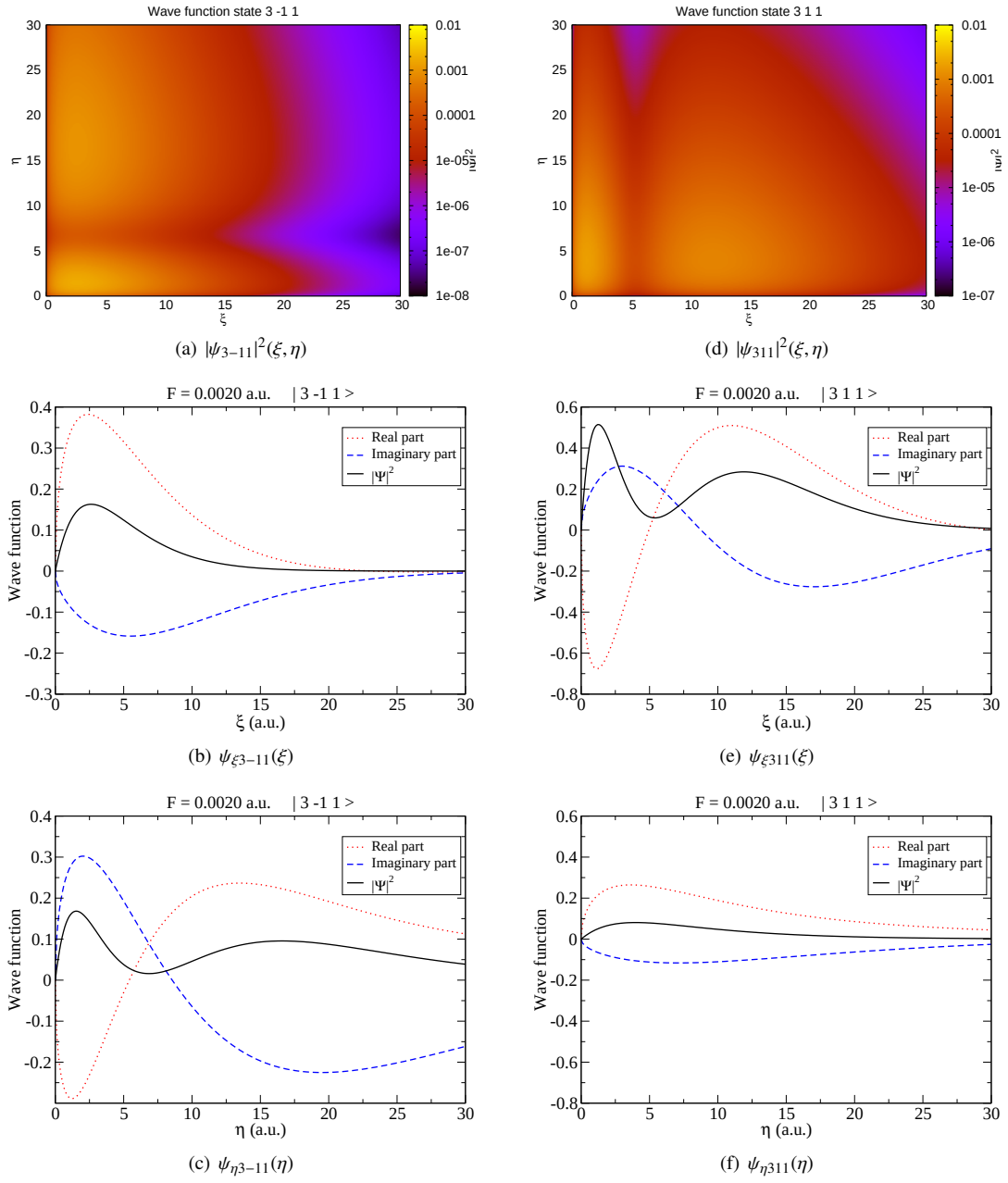

(a) $|\psi_{3-11}|^2(\xi,\eta)$ (d) $|\psi_{311}|^2(\xi,\eta)$

(b) $\psi_{\xi 3-11}(\xi)$ (e) $\psi_{\xi 311}(\xi)$

(c) $\psi_{\eta 3-11}(\eta)$ (f) $\psi_{\eta 311}(\eta)$

Figure 4.8: Wave function of the Stark states $|\,3\ -1\ 1\,\rangle$ and $|\,3\ 1\ 1\,\rangle$ for a field intensity of $F = 0.0020$ a.u..

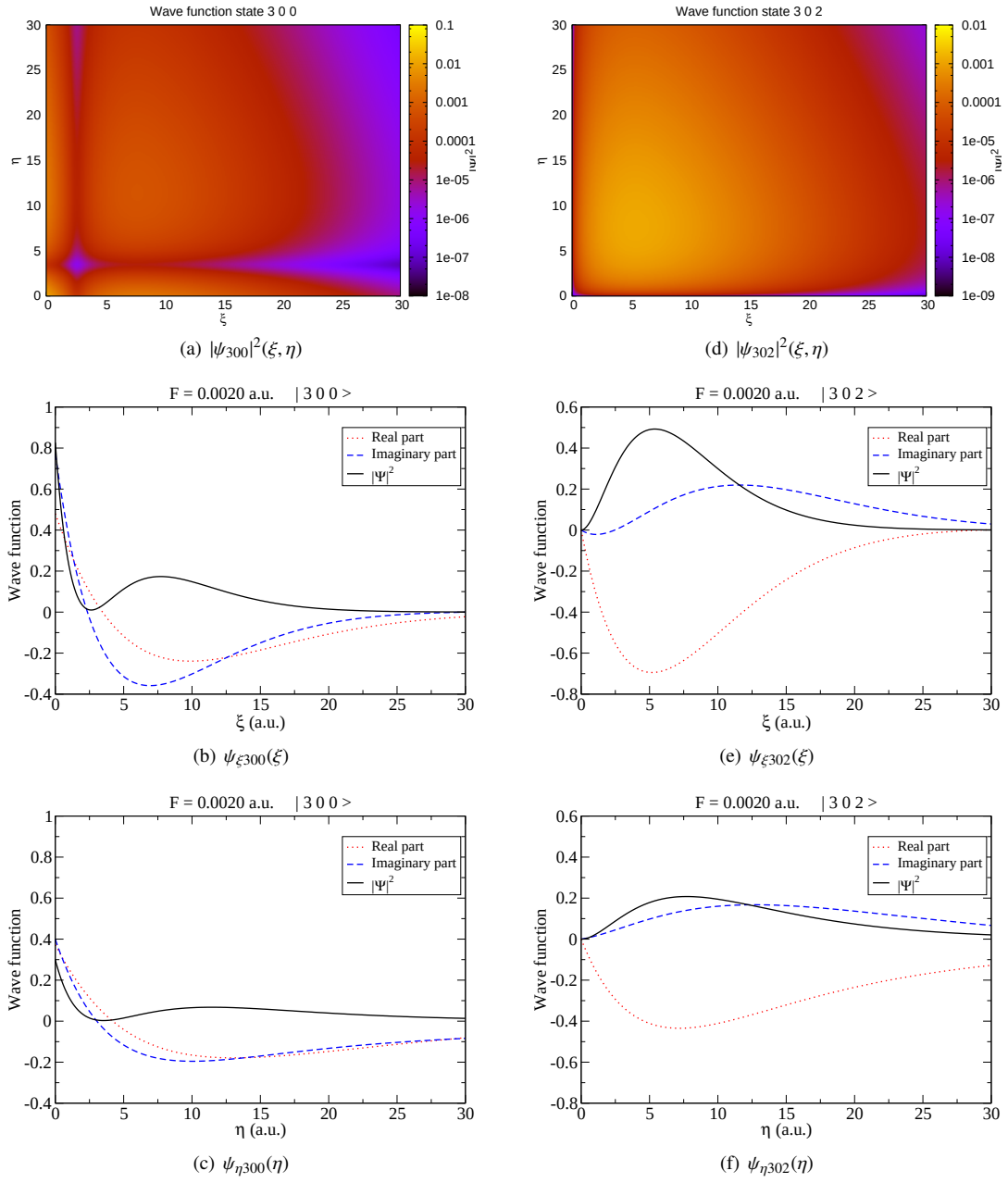

(a) $|\psi_{300}|^2(\xi,\eta)$ (d) $|\psi_{302}|^2(\xi,\eta)$

(b) $\psi_{\xi 300}(\xi)$ (e) $\psi_{\xi 302}(\xi)$

(c) $\psi_{\eta 300}(\eta)$ (f) $\psi_{\eta 302}(\eta)$

Figure 4.9: Wave function of the Stark states $|\,3\,0\,0\,\rangle$ and $|\,3\,0\,2\,\rangle$ for a field intensity of $F = 0.0020$ a.u..

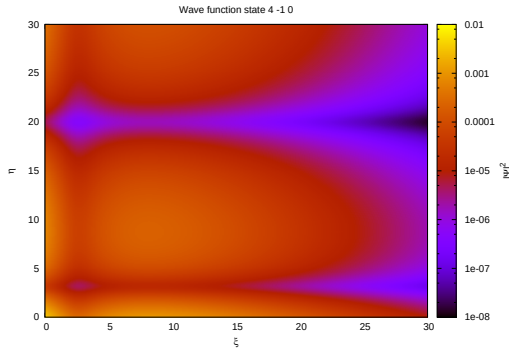

(a) $|\psi_{4-10}|^2(\xi,\eta)$

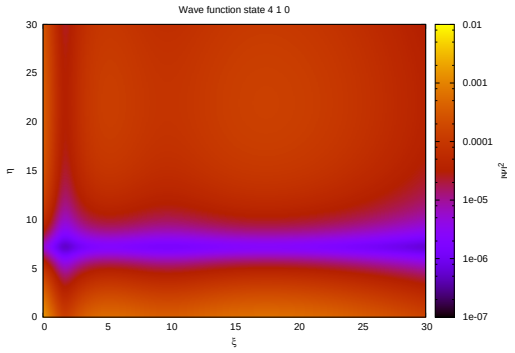

(d) $|\psi_{410}|^2(\xi,\eta)$

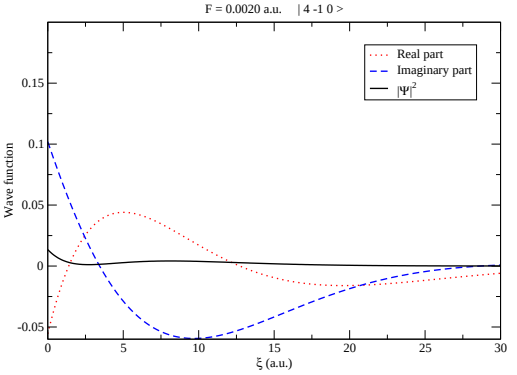

(b) $\psi_{\xi 4-10}(\xi)$

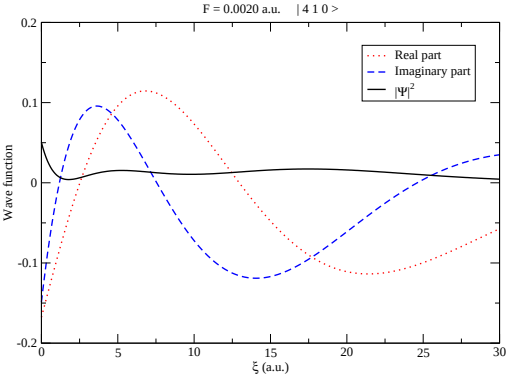

(e) $\psi_{\xi 410}(\xi)$

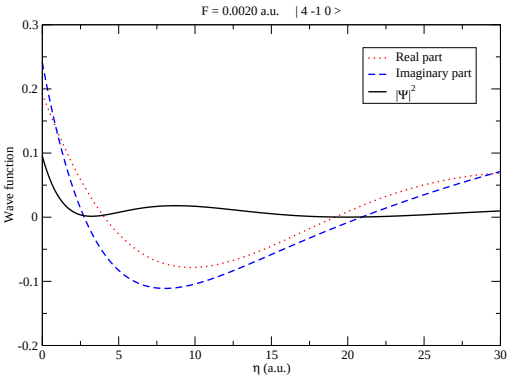

(c) $\psi_{\eta 4-10}(\eta)$

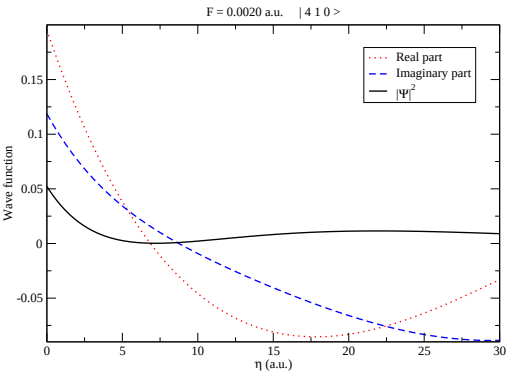

(f) $\psi_{\eta 410}(\eta)$

Figure 4.10: Wave function of the Stark states $|4\ -1\ 0\rangle$ and $|4\ 1\ 0\rangle$ for a field intensity of $F = 0.0020$ a.u..

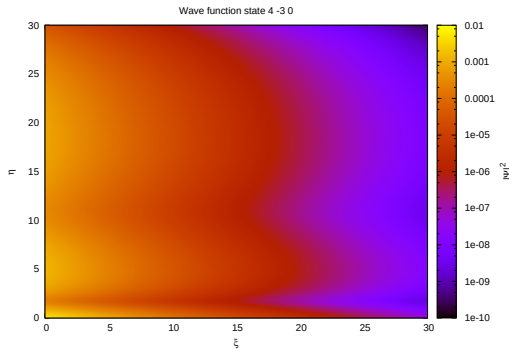

(a) $|\psi_{4-30}|^2(\xi,\eta)$

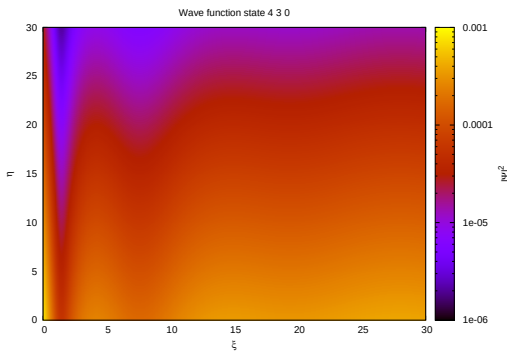

(d) $|\psi_{430}|^2(\xi,\eta)$

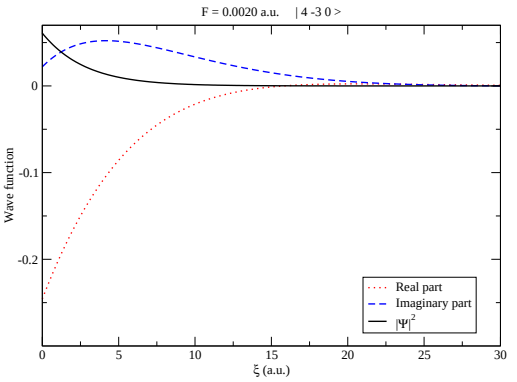

(b) $\psi_{\xi 4-30}(\xi)$

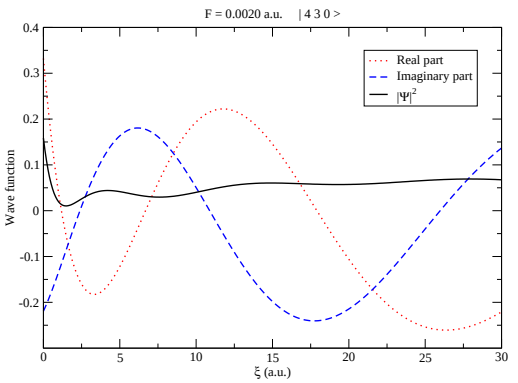

(e) $\psi_{\xi 430}(\xi)$

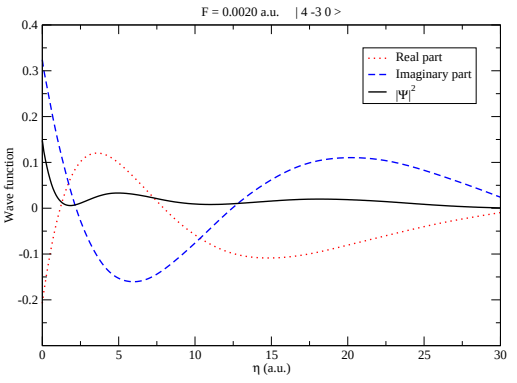

(c) $\psi_{\eta 4-30}(\eta)$

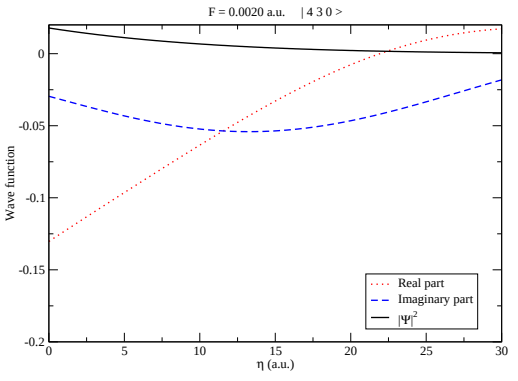

(f) $\psi_{\eta 430}(\eta)$

Figure 4.11: Wave function of the Stark states $|4\ -3\,0\rangle$ and $|4\,3\,0\rangle$ for a field intensity of $F = 0.0020$ a.u..

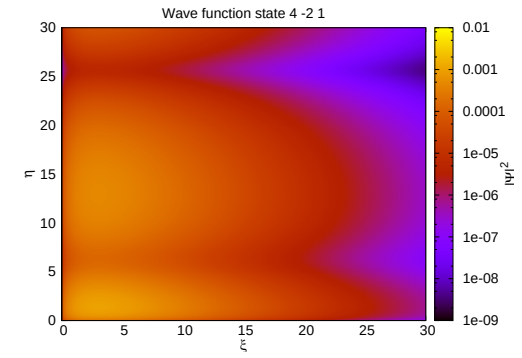

(a) $|\psi_{4-21}|^2(\xi,\eta)$

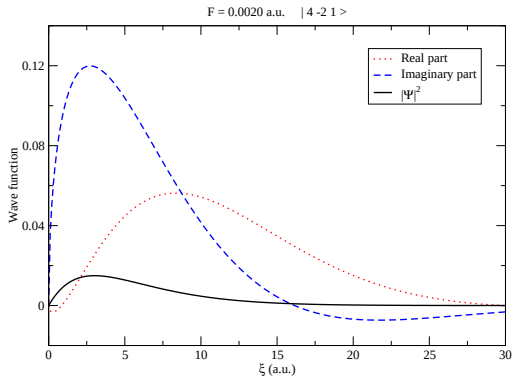

(b) $\psi_{\xi 4-21}(\xi)$

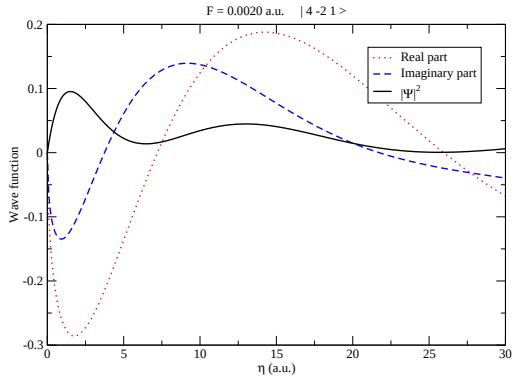

(c) $\psi_{\eta 4-21}(\eta)$

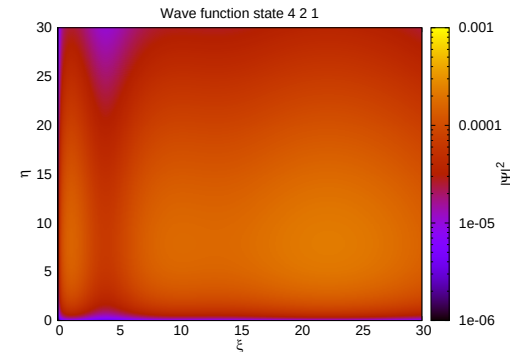

(d) $|\psi_{421}|^2(\xi,\eta)$

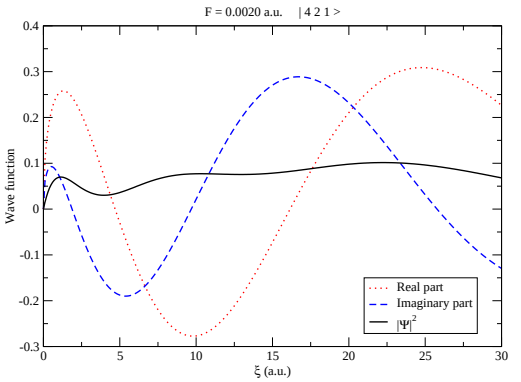

(e) $\psi_{\xi 421}(\xi)$

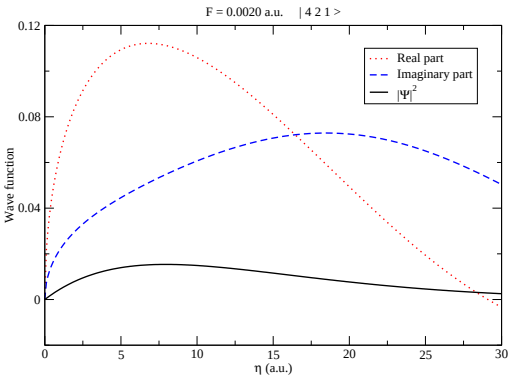

(f) $\psi_{\eta 421}(\eta)$

Figure 4.12: Wave function of the Stark states $|4\ -2\ 1\rangle$ and $|4\ 2\ 1\rangle$ for a field intensity of $F = 0.0020$ a.u..

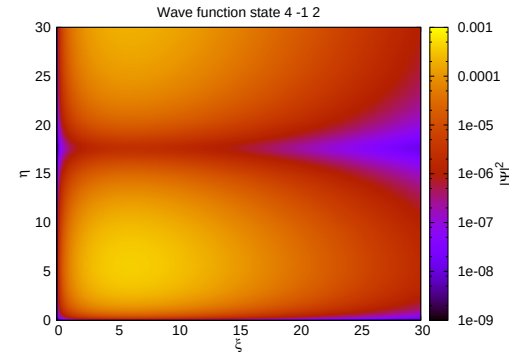

(a) $|\psi_{4-12}|^2(\xi,\eta)$

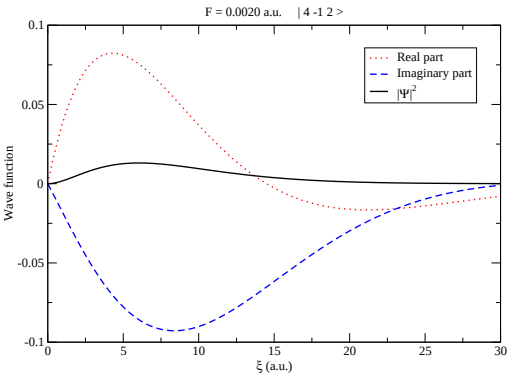

(b) $\psi_{\xi 4-12}(\xi)$

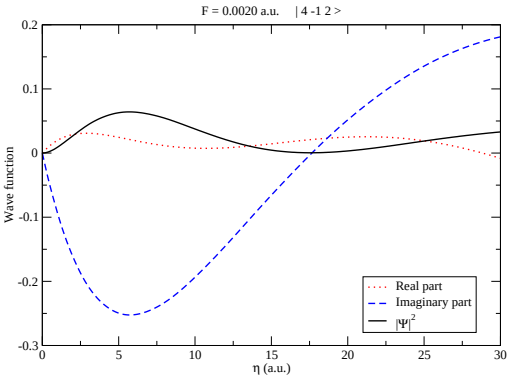

(c) $\psi_{\eta 4-12}(\eta)$

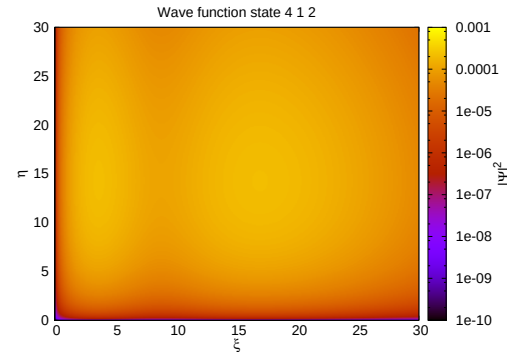

(d) $|\psi_{412}|^2(\xi,\eta)$

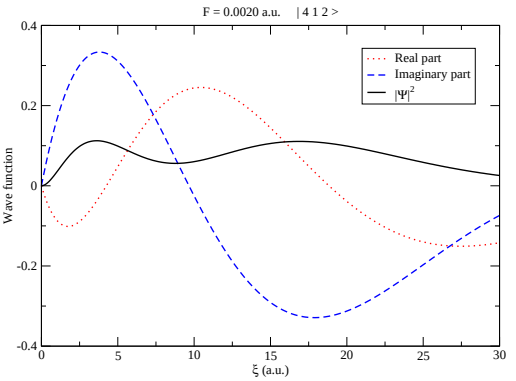

(e) $\psi_{\xi 412}(\xi)$

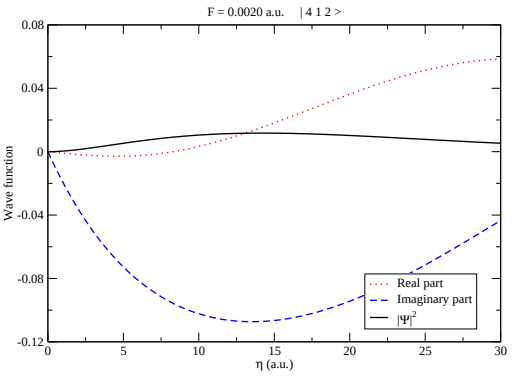

(f) $\psi_{\eta 412}(\eta)$

Figure 4.13: Wave function of the Stark states $|4\ -1\ 2\rangle$ and $|4\ 1\ 2\rangle$ for a field intensity of $F = 0.0020$ a.u..

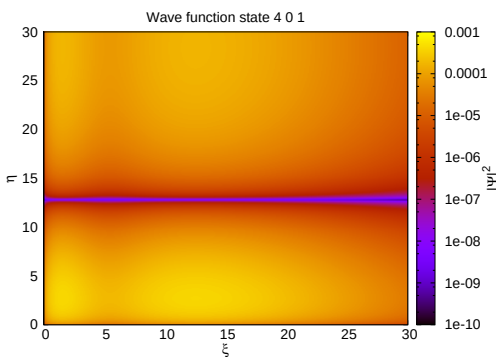

(a) $|\psi_{401}|^2(\xi,\eta)$

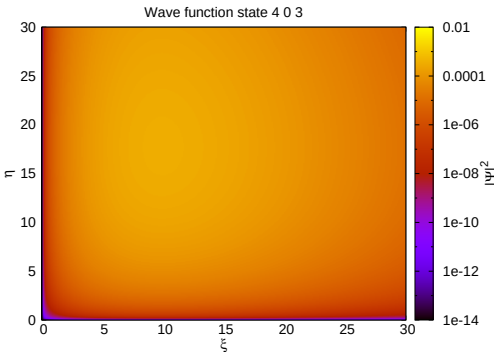

(d) $|\psi_{403}|^2(\xi,\eta)$

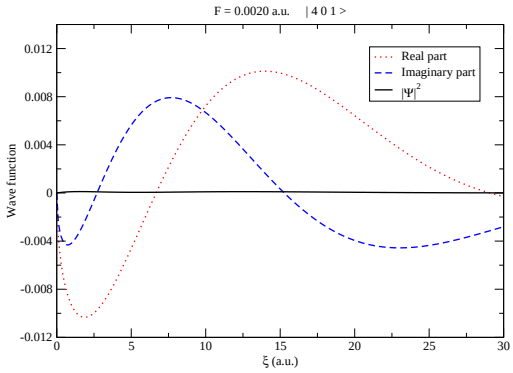

(b) $\psi_{\xi 401}(\xi)$

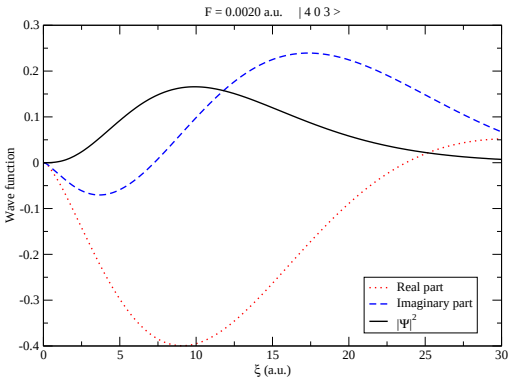

(e) $\psi_{\xi 403}(\xi)$

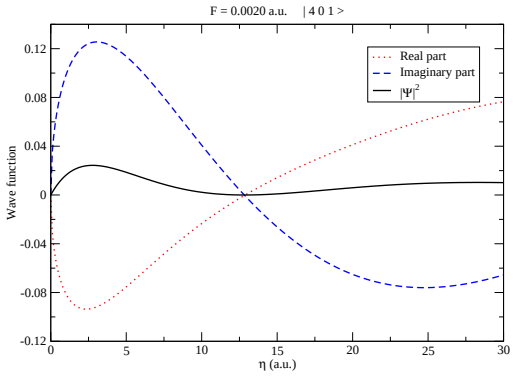

(c) $\psi_{\eta 401}(\eta)$

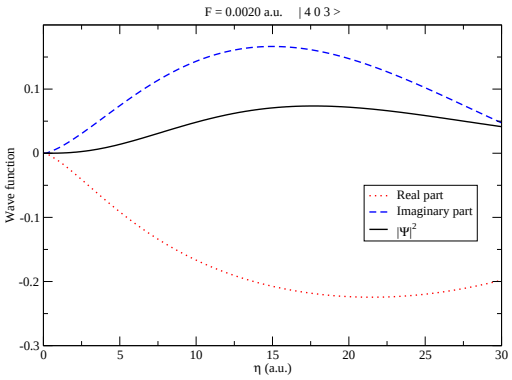

(f) $\psi_{\eta 403}(\eta)$

Figure 4.14: Wave function of the Stark states $|\,4\,0\,1\,\rangle$ and $|\,4\,0\,3\,\rangle$ for a field intensity of $F = 0.0020$ a.u..

Chapter 5

Derived quantities

The wave functions contain all the information about the system, we can obtain any physical observable from them just making the bracket.

In the following sections we explain how to get these physical observables, which will be useful tools for practical applications, as plasma diagnostic.

5.1 Isotopic correction

For the calculation of the shown energies, widths and wave functions we used the Hamiltonian 3.4, where in the kinetic term appears the electron mass as the unit. If we want to calculate the exact Stark splitting of the hydrogen spectral lines we have to consider the isotopes, so we can determine for example the difference of the Stark structure of lines H_α, D_α or T_α.

We calculate the energy difference for the individual isotopes as

$$E_\mu = \frac{1}{\mu} E_1 + \left(1 - \frac{1}{\mu}\right) \left\langle \psi \left| -\frac{e^{-i\vartheta}}{r} + e^{i\vartheta} F z \right| \psi \right\rangle , \tag{5.1}$$

where E_μ are the obtained energies for reduced mass μ. Introducing in 5.1 the expression of the matrix elements we get

$$\left\langle \psi \left| -\frac{e^{-i\vartheta}}{r} + e^{i\vartheta} F z \right| \psi \right\rangle = \int_0^\infty d\xi \int_0^\infty d\eta \, \psi^* \left(-\frac{e^{-i\vartheta}}{2} + \frac{e^{i\vartheta}}{8} F (\xi^2 - \eta^2) \right) \psi , \tag{5.2}$$

and using the expansion of ψ in its basis set

$$\begin{aligned} \left\langle \psi \left| -\frac{e^{-i\vartheta}}{r} + e^{i\vartheta} F z \right| \psi \right\rangle = & \sum_{i_1, j_1 = 1}^{N} \sum_{i_2, j_2 = 1}^{N} c^*_{i_1 j_1 m} \, c_{i_2 j_2 m} \left[-\frac{e^{-i\vartheta}}{2} \mathcal{I}_{i_1 i_2} \mathcal{I}_{j_1 j_2} \right. \\ & \left. + \frac{e^{i\vartheta}}{8} F \left(\mathcal{F}_{i_1 i_2} \mathcal{I}_{j_1 j_2} - \mathcal{I}_{i_1 i_2} \mathcal{F}_{j_1 j_2} \right) \right] . \end{aligned} \tag{5.3}$$

In figures 5.1, 5.2 and 5.3 we show the isotopic corrections for the energies and widths of the different isotopes of hydrogen for the levels of $n \leq 3$. The transitions between these levels will form the Balmer α line. The correction is smaller as the mass of the nucleus increases.

Adding these corrections to the energy we can calculate the exact splitting of the Balmer H_α and D_α lines, which are important for the MSE spectroscopy. These splittings are shown in figures 5.4 and 5.5. It is divided into its three component groups: σ for $\Delta m = \pm 1$, $\Delta k = 0$; π^+ for $\Delta m = 0$, $\Delta k = +1$ and π^- for $\Delta m = 0$, $\Delta k = -1$. δ and ϕ transitions are very weak in comparison and they will not be seen in a real spectrum with a background.

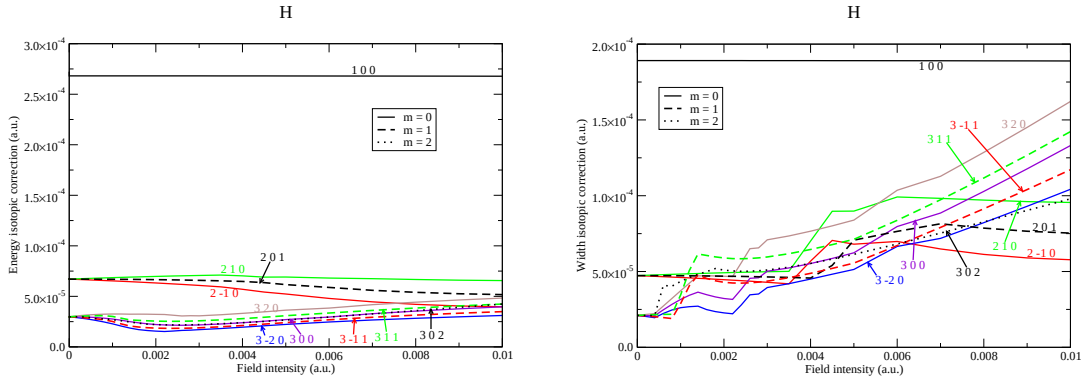

(a) Energy (b) Width

Figure 5.1: Isotopic corrections for the energies and widths of the levels $n \leq 3$ of hydrogen versus the field intensity

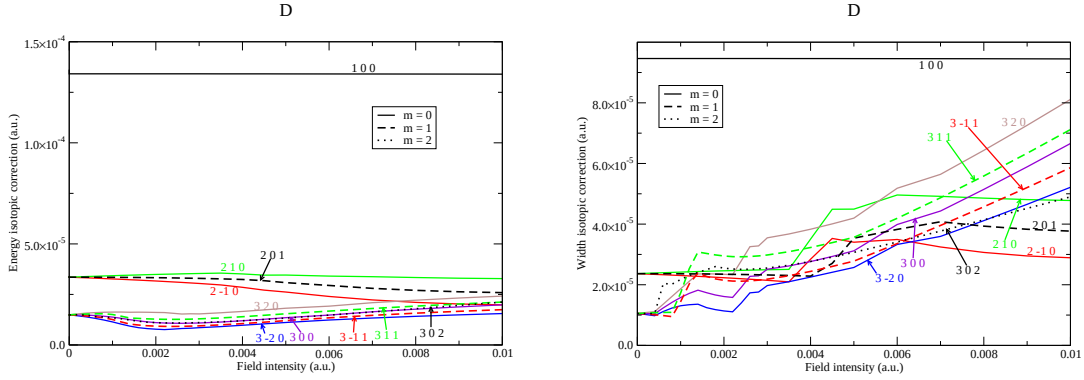

(a) Energy (b) Width

Figure 5.2: Isotopic corrections for the energies and widths of the levels $n \leq 3$ of deuterium versus the field intensity

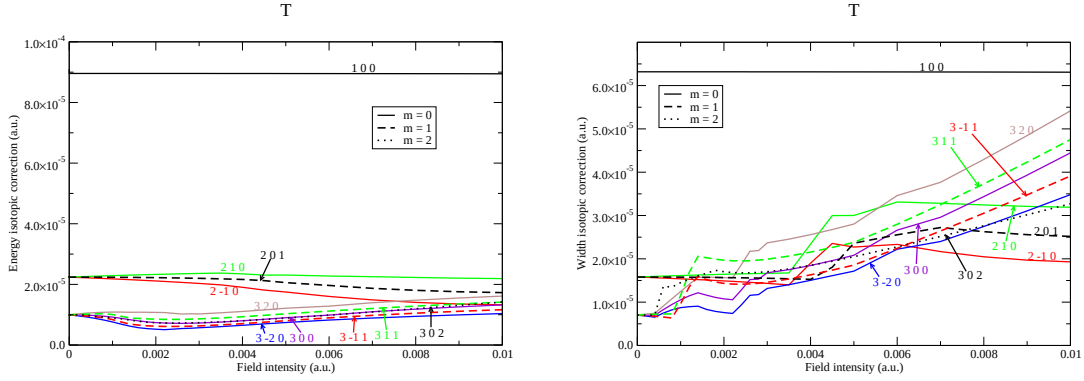

(a) Energy (b) Width

Figure 5.3: Isotopic corrections for the energies and widths of the levels $n \leq 3$ of tritium versus the field intensity

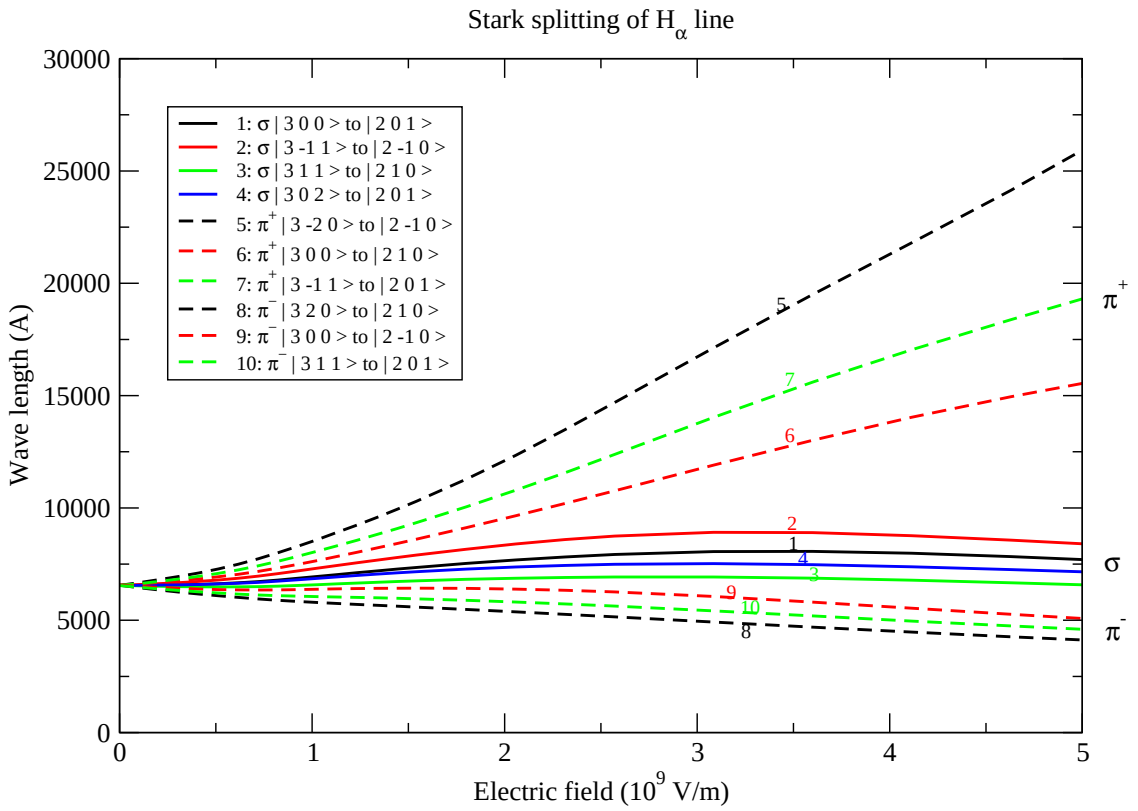

Figure 5.4: Stark splitting of the H_α line of hydrogen versus the electric field intensity.

5.2 Einstein transition coefficients

Once we get the wave functions we just have to bracket them with a physical observable to obtain its expected value. In order to calculate observables we must take in account that we rotated the coordinates in the complex plane to get the wave functions, so the physical positions and momentum must be written with the correct rotation:

$$\begin{aligned} x &\rightarrow x\,\mathrm{e}^{-i\vartheta} \\ \frac{\partial}{\partial x} &\rightarrow \frac{\partial}{\partial x}\,\mathrm{e}^{i\vartheta}\,, \end{aligned} \tag{5.4}$$

with $x = \xi, \eta$.

The first quantity we can calculate are the Einstein emission coefficients A and B, both are proportional to the modulus squared of the matrix element $|\langle\psi_1|\vec{r}|\psi_2\rangle|^2$. To calculate it we evaluate the matrix elements of each Cartesian component x, y and z as:

$$\begin{aligned} \left\langle \psi_1 \left| x\,\mathrm{e}^{-i\vartheta} \right| \psi_2 \right\rangle &= \frac{1}{2\pi}\,\mathrm{e}^{-i\vartheta} \int_0^{2\pi} \mathrm{d}\phi \int_0^{\infty} \mathrm{d}\xi \int_0^{\infty} \mathrm{d}\eta\, \frac{1}{4}\,(\xi + \eta)\,\psi_1^*(\xi,\eta)\,\mathrm{e}^{-im_1\phi}\,\sqrt{\xi\eta}\,\cos\phi\,\psi_2(\xi,\eta)\,\mathrm{e}^{im_2\phi} \\ &= \frac{1}{16\pi}\,\mathrm{e}^{-i\vartheta} \int_0^{2\pi} \mathrm{d}\phi \left(\mathrm{e}^{i(m_2-m_1+1)\phi} + \mathrm{e}^{i(m_2-m_1-1)\phi}\right) \int_0^{\infty} \mathrm{d}\xi \int_0^{\infty} \mathrm{d}\eta\,(\xi + \eta)\,\psi_1^*(\xi,\eta)\,\sqrt{\xi\eta}\,\psi_2(\xi,\eta) \\ &= \frac{1}{8}\,\mathrm{e}^{-i\vartheta}\,(\delta_{m_2 m_1 - 1} + \delta_{m_2 m_1 + 1}) \int_0^{\infty} \mathrm{d}\xi \int_0^{\infty} \mathrm{d}\eta\,\psi_1^*(\xi,\eta)\,(\xi + \eta)\,\sqrt{\xi\eta}\,\psi_2(\xi,\eta) \end{aligned} \tag{5.5}$$

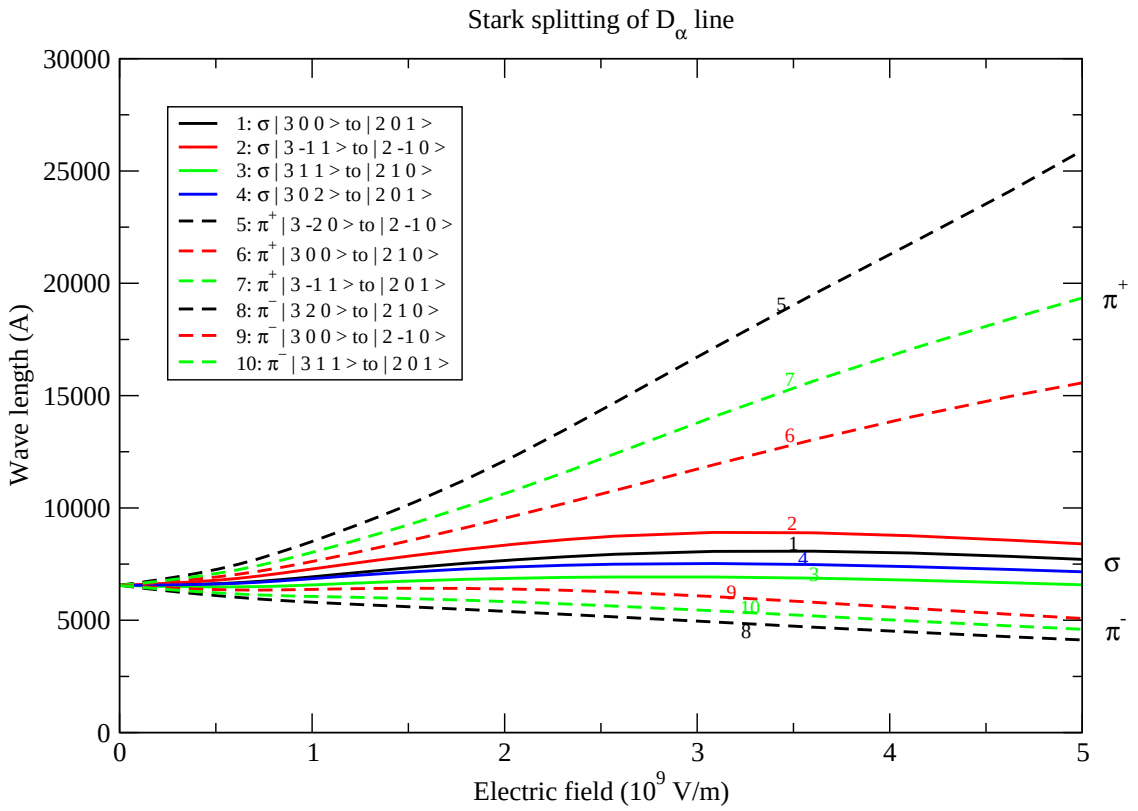

Figure 5.5: Stark splitting of the D_α line of deuterium versus the electric field intensity.

$$\begin{aligned}
\left\langle \psi_1 \left| y\, e^{-i\vartheta} \right| \psi_2 \right\rangle &= \frac{1}{2\pi} e^{-i\vartheta} \int_0^{2\pi} d\phi \int_0^\infty d\xi \int_0^\infty d\eta\, \frac{1}{4} (\xi + \eta)\, \psi_1^*(\xi,\eta)\, e^{-im_1\phi} \sqrt{\xi\eta}\, \sin\phi\, \psi_2(\xi,\eta)\, e^{im_2\phi} \\
&= \frac{1}{16\pi i} e^{-i\vartheta} \int_0^{2\pi} d\phi \left(e^{i(m_2-m_1+1)\phi} - e^{i(m_2-m_1-1)\phi} \right) \int_0^\infty d\xi \int_0^\infty d\eta\, (\xi + \eta)\, \psi_1^*(\xi,\eta)\, \sqrt{\xi\eta}\, \psi_2(\xi,\eta) \\
&= \frac{1}{8i} e^{-i\vartheta} \left(\delta_{m_2 m_1 - 1} - \delta_{m_2 m_1 + 1} \right) \int_0^\infty d\xi \int_0^\infty d\eta\, \psi_1^*(\xi,\eta)\, (\xi + \eta)\, \sqrt{\xi\eta}\, \psi_2(\xi,\eta) \qquad (5.6)
\end{aligned}$$

$$\begin{aligned}
\left\langle \psi_1 \left| z\, e^{-i\vartheta} \right| \psi_2 \right\rangle &= \frac{1}{2\pi} e^{-i\vartheta} \int_0^{2\pi} d\phi \int_0^\infty d\xi \int_0^\infty d\eta\, \frac{1}{4} (\xi + \eta)\, \psi_1^*(\xi,\eta)\, e^{-im_1\phi}\, \frac{1}{2} (\xi - \eta)\, \psi_2(\xi,\eta)\, e^{im_2\phi} \\
&= \frac{1}{16\pi} e^{-i\vartheta} \int_0^{2\pi} d\phi\, e^{i(m_2-m_1)\phi} \int_0^\infty d\xi \int_0^\infty d\eta\, (\xi + \eta)\, \psi_1^*(\xi,\eta)\, (\xi - \eta)\, \psi_2(\xi,\eta) \\
&= \frac{1}{8} e^{-i\vartheta}\, \delta_{m_1 m_2} \int_0^\infty d\xi \int_0^\infty d\eta\, \psi_1^*(\xi,\eta)\, (\xi^2 - \eta^2)\, \psi_2(\xi,\eta)\,. \qquad (5.7)
\end{aligned}$$

After splitting the angular part we obtain the first selection rule for electric dipole transition $\Delta m = 0, \pm 1$, which is exact for the Stark effect.

If we introduce in the parabolic parts of the wave function $\psi(\xi,\eta)$ the zero-field expressions 2.9 of the product of Laguerre polynomials, the operator $\xi\sqrt{\xi}$ which appears in the integrals for x and y can couple any pair of Laguerre polynomials, so we do not obtain any additional selection rule in the case $\Delta m = \pm 1$. Nevertheless in the integral for z, the operator ξ^2 only couples Laguerre polynomials with a difference of grad lower or equal to two [49], so we obtain a selection rule $\Delta n_1 = 0, \pm 1, \pm 2$, $\Delta n_2 = 0, \pm 1, \pm 2$, if $\Delta m = 0$, which corresponds to the radiation linearly polarised. As the wave functions for finite field are quite similar qualitatively to the ones for zero field, this selection rule should be fulfilled approximately for the approximate quantum numbers and $\tilde{n}_1$ and $\tilde{n}_2$.

To integrate the parabolic parts we use the wave functions expansions in the basis set 3.5:

$$\begin{aligned}
\psi_1(\xi,\eta) &= \sum_{i_1=1}^{N}\sum_{j_1=1}^{N} c_{1i_1j_1m_1}\,(\xi\eta)^{\frac{m_1}{2}}\,\mathrm{e}^{-\frac{\xi+\eta}{2}}\,\Lambda_{Ni_1}(\xi)\,\Lambda_{Nj_1}(\eta)\\
\psi_2(\xi,\eta) &= \sum_{i_2=1}^{N}\sum_{j_2=1}^{N} c_{2i_2j_2m_2}\,(\xi\eta)^{\frac{m_2}{2}}\,\mathrm{e}^{-\frac{\xi+\eta}{2}}\,\Lambda_{Ni_2}(\xi)\,\Lambda_{Nj_2}(\eta)
\end{aligned} \tag{5.8}$$

$$\begin{aligned}
\left\langle\psi_1\left|\,x\,\mathrm{e}^{-i\vartheta}\right|\psi_2\right\rangle &= \frac{1}{8}\,\mathrm{e}^{-i\vartheta}\,(\delta_{m_2m_1-1}+\delta_{m_2m_1+1})\sum_{i_1,j_1=1}^{N}\sum_{i_2,j_2=1}^{N} c^*_{1i_1j_1m_1}\,c_{2i_2j_2m_2}\\
&\quad\times\int_0^\infty \mathrm{d}\xi\int_0^\infty \mathrm{d}\eta\,(\xi+\eta)\,\sqrt{\xi\eta}\,(\xi\eta)^{\frac{|m_1|+|m_2|}{2}}\,\mathrm{e}^{-(\xi+\eta)}\,\Lambda^*_{Ni_1}(\xi)\,\Lambda^*_{Nj_1}(\eta)\,\Lambda_{Ni_2}(\xi)\,\Lambda_{Nj_2}(\eta)\\
&= \frac{1}{8}\,\mathrm{e}^{-i\vartheta}\,\delta_{m_2m_1-1}\sum_{i_1,j_1=1}^{N}\sum_{i_2,j_2=1}^{N} c^*_{1i_1j_1m_1}\,c_{2i_2j_2m_2}\,(\mathcal{S}_{i_1i_2m_2}\,\mathcal{I}_{j_1j_2m_2}+\mathcal{I}_{i_1i_2m_2}\,\mathcal{S}_{j_1j_2m_2})\\
&\quad+\frac{1}{8}\,\mathrm{e}^{-i\vartheta}\,\delta_{m_2m_1+1}\sum_{i_1,j_1=1}^{N}\sum_{i_2,j_2=1}^{N} c^*_{1i_1j_1m_1}\,c_{2i_2j_2m_2}\,(\mathcal{S}_{i_1i_2m_1}\,\mathcal{I}_{j_1j_2m_1}+\mathcal{I}_{i_1i_2m_1}\,\mathcal{S}_{j_1j_2m_1})
\end{aligned} \tag{5.9}$$

$$\begin{aligned}
\left\langle\psi_1\left|\,y\,\mathrm{e}^{-i\vartheta}\right|\psi_2\right\rangle &= \frac{1}{8i}\,\mathrm{e}^{-i\vartheta}\,(\delta_{m_2m_1-1}-\delta_{m_2m_1+1})\sum_{i_1,j_1=1}^{N}\sum_{i_2,j_2=1}^{N} c^*_{1i_1j_1m_1}\,c_{2i_2j_2m_2}\\
&\quad\times\int_0^\infty \mathrm{d}\xi\int_0^\infty \mathrm{d}\eta\,(\xi+\eta)\,\sqrt{\xi\eta}\,(\xi\eta)^{\frac{|m_1|+|m_2|}{2}}\,\mathrm{e}^{-(\xi+\eta)}\,\Lambda^*_{Ni_1}(\xi)\,\Lambda^*_{Nj_1}(\eta)\,\Lambda_{Ni_2}(\xi)\,\Lambda_{Nj_2}(\eta)\\
&= \frac{1}{8i}\,\mathrm{e}^{-i\vartheta}\,\delta_{m_2m_1-1}\sum_{i_1,j_1=1}^{N}\sum_{i_2,j_2=1}^{N} c^*_{1i_1j_1m_1}\,c_{2i_2j_2m_2}\,(\mathcal{S}_{i_1i_2m_2}\,\mathcal{I}_{j_1j_2m_2}+\mathcal{I}_{i_1i_2m_2}\,\mathcal{S}_{j_1j_2m_2})\\
&\quad-\frac{1}{8i}\,\mathrm{e}^{-i\vartheta}\,\delta_{m_2m_1+1}\sum_{i_1,j_1=1}^{N}\sum_{i_2,j_2=1}^{N} c^*_{1i_1j_1m_1}\,c_{2i_2j_2m_2}\,(\mathcal{S}_{i_1i_2m_1}\,\mathcal{I}_{j_1j_2m_1}+\mathcal{I}_{i_1i_2m_1}\,\mathcal{S}_{j_1j_2m_1})
\end{aligned} \tag{5.10}$$

$$\begin{aligned}
\left\langle\psi_1\left|\,z\,\mathrm{e}^{-i\vartheta}\right|\psi_2\right\rangle &= \frac{1}{8}\,\mathrm{e}^{-i\vartheta}\,\delta_{m_2m_1}\sum_{i_1,j_1=1}^{N}\sum_{i_2,j_2=1}^{N} c^*_{1i_1j_1m_1}\,c_{2i_2j_2m_2}\\
&\quad\times\int_0^\infty \mathrm{d}\xi\int_0^\infty \mathrm{d}\eta\,(\xi+\eta)\,(\xi-\eta)\,(\xi\eta)^{\frac{|m_1|+|m_2|}{2}}\,\mathrm{e}^{-(\xi+\eta)}\,\Lambda^*_{Ni_1}(\xi)\,\Lambda^*_{Nj_1}(\eta)\,\Lambda_{Ni_2}(\xi)\,\Lambda_{Nj_2}(\eta)\\
&= \frac{1}{8}\,\mathrm{e}^{-i\vartheta}\,\delta_{m_2m_1}\sum_{i_1,j_1=1}^{N}\sum_{i_2,j_2=1}^{N} c^*_{1i_1j_1m_1}\,c_{2i_2j_2m_2}\,(\mathcal{F}_{i_1i_2m_1}\,\mathcal{I}_{j_1j_2m_1}-\mathcal{I}_{i_1i_2m_1}\,\mathcal{F}_{j_1j_2m_1})\,.
\end{aligned} \tag{5.11}$$

So the dipole moment can be calculated in terms of the ground integrals 3.27 and the expansion coefficients. Once the modulus square of the matrix element is calculated the phase simplifies, so the Einstein coefficients remain independent of the complex rotation angle

$$\begin{aligned}
B_{21} &= \frac{4\pi^2}{3}\,\frac{e^2}{\hbar^2}\,\frac{g_2}{g_1}\,\left|\left\langle\psi_1\left|\,\vec{r}\,\right|\psi_2\right\rangle\right|^2\\
A_{21} &= \frac{(E_2-E_1)^3}{\hbar^2\pi^2c^3}\,B_{12}
\end{aligned} \tag{5.12}$$

Figure 5.6 shows the Einstein spontaneous emission coefficients for the transitions involved in the Balmer α line.

Combining figures 5.4, 5.5 and 5.6, we show in figure 5.7 the modelled profile of the Balmer D_α and H_α lines for two field intensities of relevance to plasma physics. The illustrated profile corresponds to the corona regime, when only radiative decay is included and collisional redistribution is negligible. We have also not included the Doppler shift and broadening contributions, which will depend on plasma parameters not considered in present work, including the energy of the injected neutrals, the arrangement of the lines-of-sight and the electron temperature.

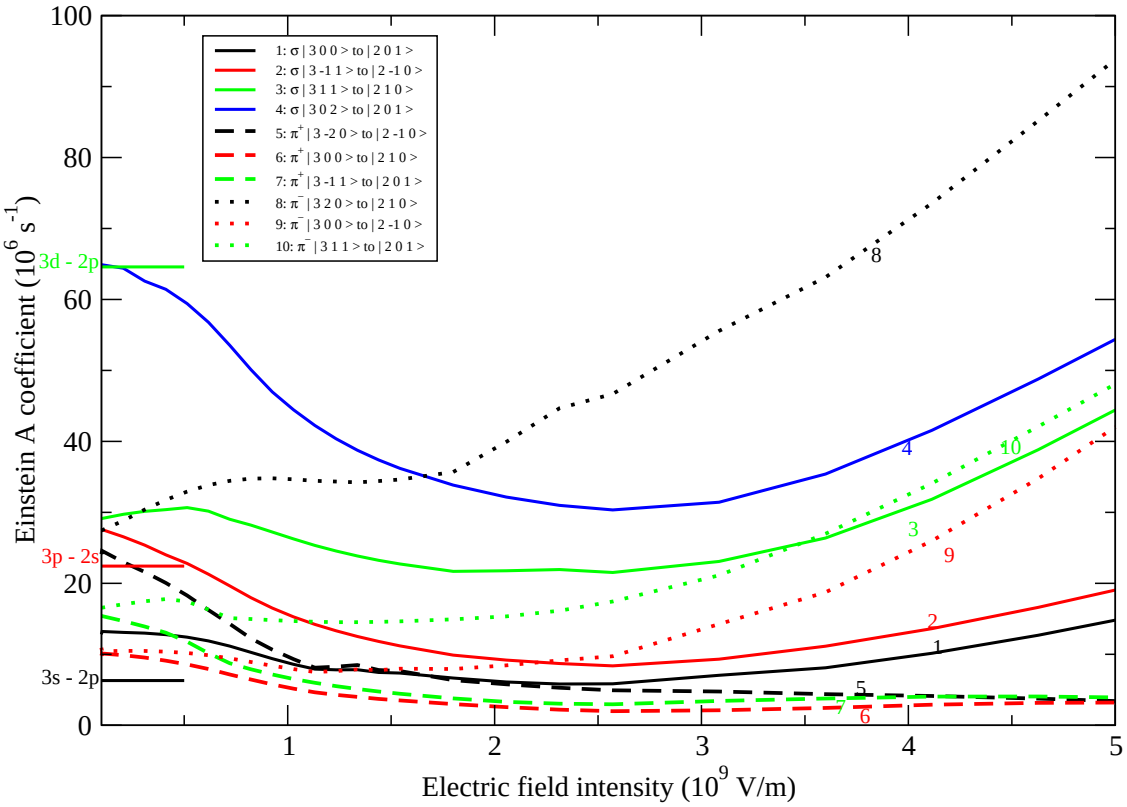

Figure 5.6: Einstein spontaneous emission coefficients of neutral hydrogen versus the electric field intensity. Marked the values for field zero for the Rydberg Hydrogen atom.

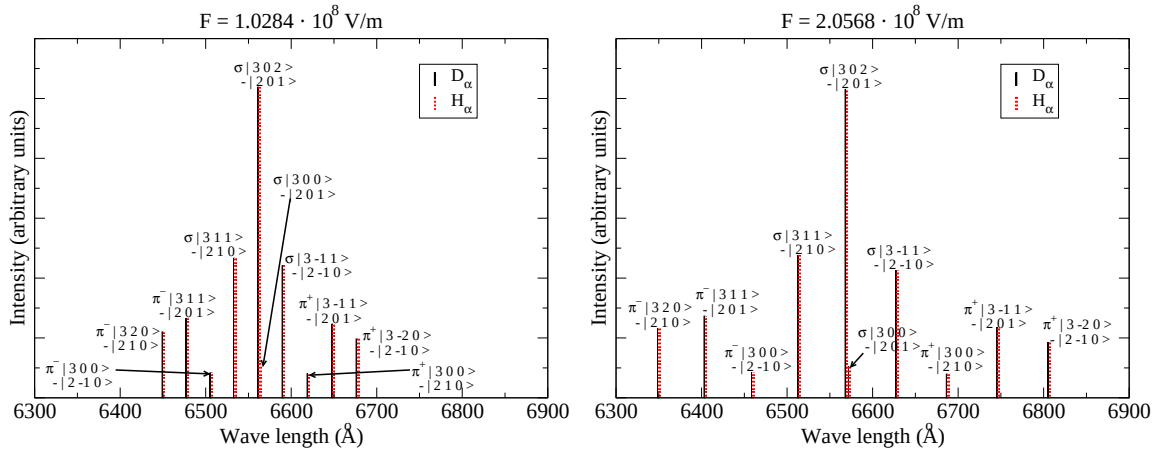

(a) $F = 1.0284 \cdot 10^8$ V/m (b) $F = 2.0568 \cdot 10^8$ V/m

Figure 5.7: Emission profile of the Balmer D_α and H_α lines for two different field intensities in corona equilibrium.

5.3 Motional Stark Effect, orbital angular momentum

In a real situation in the neutral beam injectors of a fusion device, the electric field is produced by the fast motion of the neutrals in the intense magnetic field, which is known as the Lorentz field

$$\vec{F} \;=\; \vec{v}\times\vec{B}\,, \tag{5.13}$$

with $\vec{v}$ the velocity of the neutrals and $\vec{B}$ the magnetic field. Then the electric and magnetic fields are present together and pointing in different directions. The magnetic field can be treated as a perturbation, as the field in a tokamak or stellarator is quite large, between 1 and 10 T, then the magnetic perturbation is higher than the fine structure, so we are in the Paschen-Bach regime, and we have to treat the orbital and spin angular momenta as uncoupled.

$$H_{PB} \;=\; \frac{\mu_B}{\hbar}\,\vec{B}\cdot(\vec{L} \,+\, g_e\vec{S})\,, \tag{5.14}$$

where $\vec{L}$ is the orbital angular momentum, which in Stark effect is not an operator which commutes with the Hamiltonian, $\vec{S}$ is the spin angular momentum operator, μ_B is the Bohr magneton and g_e the gyromagnetic constant of the electron, which values

$$g_e \;=\; 2 \,+\, \frac{\alpha}{\pi} \,+\, \ldots \;=\; 2.0023\,, \tag{5.15}$$

α is the fine structure constant

$$\alpha \;=\; \frac{e}{4\pi\epsilon_0\hbar c} \approx \frac{1}{137}\,. \tag{5.16}$$

Any anomalous angular momentum coming from relativistic corrections can also be included.

As the electric and magnetic fields are not parallel, we can not choose the magnetic field pointing in the z direction as it is usually made when treating Paschen-Bach effect, and we must calculate all the spacial components of the orbital angular momentum. The transformation equations for the momenta from cartesian to parabolic coordinates are

$$\begin{aligned}
p_x &= 2\,\frac{\sqrt{\xi\eta}}{\xi \,+\, \eta}\,\cos\phi\,(p_\xi \,+\, p_\eta) \,-\, \frac{1}{\sqrt{\xi\eta}}\,\sin\phi\,p_\phi \\
p_y &= 2\,\frac{\sqrt{\xi\eta}}{\xi \,+\, \eta}\,\sin\phi\,(p_\xi \,+\, p_\eta) \,+\, \frac{1}{\sqrt{\xi\eta}}\,\cos\phi\,p_\phi \\
p_z &= \frac{2}{\xi \,+\, \eta}\,(\xi p_\xi \,-\, \eta p_\eta)\,.
\end{aligned} \tag{5.17}$$

When the vectorial product is done, the coordinate is multiplied by a factor $e^{-i\vartheta}$ of the complex coordinate rotation angle, and the momentum by a $e^{i\vartheta}$, so both cancel each other and the angular momentum matrix elements remain independent of this complex rotation angle. Then the orbital angular momentum vector $\vec{L}$ can be split in its three cartesian components as follows:

$$\begin{aligned}
\vec{L} &= (yp_z \,-\, zp_y)\,\hat{x} \,+\, (zp_x \,-\, xp_z)\,\hat{y} \,+\, (xp_y \,-\, yp_x)\,\hat{z} \\
&= -\,i\hbar\left[\sqrt{\xi\eta}\,\sin\phi\left(\frac{\partial}{\partial\xi} \,-\, \frac{\partial}{\partial\eta}\right) \,-\, \frac{1}{2}\,\frac{\xi \,-\, \eta}{\sqrt{\xi\eta}}\,\cos\phi\,\frac{\partial}{\partial\phi}\right]\hat{x} \\
&\quad +\,i\hbar\left[\sqrt{\xi\eta}\,\cos\phi\left(\frac{\partial}{\partial\xi} \,-\, \frac{\partial}{\partial\eta}\right) \,+\, \frac{1}{2}\,\frac{\xi \,-\, \eta}{\sqrt{\xi\eta}}\,\sin\phi\,\frac{\partial}{\partial\phi}\right]\hat{y} \\
&\quad -\,i\hbar\,\frac{\partial}{\partial\phi}\,\hat{z}\,.
\end{aligned} \tag{5.18}$$

In Stark effect the operator L^2 is no more conserved, so it is not useful to get its mean value, anyway it can be expressed in parabolic coordinates as

$$L^2 \;=\; (\xi \,+\, \eta)\left[-\eta\,\frac{\partial^2}{\partial\xi^2} \;-\; \xi\,\frac{\partial^2}{\partial\eta^2} \;-\; 2\,(\xi \,+\, \eta)\,\frac{\partial^2}{\partial\xi\partial\eta} \;-\; 3\left(\frac{\partial}{\partial\xi} \,+\, \frac{\partial}{\partial\eta}\right) \,+\, \frac{1}{4}\,\frac{\xi \,+\, \eta}{\xi\eta}\,\frac{\partial^2}{\partial\phi^2}\right]. \tag{5.19}$$

We calculate now the cartesian components of the orbital angular momentum

$$\begin{aligned}
\langle\psi_1\,|\,L_x\,|\,\psi_2\rangle &= -\frac{i\hbar}{2\pi}\int_0^{2\pi}\mathrm{d}\phi\int_0^{\infty}\mathrm{d}\xi\int_0^{\infty}\mathrm{d}\eta\,\frac{1}{4}\,(\xi+\eta)\,\psi_1^*(\xi,\eta)\,\mathrm{e}^{-im_1\phi}\\
&\quad\times\left[\sqrt{\xi\eta}\,\sin\phi\left(\frac{\partial}{\partial\xi}-\frac{\partial}{\partial\eta}\right)-\frac{1}{2}\,\frac{\xi-\eta}{\sqrt{\xi\eta}}\,\cos\phi\,\frac{\partial}{\partial\phi}\right]\psi_2(\xi,\eta)\,\mathrm{e}^{im_2\phi}\\
&= -\frac{\hbar}{8}\,(\delta_{m_1m_2+1}-\delta_{m_1m_2-1})\int_0^{\infty}\mathrm{d}\xi\int_0^{\infty}\mathrm{d}\eta\,\psi_1^*(\xi,\eta)\,(\xi+\eta)\,\sqrt{\xi\eta}\left(\frac{\partial}{\partial\xi}-\frac{\partial}{\partial\eta}\right)\psi_2(\xi,\eta)\\
&\quad-\frac{m_2\hbar}{16}\,(\delta_{m_1m_2-1}+\delta_{m_1m_2+1})\int_0^{\infty}\mathrm{d}\xi\int_0^{\infty}\mathrm{d}\eta\,\psi_1^*(\xi,\eta)\,\frac{\xi^2-\eta^2}{\sqrt{\xi\eta}}\,\psi_2(\xi,\eta)
\end{aligned}\tag{5.20}$$

$$\begin{aligned}
\left\langle\psi_1\,|\,L_y\,|\,\psi_2\right\rangle &= \frac{i\hbar}{2\pi}\int_0^{2\pi}\mathrm{d}\phi\int_0^{\infty}\mathrm{d}\xi\int_0^{\infty}\mathrm{d}\eta\,\frac{1}{4}\,(\xi+\eta)\,\psi_1^*(\xi,\eta)\,\mathrm{e}^{-im_1\phi}\\
&\quad\times\left[\sqrt{\xi\eta}\,\sin\phi\left(\frac{\partial}{\partial\xi}-\frac{\partial}{\partial\eta}\right)-\frac{1}{2}\,\frac{\xi-\eta}{\sqrt{\xi\eta}}\,\cos\phi\,\frac{\partial}{\partial\phi}\right]\psi_2(\xi,\eta)\,\mathrm{e}^{im_2\phi}\\
&= \frac{i\hbar}{8}\,(\delta_{m_1m_2+1}+\delta_{m_1m_2-1})\int_0^{\infty}\mathrm{d}\xi\int_0^{\infty}\mathrm{d}\eta\,\psi_1^*(\xi,\eta)\,(\xi+\eta)\,\sqrt{\xi\eta}\left(\frac{\partial}{\partial\xi}-\frac{\partial}{\partial\eta}\right)\psi_2(\xi,\eta)\\
&\quad+\frac{im_2\hbar}{16}\,(\delta_{m_1m_2+1}-\delta_{m_1m_2-1})\int_0^{\infty}\mathrm{d}\xi\int_0^{\infty}\mathrm{d}\eta\,\psi_1^*(\xi,\eta)\,\frac{\xi^2-\eta^2}{\sqrt{\xi\eta}}\,\psi_2(\xi,\eta)
\end{aligned}\tag{5.21}$$

$$\begin{aligned}
\langle\psi_1\,|\,L_z\,|\,\psi_2\rangle &= -\frac{i\hbar}{2\pi}\int_0^{2\pi}\mathrm{d}\phi\int_0^{\infty}\mathrm{d}\xi\int_0^{\infty}\mathrm{d}\eta\,\frac{1}{4}\,(\xi+\eta)\,\psi_1^*(\xi,\eta)\,\mathrm{e}^{-im_1\phi}\,\frac{\partial}{\partial\phi}\,\psi_2(\xi,\eta)\,\mathrm{e}^{im_2\phi}\\
&= \hbar m_2\,\delta_{m_1m_2}\,\delta_{12}\,.
\end{aligned}\tag{5.22}$$

The L_z component is already a conserved quantity, and the other components just couple states with $\Delta m = \pm 1$. To determine the integrals we write the wave functions ψ_1 and ψ_2 as their expansions in the basis set as usually 5.8

$$\begin{aligned}
\langle\psi_1\,|\,L_x\,|\,\psi_2\rangle &= -\frac{\hbar}{8}\,(\delta_{m_1m_2+1}-\delta_{m_1m_2-1})\sum_{i_1j_1=1}^{N}\sum_{i_2j_2=1}^{N}c^*_{1i_1j_1m_1}\,c_{2i_2j_2m_2}\\
&\quad\times\int_0^{\infty}\mathrm{d}\xi\int_0^{\infty}\mathrm{d}\eta\,\mathrm{e}^{-\frac{\xi+\eta}{2}}\,(\xi\eta)^{\frac{|m_1|}{2}}\,\Lambda^*_{Ni_1}(\xi)\,\Lambda^*_{Nj_1}(\eta)\,(\xi+\eta)\,\sqrt{\xi\eta}\left(\frac{\partial}{\partial\xi}-\frac{\partial}{\partial\eta}\right)\mathrm{e}^{-\frac{\xi+\eta}{2}}\,(\xi\eta)^{\frac{|m_2|}{2}}\,\Lambda_{Ni_2}(\xi)\,\Lambda_{Nj_2}(\eta)\\
&\quad-\frac{m_2\hbar}{16}\,(\delta_{m_1m_2+1}+\delta_{m_1m_2-1})\sum_{i_1j_1=1}^{N}\sum_{i_2j_2=1}^{N}c^*_{1i_1j_1m_1}\,c_{2i_2j_2m_2}\\
&\quad\times\int_0^{\infty}\mathrm{d}\xi\int_0^{\infty}\mathrm{d}\eta\,\mathrm{e}^{-\frac{\xi+\eta}{2}}\,(\xi\eta)^{\frac{|m_1|}{2}}\,\Lambda^*_{Ni_1}(\xi)\,\Lambda^*_{Nj_1}(\eta)\,\frac{\xi^2-\eta^2}{\sqrt{\xi\eta}}\,\mathrm{e}^{-\frac{\xi+\eta}{2}}\,(\xi\eta)^{\frac{|m_2|}{2}}\,\Lambda_{Ni_2}(\xi)\,\Lambda_{Nj_2}(\eta)
\end{aligned}\tag{5.23}$$

$$\begin{aligned}
\left\langle\psi_1\,|\,L_y\,|\,\psi_2\right\rangle &= \frac{i\hbar}{8}\,(\delta_{m_1m_2+1}+\delta_{m_1m_2-1})\sum_{i_1j_1=1}^{N}\sum_{i_2j_2=1}^{N}c^*_{1i_1j_1m_1}\,c_{2i_2j_2m_2}\\
&\quad\times\int_0^{\infty}\mathrm{d}\xi\int_0^{\infty}\mathrm{d}\eta\,\mathrm{e}^{-\frac{\xi+\eta}{2}}\,(\xi\eta)^{\frac{|m_1|}{2}}\,\Lambda^*_{Ni_1}(\xi)\,\Lambda^*_{Nj_1}(\eta)\,(\xi+\eta)\,\sqrt{\xi\eta}\left(\frac{\partial}{\partial\xi}-\frac{\partial}{\partial\eta}\right)\mathrm{e}^{-\frac{\xi+\eta}{2}}\,(\xi\eta)^{\frac{|m_2|}{2}}\,\Lambda_{Ni_2}(\xi)\,\Lambda_{Nj_2}(\eta)\\
&\quad-\frac{im_2\hbar}{16}\,(\delta_{m_1m_2+1}-\delta_{m_1m_2-1})\sum_{i_1j_1=1}^{N}\sum_{i_2j_2=1}^{N}c^*_{1i_1j_1m_1}\,c_{2i_2j_2m_2}\\
&\quad\times\int_0^{\infty}\mathrm{d}\xi\int_0^{\infty}\mathrm{d}\eta\,\mathrm{e}^{-\frac{\xi+\eta}{2}}\,(\xi\eta)^{\frac{|m_1|}{2}}\,\Lambda^*_{Ni_1}(\xi)\,\Lambda^*_{Nj_1}(\eta)\,\frac{\xi^2-\eta^2}{\sqrt{\xi\eta}}\,\mathrm{e}^{-\frac{\xi+\eta}{2}}\,(\xi\eta)^{\frac{|m_2|}{2}}\,\Lambda_{Ni_2}(\xi)\,\Lambda_{Nj_2}(\eta)
\end{aligned}\tag{5.24}$$

And operating them:

$$\begin{aligned}
\langle \psi_1 \,|\, L_x \,|\, \psi_2 \rangle &= -\frac{\hbar}{8}\,\delta_{m_1 m_2+1} \sum_{i_1 j_1=1}^{N} \sum_{i_2 j_2=1}^{N} c^*_{1 i_1 j_1 m_1}\, c_{2 i_2 j_2 m_2} \\
&\times \left[\mathcal{D}_{i_1 i_2 m_2}\, \mathcal{A}_{j_1 j_2 m_2} + C_{i_1 i_2 m_2}\, \mathcal{B}_{j_1 j_2 m_2} - \mathcal{B}_{i_1 i_2 m_2}\, C_{j_1 j_2 m_2} - \mathcal{A}_{i_1 i_2 m_2}\, \mathcal{D}_{j_1 j_2 m_2} \right] \\
&+ \frac{\hbar}{8}\,\delta_{m_1 m_2-1} \sum_{i_1 j_1=1}^{N} \sum_{i_2 j_2=1}^{N} c^*_{1 i_1 j_1 m_1}\, c_{2 i_2 j_2 m_2} \\
&\times \left[\mathcal{D}_{i_1 i_2 m_1}\, \mathcal{A}_{j_1 j_2 m_1} + C_{i_1 i_2 m_1}\, \mathcal{B}_{j_1 j_2 m_1} - \mathcal{B}_{i_1 i_2 m_1}\, C_{j_1 j_2 m_1} - \mathcal{A}_{i_1 i_2 m_1}\, \mathcal{D}_{j_1 j_2 m_1} \right], \qquad (5.25)
\end{aligned}$$

$$\begin{aligned}
\left\langle \psi_1 \,|\, L_y \,|\, \psi_2 \right\rangle &= \frac{i\hbar}{8}\,\delta_{m_1 m_2+1} \sum_{i_1 j_1=1}^{N} \sum_{i_2 j_2=1}^{N} c^*_{1 i_1 j_1 m_1}\, c_{2 i_2 j_2 m_2} \\
&\times \left[\mathcal{D}_{i_1 i_2 m_2}\, \mathcal{A}_{j_1 j_2 m_2} + C_{i_1 i_2 m_2}\, \mathcal{B}_{j_1 j_2 m_2} - \mathcal{B}_{i_1 i_2 m_2}\, C_{j_1 j_2 m_2} - \mathcal{A}_{i_1 i_2 m_2}\, \mathcal{D}_{j_1 j_2 m_2} \right] \\
&+ \frac{i\hbar}{8}\,\delta_{m_1 m_2-1} \sum_{i_1 j_1=1}^{N} \sum_{i_2 j_2=1}^{N} c^*_{1 i_1 j_1 m_1}\, c_{2 i_2 j_2 m_2} \\
&\times \left[\mathcal{D}_{i_1 i_2 m_1}\, \mathcal{A}_{j_1 j_2 m_1} + C_{i_1 i_2 m_1}\, \mathcal{B}_{j_1 j_2 m_1} - \mathcal{B}_{i_1 i_2 m_1}\, C_{j_1 j_2 m_1} - \mathcal{A}_{i_1 i_2 m_1}\, \mathcal{D}_{j_1 j_2 m_1} \right]. \qquad (5.26)
\end{aligned}$$

where we have defined new ground matrixes

$$\begin{aligned}
\mathcal{I}_{ijm} &= \int_0^\infty \mathrm{d}x\, \mathrm{e}^{-x}\, x^{|m|}\, \Lambda^*_{Ni}(x)\, \Lambda_{Nj}(x) \\
\mathcal{A}_{ijm} &= \int_0^\infty \mathrm{d}x\, \mathrm{e}^{-x}\, x^{|m|}\, x\, \Lambda^*_{Ni}(x)\, \Lambda_{Nj}(x) \\
\mathcal{B}_{ijm} &= \int_0^\infty \mathrm{d}x\, \mathrm{e}^{-x}\, x^{|m|}\, x^2\, \Lambda^*_{Ni}(x)\, \Lambda_{Nj}(x) \\
C_{ijm} &= \int_0^\infty \mathrm{d}x\, \mathrm{e}^{-x}\, x^{|m|}\, x\, \Lambda^*_{Ni}(x)\, \Lambda'_{Nj}(x) \\
\mathcal{D}_{ijm} &= \int_0^\infty \mathrm{d}x\, \mathrm{e}^{-x}\, x^{|m|}\, x^2\, \Lambda^*_{Ni}(x)\, \Lambda'_{Nj}(x)\,. \qquad (5.27)
\end{aligned}$$

With expressions 5.22, 5.25 and 5.26 we can calculate the orbital part for the magnetic perturbation, now we have to add the spin part. To calculate the components x and y of the spin operator we write them in terms of the raising and lowering operators of the angular momentum j_+ and j_- as:

$$\begin{aligned}
j_+ &= j_x + i j_y \\
j_- &= j_x - i j_y\,, \qquad (5.28)
\end{aligned}$$

which fulfil

$$\begin{aligned}
j_z \,|\, j\, m\rangle &= \hbar\, j \,|\, j\, m\rangle \\
j_+ \,|\, j\, m\rangle &= \hbar \sqrt{j(j+1) - m(m+1)}\,|\, j\, m+1\rangle \\
j_- \,|\, j\, m\rangle &= \sqrt{j(j+1) - m(m-1)}\,|\, j\, m-1\rangle\,. \qquad (5.29)
\end{aligned}$$

That leads to a expression for the spin operator ($j = \frac{1}{2}$) as

$$\begin{aligned}
\langle s\, m_{s1} \,|\, S_z \,|\, s\, m_{s2}\rangle &= \frac{\hbar}{2}\,\delta_{m_{s1} m_{s2}} \\
\langle s\, m_{s1} \,|\, S_x \,|\, s\, m_{s2}\rangle &= \frac{\hbar}{2}\left(\sqrt{3/4 - m_{s2}(m_{s2}+1)}\,\delta_{m_{s1} m_{s2}+1} + \sqrt{3/4 - m_{s2}(m_{s2}-1)}\,\delta_{m_{s1} m_{s2}-1} \right) \\
\left\langle s\, m_{s1} \left| S_y \right| s\, m_{s2} \right\rangle &= \frac{\hbar}{2i}\left(\sqrt{3/4 - m_{s2}(m_{s2}+1)}\,\delta_{m_{s1} m_{s2}+1} - \sqrt{3/4 - m_{s2}(m_{s2}-1)}\,\delta_{m_{s1} m_{s2}-1} \right), \qquad (5.30)
\end{aligned}$$

so we can now get the total magnetic perturbation matrix as

$$H_B^{(1)} = \frac{\mu_B}{\hbar} \left\langle \psi_1\, m_{s1} \left| \vec{B} \cdot (\vec{L} + g_e \vec{S}) \right| \psi_2\, m_{s2} \right\rangle \qquad (5.31)$$

Chapter 6

Summary

The present work is focused mainly in the development of an *ab initio* method to obtain the energies, widths and wave functions of the neutral hydrogen atom under a constant electric field. The characteristics of the system makes that perturbation theory is not applicable to describe the effect of the external electric field on the atom. We chose a complex coordinate rotation method to extract the resonances of the Stark hydrogen atom from the continuum background, we expanded the wave functions in a linear independent basis set of 900 Laguerre-mesh polynomials ($N = 30$), we calculated with a good accuracy all the resonances for the shells with approximate principal quantum number $\tilde{n} \leq 5$.

The hole information about the system lays on the wave functions of the resonances, so in the expansion coefficients c_{ijm} of equation 3.5. In chapter 5 it was shown how any physical observable can be calculated as a linear combination of the ground integrals of the basis functions with these expansion coefficients. The shown results were obtained in terms of a Laguerre-mesh polynomials basis set, but the treatment is general and it can be applied to any other basis set.

Present work is a first step to get a tool for plasma diagnosis through the MSE spectroscopy. The determination of the wave functions of the Stark states of neutral hydrogen is the starting point to obtain the collision radiative parameters which will allow simulate MSE spectra. A challenging problem for the future is to get the collisional part, one has to determine the collision cross sections for the processes involved in the neutral beam: electron impact, ion impact and charge exchange. They are directional cross sections, with an atom which has no spherical symmetry, but it is polarized and oriented in the direction of the electric field. These directional cross sections are different to the usual tabulated ones.

The implementation is complete and can be expanded to obtain results for higher excited shells by increasing the basis set. For a basis set of dimension N, which means N^2 functions, one gets approximately N resonances for a fixed value of m. The computation time and storage capacity increases as N^4. In our case, $N = 30$, we have to store a complex matrix 900×900 for each value of the field intensity and the complex rotation angle, which is more than six megabytes for each value of (F, ϑ) for each m.

The true wave functions for the Stark atom is an important advance in atomic physics and it opens new research lines. In a next step of the work, we use these calculated wave functions to evaluate collision cross sections and rate coefficients relevant to the collisional-radiative models for neutral beam injection in fusion plasmas. Both electron impact and ion impact excitation matter as well as ionization and charge exchange. With the motional Stark field present, the collisions are with oriented atoms. Also the ion collisions are semi-directional in a cone of attack depending on the ion thermal speeds versus the beam speed. Impact parameter models can take account of these effects with matrix elements evaluated using the true atom wave functions described here. Up to now cross sections and Einstein coefficients for the isolated hydrogen atom ($F = 0$) were used for the collision radiative modelling of BMS.

Once all the steps are done, including the directional cross sections, all will be put together in the routine ADAS305, which will improve considerably the quality of the spectra predicted.

Appendix A

Fundamental constants and conversion factors used

Fundamental constants.

Fine structure constant	α	$\frac{e^2}{\hbar c} = 7.297 \cdot 10^3 = \frac{1}{137}$
Electron gyromagnetic constant	g_e	$2 + \frac{\alpha}{\pi} = 2.0023$
Light velocity in vacuum	c	$\frac{1}{\alpha} v_H = 3 \cdot 10^8\,\mathrm{m/s}$
Plank constant	h	$2\pi\hbar = 6.626 \cdot 10^{-34}\,\mathrm{J\,s}$
Proton mass	m_P	$1836.15\,m = 1.672 \cdot 10^{-27}\,\mathrm{kg}$
Deuteron mass	m_D	$3670.48\,m = 3.343 \cdot 10^{-27}\,\mathrm{kg}$
Triton mass	m_T	$5496.92\,m = 5.007 \cdot 10^{-27}\,\mathrm{kg}$
Bohr magneton	μ_B	$\frac{1}{2}\frac{e\hbar}{m} = 9.275 \cdot 10^{-24}\,\mathrm{J/T}$

Fundamental atomic units and equivalent in International Unit System.

mass	m	$9.109 \cdot 10^{-31}\,\mathrm{kg}$
electric charge	e	$1.602 \cdot 10^{-19}\,\mathrm{C}$
angular momentum	$\hbar$	$1.054 \cdot 10^{-34}\,\mathrm{J\,s}$
dielectric constant	$\frac{1}{4\pi\epsilon_0}$	$8.987 \cdot 10^9\,\mathrm{kg\,m^3\,s^{-2}\,C^{-2}}$
magnetic moment	$\frac{e\hbar}{m}$	$1.855 \cdot 10^{-23}\,\mathrm{J/T}$

Derived atomic units and equivalent in International Unit System.

energy	$E_H = \frac{me^4}{\hbar 4\pi\epsilon_0}$	$4.359 \cdot 10^{-19}\,\mathrm{J} = 27.211\,\mathrm{eV}$
length	$a_0 = \frac{\hbar^2 4\pi\epsilon_0}{me^2}$	$5.29 \cdot 10^{-11}\,\mathrm{m}$
time	$t_H = \frac{\hbar}{E_H}$	$2.419 \cdot 10^{-17}\,\mathrm{s}$
velocity	$v_H = \frac{a_0}{t_H}$	$2.188 \cdot 10^6\,\mathrm{m/s}$
electric field	$F_0 = \frac{E_H}{ea_0}$	$5.142 \cdot 10^{11}\,\mathrm{V/m}$
Magnetic field	$B_0 = \frac{\hbar}{ea_0^2}$	$2.35 \cdot 10^5\,\mathrm{T}$

Appendix B

Calculated roots of Laguerre polynomials

We show the calculated roots of the Laguerre polynomials $L_N(x)$ for $N \leq 40$. The roots were obtained through a bisection method with an accuracy of 10^{-12}, taking in advantage that all the roots of the Laguerre polynomials are real, greater than zero and of multiplicity one. The Laguerre polynomials were calculated using the recurrence relation

$$\begin{aligned} L_0(x) &= 1 \\ L_1(x) &= 1 - x \\ N L_N(x) &= (2N - 1 - x) L_{N-1}(x) - (N - 1) L_{N-2}(x) . \end{aligned} \tag{B.1}$$

N				
1	$1.000000000 \cdot 10^{0}$			
2	$5.857864376 \cdot 10^{-1}$	$3.414213562 \cdot 10^{0}$		
3	$4.157745568 \cdot 10^{-1}$	$2.294280360 \cdot 10^{0}$	$6.289945083 \cdot 10^{0}$	
4	$3.225476896 \cdot 10^{-1}$	$1.745761101 \cdot 10^{0}$	$4.536620297 \cdot 10^{0}$	$9.395070912 \cdot 10^{0}$
5	$2.635603197 \cdot 10^{-1}$	$1.413403059 \cdot 10^{0}$	$3.596425771 \cdot 10^{0}$	$7.085810006 \cdot 10^{0}$
	$1.264080084 \cdot 10^{1}$			
6	$2.228466042 \cdot 10^{-1}$	$1.188932102 \cdot 10^{0}$	$2.992736326 \cdot 10^{0}$	$5.775143569 \cdot 10^{0}$
	$9.837467418 \cdot 10^{0}$	$1.598287398 \cdot 10^{1}$		
7	$1.930436766 \cdot 10^{-1}$	$1.026664895 \cdot 10^{0}$	$2.567876745 \cdot 10^{0}$	$4.900353085 \cdot 10^{0}$
	$8.182153445 \cdot 10^{0}$	$1.273418029 \cdot 10^{1}$	$1.939572786 \cdot 10^{1}$	
8	$1.702796323 \cdot 10^{-1}$	$9.037017768 \cdot 10^{-1}$	$2.251086630 \cdot 10^{0}$	$4.266700170 \cdot 10^{0}$
	$7.045905402 \cdot 10^{0}$	$1.075851601 \cdot 10^{1}$	$1.574067864 \cdot 10^{1}$	$2.286313174 \cdot 10^{1}$
9	$1.523222277 \cdot 10^{-1}$	$8.072200227 \cdot 10^{-1}$	$2.005135156 \cdot 10^{0}$	$3.783473973 \cdot 10^{0}$
	$6.204956778 \cdot 10^{0}$	$9.372985252 \cdot 10^{0}$	$1.346623691 \cdot 10^{1}$	$1.883359779 \cdot 10^{1}$
	$2.637407189 \cdot 10^{1}$			
10	$1.377934705 \cdot 10^{-1}$	$7.294545495 \cdot 10^{-1}$	$1.808342902 \cdot 10^{0}$	$3.401433698 \cdot 10^{0}$
	$5.552496140 \cdot 10^{0}$	$8.330152747 \cdot 10^{0}$	$1.184378584 \cdot 10^{1}$	$1.627925783 \cdot 10^{1}$
	$2.199658581 \cdot 10^{1}$	$2.992069701 \cdot 10^{1}$		
11	$1.257964422 \cdot 10^{-1}$	$6.654182558 \cdot 10^{-1}$	$1.647150546 \cdot 10^{0}$	$3.091138143 \cdot 10^{0}$
	$5.029284402 \cdot 10^{0}$	$7.509887864 \cdot 10^{0}$	$1.060595100 \cdot 10^{1}$	$1.443161376 \cdot 10^{1}$
	$1.917885740 \cdot 10^{1}$	$2.521770934 \cdot 10^{1}$	$3.349719285 \cdot 10^{1}$	
12	$1.157221174 \cdot 10^{-1}$	$6.117574845 \cdot 10^{-1}$	$1.512610270 \cdot 10^{0}$	$2.833751338 \cdot 10^{0}$
	$4.599227639 \cdot 10^{0}$	$6.844525453 \cdot 10^{0}$	$9.621316842 \cdot 10^{0}$	$1.300605499 \cdot 10^{1}$
	$1.711685519 \cdot 10^{1}$	$2.215109038 \cdot 10^{1}$	$2.848796725 \cdot 10^{1}$	$3.709912104 \cdot 10^{1}$
13	$1.071423885 \cdot 10^{-1}$	$5.661318990 \cdot 10^{-1}$	$1.398564336 \cdot 10^{0}$	$2.616597108 \cdot 10^{0}$
	$4.238845929 \cdot 10^{0}$	$6.292256271 \cdot 10^{0}$	$8.815001941 \cdot 10^{0}$	$1.186140359 \cdot 10^{1}$
	$1.551076204 \cdot 10^{1}$	$1.988463566 \cdot 10^{1}$	$2.518526386 \cdot 10^{1}$	$3.180038630 \cdot 10^{1}$

N				
	$4.072300867 \cdot 10^{1}$			
14	$9.974750703 \cdot 10^{-2}$	$5.268576489 \cdot 10^{-1}$	$1.300629121 \cdot 10^{0}$	$2.430801079 \cdot 10^{0}$
	$3.932102822 \cdot 10^{0}$	$5.825536218 \cdot 10^{0}$	$8.140240142 \cdot 10^{0}$	$1.091649951 \cdot 10^{1}$
	$1.421080501 \cdot 10^{1}$	$1.810489222 \cdot 10^{1}$	$2.272338163 \cdot 10^{1}$	$2.827298172 \cdot 10^{1}$
	$3.514944366 \cdot 10^{1}$	$4.436608171 \cdot 10^{1}$		
15	$9.330781202 \cdot 10^{-2}$	$4.926917403 \cdot 10^{-1}$	$1.215595412 \cdot 10^{0}$	$2.269949526 \cdot 10^{0}$
	$3.667622722 \cdot 10^{0}$	$5.425336627 \cdot 10^{0}$	$7.565916227 \cdot 10^{0}$	$1.012022857 \cdot 10^{1}$
	$1.313028248 \cdot 10^{1}$	$1.665440771 \cdot 10^{1}$	$2.077647890 \cdot 10^{1}$	$2.562389423 \cdot 10^{1}$
	$3.140751917 \cdot 10^{1}$	$3.853068331 \cdot 10^{1}$	$4.802608557 \cdot 10^{1}$	
16	$8.764941048 \cdot 10^{-2}$	$4.626963289 \cdot 10^{-1}$	$1.141057775 \cdot 10^{0}$	$2.129283645 \cdot 10^{0}$
	$3.437086634 \cdot 10^{0}$	$5.078018615 \cdot 10^{0}$	$7.070338535 \cdot 10^{0}$	$9.438314336 \cdot 10^{0}$
	$1.221422337 \cdot 10^{1}$	$1.544152737 \cdot 10^{1}$	$1.918015686 \cdot 10^{1}$	$2.351590569 \cdot 10^{1}$
	$2.857872974 \cdot 10^{1}$	$3.458339870 \cdot 10^{1}$	$4.194045265 \cdot 10^{1}$	$5.170116034 \cdot 10^{1}$
17	$8.263821471 \cdot 10^{-2}$	$4.361503236 \cdot 10^{-1}$	$1.075176578 \cdot 10^{0}$	$2.005193532 \cdot 10^{0}$
	$3.234256124 \cdot 10^{0}$	$4.773513514 \cdot 10^{0}$	$6.637829205 \cdot 10^{0}$	$8.846685511 \cdot 10^{0}$
	$1.142552932 \cdot 10^{1}$	$1.440782304 \cdot 10^{1}$	$1.783828473 \cdot 10^{1}$	$2.177826826 \cdot 10^{1}$
	$2.631531781 \cdot 10^{1}$	$3.158177168 \cdot 10^{1}$	$3.779609384 \cdot 10^{1}$	$4.537571653 \cdot 10^{1}$
	$5.538975179 \cdot 10^{1}$			
18	$7.816916667 \cdot 10^{-2}$	$4.124900853 \cdot 10^{-1}$	$1.016520180 \cdot 10^{0}$	$1.894888510 \cdot 10^{0}$
	$3.054353113 \cdot 10^{0}$	$4.504205539 \cdot 10^{0}$	$6.256725074 \cdot 10^{0}$	$8.327825157 \cdot 10^{0}$
	$1.073799005 \cdot 10^{1}$	$1.351365621 \cdot 10^{1}$	$1.668930628 \cdot 10^{1}$	$2.031076763 \cdot 10^{1}$
	$2.444068136 \cdot 10^{1}$	$2.916820866 \cdot 10^{1}$	$3.462792707 \cdot 10^{1}$	$4.104181677 \cdot 10^{1}$
	$4.883392272 \cdot 10^{1}$	$5.909054644 \cdot 10^{1}$		
19	$7.415878376 \cdot 10^{-2}$	$3.912686133 \cdot 10^{-1}$	$9.639573440 \cdot 10^{-1}$	$1.796175582 \cdot 10^{0}$
	$2.893651382 \cdot 10^{0}$	$4.264215540 \cdot 10^{0}$	$5.918141562 \cdot 10^{0}$	$7.868618915 \cdot 10^{0}$
	$1.013242372 \cdot 10^{1}$	$1.273088146 \cdot 10^{1}$	$1.569127834 \cdot 10^{1}$	$1.904899321 \cdot 10^{1}$
	$2.285084976 \cdot 10^{1}$	$2.716066933 \cdot 10^{1}$	$3.206912225 \cdot 10^{1}$	$3.771290580 \cdot 10^{1}$
	$4.431736280 \cdot 10^{1}$	$5.231290246 \cdot 10^{1}$	$6.280242315 \cdot 10^{1}$	
20	$7.053988969 \cdot 10^{-2}$	$3.721268180 \cdot 10^{-1}$	$9.165821025 \cdot 10^{-1}$	$1.707306531 \cdot 10^{0}$
	$2.749199255 \cdot 10^{0}$	$4.048925314 \cdot 10^{0}$	$5.615174971 \cdot 10^{0}$	$7.459017454 \cdot 10^{0}$
	$9.594392870 \cdot 10^{0}$	$1.203880255 \cdot 10^{1}$	$1.481429344 \cdot 10^{1}$	$1.794889552 \cdot 10^{1}$
	$2.147878824 \cdot 10^{1}$	$2.545170279 \cdot 10^{1}$	$2.993255463 \cdot 10^{1}$	$3.501343424 \cdot 10^{1}$
	$4.083305706 \cdot 10^{1}$	$4.761999405 \cdot 10^{1}$	$5.581079575 \cdot 10^{1}$	$6.652441653 \cdot 10^{1}$
21	$6.725781792 \cdot 10^{-2}$	$3.547728953 \cdot 10^{-1}$	$8.736601668 \cdot 10^{-1}$	$1.626869942 \cdot 10^{0}$
	$2.618626411 \cdot 10^{0}$	$3.854652138 \cdot 10^{0}$	$5.342369281 \cdot 10^{0}$	$7.091168813 \cdot 10^{0}$
	$9.112778854 \cdot 10^{0}$	$1.142177176 \cdot 10^{1}$	$1.403627070 \cdot 10^{1}$	$1.697895269 \cdot 10^{1}$
	$2.027850941 \cdot 10^{1}$	$2.397184559 \cdot 10^{1}$	$2.810752860 \cdot 10^{1}$	$3.275149741 \cdot 10^{1}$
	$3.799718782 \cdot 10^{1}$	$4.398524576 \cdot 10^{1}$	$5.094735119 \cdot 10^{1}$	$5.932599412 \cdot 10^{1}$
	$7.025568863 \cdot 10^{1}$			
22	$6.426762874 \cdot 10^{-2}$	$3.389672548 \cdot 10^{-1}$	$8.345899854 \cdot 10^{-1}$	$1.553713387 \cdot 10^{0}$
	$2.500006237 \cdot 10^{0}$	$3.678420344 \cdot 10^{0}$	$5.095349069 \cdot 10^{0}$	$6.758835516 \cdot 10^{0}$
	$8.678853314 \cdot 10^{0}$	$1.086768689 \cdot 10^{1}$	$1.334045105 \cdot 10^{1}$	$1.611581134 \cdot 10^{1}$
	$1.921700368 \cdot 10^{1}$	$2.267331660 \cdot 10^{1}$	$2.652231959 \cdot 10^{1}$	$3.081335794 \cdot 10^{1}$
	$3.561333520 \cdot 10^{1}$	$4.101696860 \cdot 10^{1}$	$4.716675785 \cdot 10^{1}$	$5.429738526 \cdot 10^{1}$
	$6.285709625 \cdot 10^{1}$	$7.399550701 \cdot 10^{1}$		
23	$6.153203776 \cdot 10^{-2}$	$3.245113292 \cdot 10^{-1}$	$7.988739687 \cdot 10^{-1}$	$1.486886334 \cdot 10^{0}$
	$2.391755830 \cdot 10^{0}$	$3.517797443 \cdot 10^{0}$	$4.870560369 \cdot 10^{0}$	$6.456991307 \cdot 10^{0}$
	$8.285651893 \cdot 10^{0}$	$1.036700904 \cdot 10^{1}$	$1.271382503 \cdot 10^{1}$	$1.534168757 \cdot 10^{1}$
	$1.826974239 \cdot 10^{1}$	$2.152172785 \cdot 10^{1}$	$2.512747713 \cdot 10^{1}$	$2.912517511 \cdot 10^{1}$
	$3.356489656 \cdot 10^{1}$	$3.851445968 \cdot 10^{1}$	$4.406980781 \cdot 10^{1}$	$5.037522660 \cdot 10^{1}$
	$5.766830435 \cdot 10^{1}$	$6.640287307 \cdot 10^{1}$	$7.774322728 \cdot 10^{1}$	

N				
24	$5.901985218 \cdot 10^{-2}$	$3.112391462 \cdot 10^{-1}$	$7.660969055 \cdot 10^{-1}$	$1.425597591 \cdot 10^{0}$
	$2.292562059 \cdot 10^{0}$	$3.370774264 \cdot 10^{0}$	$4.665083703 \cdot 10^{0}$	$6.181535119 \cdot 10^{0}$
	$7.927539247 \cdot 10^{0}$	$9.912098015 \cdot 10^{0}$	$1.214610271 \cdot 10^{1}$	$1.464273229 \cdot 10^{1}$
	$1.741799265 \cdot 10^{1}$	$2.049146008 \cdot 10^{1}$	$2.388732985 \cdot 10^{1}$	$2.763593717 \cdot 10^{1}$
	$3.177604135 \cdot 10^{1}$	$3.635840580 \cdot 10^{1}$	$4.145172048 \cdot 10^{1}$	$4.715310645 \cdot 10^{1}$
	$5.360857454 \cdot 10^{1}$	$6.105853145 \cdot 10^{1}$	$6.996224004 \cdot 10^{1}$	$8.149827923 \cdot 10^{1}$
25	$5.670477545 \cdot 10^{-2}$	$2.990108986 \cdot 10^{-1}$	$7.359095554 \cdot 10^{-1}$	$1.369183116 \cdot 10^{0}$
	$2.201326054 \cdot 10^{0}$	$3.235675804 \cdot 10^{0}$	$4.476496615 \cdot 10^{0}$	$5.929083763 \cdot 10^{0}$
	$7.599899310 \cdot 10^{0}$	$9.496749221 \cdot 10^{0}$	$1.162901491 \cdot 10^{1}$	$1.400795798 \cdot 10^{1}$
	$1.664712560 \cdot 10^{1}$	$1.956289801 \cdot 10^{1}$	$2.277524199 \cdot 10^{1}$	$2.630877239 \cdot 10^{1}$
	$3.019429116 \cdot 10^{1}$	$3.447109757 \cdot 10^{1}$	$3.919060880 \cdot 10^{1}$	$4.442234934 \cdot 10^{1}$
	$5.026457499 \cdot 10^{1}$	$5.686496717 \cdot 10^{1}$	$6.446667062 \cdot 10^{1}$	$7.353423479 \cdot 10^{1}$
	$8.526015556 \cdot 10^{1}$			
26	$5.456448272 \cdot 10^{-2}$	$2.877079791 \cdot 10^{-1}$	$7.080160195 \cdot 10^{-1}$	$1.317081366 \cdot 10^{0}$
	$2.117120945 \cdot 10^{0}$	$3.111093879 \cdot 10^{0}$	$4.302770876 \cdot 10^{0}$	$5.696818826 \cdot 10^{0}$
	$7.298909963 \cdot 10^{0}$	$9.115862897 \cdot 10^{0}$	$1.115582495 \cdot 10^{1}$	$1.342850903 \cdot 10^{1}$
	$1.594550395 \cdot 10^{1}$	$1.872068615 \cdot 10^{1}$	$2.177077461 \cdot 10^{1}$	$2.511609366 \cdot 10^{1}$
	$2.878164687 \cdot 10^{1}$	$3.279867322 \cdot 10^{1}$	$3.720698263 \cdot 10^{1}$	$4.205861592 \cdot 10^{1}$
	$4.742389936 \cdot 10^{1}$	$5.340218520 \cdot 10^{1}$	$6.014277569 \cdot 10^{1}$	$6.789147971 \cdot 10^{1}$
	$7.711799907 \cdot 10^{1}$	$8.902840275 \cdot 10^{1}$		
27	$5.257989821 \cdot 10^{-2}$	$2.772291060 \cdot 10^{-1}$	$6.821639114 \cdot 10^{-1}$	$1.268814181 \cdot 10^{0}$
	$2.039159278 \cdot 10^{0}$	$2.995835582 \cdot 10^{0}$	$4.142194483 \cdot 10^{0}$	$5.482371716 \cdot 10^{0}$
	$7.021376025 \cdot 10^{0}$	$8.765202717 \cdot 10^{0}$	$1.072097905 \cdot 10^{1}$	$1.289715090 \cdot 10^{1}$
	$1.530372420 \cdot 10^{1}$	$1.795258016 \cdot 10^{1}$	$2.085789274 \cdot 10^{1}$	$2.403669039 \cdot 10^{1}$
	$2.750962763 \cdot 10^{1}$	$3.130207079 \cdot 10^{1}$	$3.544567067 \cdot 10^{1}$	$3.998072262 \cdot 10^{1}$
	$4.495986479 \cdot 10^{1}$	$5.045419615 \cdot 10^{1}$	$5.656413090 \cdot 10^{1}$	$6.344054668 \cdot 10^{1}$
	$7.133184806 \cdot 10^{1}$	$8.071276385 \cdot 10^{1}$	$9.280261353 \cdot 10^{1}$	
28	$5.073462485 \cdot 10^{-2}$	$2.674872686 \cdot 10^{-1}$	$6.581366284 \cdot 10^{-1}$	$1.223971808 \cdot 10^{0}$
	$1.966767612 \cdot 10^{0}$	$2.888883326 \cdot 10^{0}$	$3.993311659 \cdot 10^{0}$	$5.283736063 \cdot 10^{0}$
	$6.764603404 \cdot 10^{0}$	$8.441216328 \cdot 10^{0}$	$1.031985046 \cdot 10^{1}$	$1.240790341 \cdot 10^{1}$
	$1.471408516 \cdot 10^{1}$	$1.724866342 \cdot 10^{1}$	$2.002378333 \cdot 10^{1}$	$2.305389014 \cdot 10^{1}$
	$2.635629737 \cdot 10^{1}$	$2.995196683 \cdot 10^{1}$	$3.386660552 \cdot 10^{1}$	$3.813225441 \cdot 10^{1}$
	$4.278967237 \cdot 10^{1}$	$4.789207163 \cdot 10^{1}$	$5.351129796 \cdot 10^{1}$	$5.974879608 \cdot 10^{1}$
	$6.675697728 \cdot 10^{1}$	$7.478677815 \cdot 10^{1}$	$8.431783711 \cdot 10^{1}$	$9.658242063 \cdot 10^{1}$
29	$4.901448999 \cdot 10^{-2}$	$2.584072979 \cdot 10^{-1}$	$6.357472158 \cdot 10^{-1}$	$1.182201056 \cdot 10^{0}$
	$1.899366498 \cdot 10^{0}$	$2.789363538 \cdot 10^{0}$	$3.854876158 \cdot 10^{0}$	$5.099200089 \cdot 10^{0}$
	$6.526302885 \cdot 10^{0}$	$8.140899733 \cdot 10^{0}$	$9.948548894 \cdot 10^{0}$	$1.195577194 \cdot 10^{1}$
	$1.417020584 \cdot 10^{1}$	$1.660079655 \cdot 10^{1}$	$1.925804791 \cdot 10^{1}$	$2.215434543 \cdot 10^{1}$
	$2.530438376 \cdot 10^{1}$	$2.872574103 \cdot 10^{1}$	$3.243966674 \cdot 10^{1}$	$3.647218971 \cdot 10^{1}$
	$4.085572234 \cdot 10^{1}$	$4.563146770 \cdot 10^{1}$	$5.085319152 \cdot 10^{1}$	$5.659346290 \cdot 10^{1}$
	$6.295472850 \cdot 10^{1}$	$7.009089460 \cdot 10^{1}$	$7.825537042 \cdot 10^{1}$	$8.793259364 \cdot 10^{1}$
	$1.003674916 \cdot 10^{2}$			
30	$4.740718054 \cdot 10^{-2}$	$2.499239168 \cdot 10^{-1}$	$6.148334544 \cdot 10^{-1}$	$1.143195826 \cdot 10^{0}$
	$1.836454555 \cdot 10^{0}$	$2.696521875 \cdot 10^{0}$	$3.725814508 \cdot 10^{0}$	$4.927293766 \cdot 10^{0}$
	$6.304515591 \cdot 10^{0}$	$7.861693293 \cdot 10^{0}$	$9.603775985 \cdot 10^{0}$	$1.153654660 \cdot 10^{1}$
	$1.366674469 \cdot 10^{1}$	$1.600222119 \cdot 10^{1}$	$1.855213484 \cdot 10^{1}$	$2.132720432 \cdot 10^{1}$
	$2.434003576 \cdot 10^{1}$	$2.760555480 \cdot 10^{1}$	$3.114158670 \cdot 10^{1}$	$3.496965201 \cdot 10^{1}$
	$3.911608495 \cdot 10^{1}$	$4.361365291 \cdot 10^{1}$	$4.850398616 \cdot 10^{1}$	$5.384138541 \cdot 10^{1}$
	$5.969912186 \cdot 10^{1}$	$6.618061779 \cdot 10^{1}$	$7.344123860 \cdot 10^{1}$	$8.173681051 \cdot 10^{1}$
	$9.155646652 \cdot 10^{1}$	$1.041575244 \cdot 10^{2}$		
31	$4.590194762 \cdot 10^{-2}$	$2.419801638 \cdot 10^{-1}$	$5.952538942 \cdot 10^{-1}$	$1.106689500 \cdot 10^{0}$

N				
	$1.777595693 \cdot 10^{0}$	$2.609703415 \cdot 10^{0}$	$3.605196802 \cdot 10^{0}$	$4.766747084 \cdot 10^{0}$
	$6.097554567 \cdot 10^{0}$	$7.601400949 \cdot 10^{0}$	$9.282714313 \cdot 10^{0}$	$1.114664976 \cdot 10^{1}$
	$1.319918958 \cdot 10^{1}$	$1.544726832 \cdot 10^{1}$	$1.789892983 \cdot 10^{1}$	$2.056352634 \cdot 10^{1}$
	$2.345197348 \cdot 10^{1}$	$2.657708135 \cdot 10^{1}$	$2.995399087 \cdot 10^{1}$	$3.360075953 \cdot 10^{1}$
	$3.753916441 \cdot 10^{1}$	$4.179583087 \cdot 10^{1}$	$4.640386681 \cdot 10^{1}$	$5.140531448 \cdot 10^{1}$
	$5.685499287 \cdot 10^{1}$	$6.282685591 \cdot 10^{1}$	$6.942527719 \cdot 10^{1}$	$7.680704776 \cdot 10^{1}$
	$8.523035861 \cdot 10^{1}$	$9.518893989 \cdot 10^{1}$	$1.079522438 \cdot 10^{2}$	
32	$4.448936583 \cdot 10^{-2}$	$2.345261095 \cdot 10^{-1}$	$5.768846293 \cdot 10^{-1}$	$1.072448754 \cdot 10^{0}$
	$1.722408776 \cdot 10^{0}$	$2.528336706 \cdot 10^{0}$	$3.492213273 \cdot 10^{0}$	$4.616456770 \cdot 10^{0}$
	$5.903958504 \cdot 10^{0}$	$7.358126733 \cdot 10^{0}$	$8.982940924 \cdot 10^{0}$	$1.078301863 \cdot 10^{1}$
	$1.276369799 \cdot 10^{1}$	$1.493113976 \cdot 10^{1}$	$1.729245434 \cdot 10^{1}$	$1.985586094 \cdot 10^{1}$
	$2.263088901 \cdot 10^{1}$	$2.562863602 \cdot 10^{1}$	$2.886210182 \cdot 10^{1}$	$3.234662915 \cdot 10^{1}$
	$3.610049481 \cdot 10^{1}$	$4.014571977 \cdot 10^{1}$	$4.450920800 \cdot 10^{1}$	$4.922439499 \cdot 10^{1}$
	$5.433372133 \cdot 10^{1}$	$5.989250916 \cdot 10^{1}$	$6.597537729 \cdot 10^{1}$	$7.268762809 \cdot 10^{1}$
	$8.018744698 \cdot 10^{1}$	$8.873534042 \cdot 10^{1}$	$9.882954287 \cdot 10^{1}$	$1.117513981 \cdot 10^{2}$
33	$4.316113562 \cdot 10^{-2}$	$2.275178028 \cdot 10^{-1}$	$5.596166559 \cdot 10^{-1}$	$1.040268508 \cdot 10^{0}$
	$1.670559196 \cdot 10^{0}$	$2.451920796 \cdot 10^{0}$	$3.386155338 \cdot 10^{0}$	$4.475459498 \cdot 10^{0}$
	$5.722454720 \cdot 10^{0}$	$7.130224344 \cdot 10^{0}$	$8.702359231 \cdot 10^{0}$	$1.044301365 \cdot 10^{1}$
	$1.235697376 \cdot 10^{1}$	$1.444974168 \cdot 10^{1}$	$1.672763922 \cdot 10^{1}$	$1.919793659 \cdot 10^{1}$
	$2.186901352 \cdot 10^{1}$	$2.475056291 \cdot 10^{1}$	$2.785385111 \cdot 10^{1}$	$3.119205555 \cdot 10^{1}$
	$3.478070915 \cdot 10^{1}$	$3.863829672 \cdot 10^{1}$	$4.278707208 \cdot 10^{1}$	$4.725420660 \cdot 10^{1}$
	$5.207345190 \cdot 10^{1}$	$5.728763454 \cdot 10^{1}$	$6.295256595 \cdot 10^{1}$	$6.914351338 \cdot 10^{1}$
	$7.596668701 \cdot 10^{1}$	$8.358163722 \cdot 10^{1}$	$9.225113944 \cdot 10^{1}$	$1.024778443 \cdot 10^{2}$
	$1.155547564 \cdot 10^{2}$			
34	$4.190992002 \cdot 10^{-2}$	$2.209164020 \cdot 10^{-1}$	$5.433536946 \cdot 10^{-1}$	$1.009967765 \cdot 10^{0}$
	$1.621751953 \cdot 10^{0}$	$2.380014626 \cdot 10^{0}$	$3.286400154 \cdot 10^{0}$	$4.342910167 \cdot 10^{0}$
	$5.551929289 \cdot 10^{0}$	$6.916256712 \cdot 10^{0}$	$8.439144796 \cdot 10^{0}$	$1.012434611 \cdot 10^{1}$
	$1.197617070 \cdot 10^{1}$	$1.399955595 \cdot 10^{1}$	$1.620015203 \cdot 10^{1}$	$1.858442711 \cdot 10^{1}$
	$2.115979765 \cdot 10^{1}$	$2.393479131 \cdot 10^{1}$	$2.691925258 \cdot 10^{1}$	$3.012460565 \cdot 10^{1}$
	$3.356419492 \cdot 10^{1}$	$3.725373335 \cdot 10^{1}$	$4.121190386 \cdot 10^{1}$	$4.546118331 \cdot 10^{1}$
	$5.002900054 \cdot 10^{1}$	$5.494941289 \cdot 10^{1}$	$6.026562168 \cdot 10^{1}$	$6.603391492 \cdot 10^{1}$
	$7.233019308 \cdot 10^{1}$	$7.926155449 \cdot 10^{1}$	$8.698888681 \cdot 10^{1}$	$9.577719042 \cdot 10^{1}$
	$1.061334485 \cdot 10^{2}$	$1.193621067 \cdot 10^{2}$		
35	$4.072920906 \cdot 10^{-2}$	$2.146874527 \cdot 10^{-1}$	$5.280103843 \cdot 10^{-1}$	$9.813861735 \cdot 10^{-1}$
	$1.575725948 \cdot 10^{0}$	$2.312228297 \cdot 10^{0}$	$3.192397939 \cdot 10^{0}$	$4.218064125 \cdot 10^{0}$
	$5.391402735 \cdot 10^{0}$	$6.714963280 \cdot 10^{0}$	$8.191701759 \cdot 10^{0}$	$9.825020497 \cdot 10^{0}$
	$1.161881639 \cdot 10^{1}$	$1.357753936 \cdot 10^{1}$	$1.570626340 \cdot 10^{1}$	$1.801077329 \cdot 10^{1}$
	$2.049767111 \cdot 10^{1}$	$2.317450800 \cdot 10^{1}$	$2.604994871 \cdot 10^{1}$	$2.913397921 \cdot 10^{1}$
	$3.243817184 \cdot 10^{1}$	$3.597602877 \cdot 10^{1}$	$3.976343410 \cdot 10^{1}$	$4.381926012 \cdot 10^{1}$
	$4.816619797 \cdot 10^{1}$	$5.283192506 \cdot 10^{1}$	$5.785079502 \cdot 10^{1}$	$6.326637368 \cdot 10^{1}$
	$6.913541388 \cdot 10^{1}$	$7.553443513 \cdot 10^{1}$	$8.257140552 \cdot 10^{1}$	$9.040852386 \cdot 10^{1}$
	$9.931297366 \cdot 10^{1}$	$1.097959909 \cdot 10^{2}$	$1.231732532 \cdot 10^{2}$	
36	$3.961320641 \cdot 10^{-2}$	$2.088002857 \cdot 10^{-1}$	$5.135107755 \cdot 10^{-1}$	$9.543811531 \cdot 10^{-1}$
	$1.532249225 \cdot 10^{0}$	$2.248215818 \cdot 10^{0}$	$3.103661490 \cdot 10^{0}$	$4.100262546 \cdot 10^{0}$
	$5.240010109 \cdot 10^{0}$	$6.525233330 \cdot 10^{0}$	$7.958627509 \cdot 10^{0}$	$9.543288035 \cdot 10^{0}$
	$1.128275129 \cdot 10^{1}$	$1.318104390 \cdot 10^{1}$	$1.524274227 \cdot 10^{1}$	$1.747304463 \cdot 10^{1}$
	$1.987785893 \cdot 10^{1}$	$2.246391051 \cdot 10^{1}$	$2.523887526 \cdot 10^{1}$	$2.821154568 \cdot 10^{1}$
	$3.139204037 \cdot 10^{1}$	$3.479207145 \cdot 10^{1}$	$3.842529076 \cdot 10^{1}$	$4.230774567 \cdot 10^{1}$
	$4.645849004 \cdot 10^{1}$	$5.090042150 \cdot 10^{1}$	$5.566145791 \cdot 10^{1}$	$6.077624068 \cdot 10^{1}$
	$6.628869068 \cdot 10^{1}$	$7.225601475 \cdot 10^{1}$	$7.875533816 \cdot 10^{1}$	$8.589548143 \cdot 10^{1}$
	$9.383992978 \cdot 10^{1}$	$1.028580101 \cdot 10^{2}$	$1.134651355 \cdot 10^{2}$	$1.269880152 \cdot 10^{2}$

N				
37	$3.855673419 \cdot 10^{-2}$	$2.032275099 \cdot 10^{-1}$	$4.997870664 \cdot 10^{-1}$	$9.288254993 \cdot 10^{-1}$
	$1.491115012 \cdot 10^{0}$	$2.187669072 \cdot 10^{0}$	$3.019757468 \cdot 10^{0}$	$3.988920303 \cdot 10^{0}$
	$5.096984545 \cdot 10^{0}$	$6.346084061 \cdot 10^{0}$	$7.738683814 \cdot 10^{0}$	$9.277608942 \cdot 10^{0}$
	$1.096607963 \cdot 10^{1}$	$1.280775291 \cdot 10^{1}$	$1.480677283 \cdot 10^{1}$	$1.696783086 \cdot 10^{1}$
	$1.929623895 \cdot 10^{1}$	$2.179801837 \cdot 10^{1}$	$2.448000859 \cdot 10^{1}$	$2.735000162 \cdot 10^{1}$
	$3.041690963 \cdot 10^{1}$	$3.369097614 \cdot 10^{1}$	$3.718404564 \cdot 10^{1}$	$4.090991253 \cdot 10^{1}$
	$4.488478042 \cdot 10^{1}$	$4.912787781 \cdot 10^{1}$	$5.366230174 \cdot 10^{1}$	$5.851620322 \cdot 10^{1}$
	$6.372450358 \cdot 10^{1}$	$6.933147003 \cdot 10^{1}$	$7.539475330 \cdot 10^{1}$	$8.199207200 \cdot 10^{1}$
	$8.923308273 \cdot 10^{1}$	$9.728253367 \cdot 10^{1}$	$1.064118573 \cdot 10^{2}$	$1.171405711 \cdot 10^{2}$
	$1.308062254 \cdot 10^{2}$			
38	$3.755515263 \cdot 10^{-2}$	$1.979445866 \cdot 10^{-1}$	$4.867785379 \cdot 10^{-1}$	$9.046053593 \cdot 10^{-1}$
	$1.452138374 \cdot 10^{0}$	$2.130312744 \cdot 10^{0}$	$2.940299106 \cdot 10^{0}$	$3.883515862 \cdot 10^{0}$
	$4.961643595 \cdot 10^{0}$	$6.176642449 \cdot 10^{0}$	$7.530773049 \cdot 10^{0}$	$9.026621537 \cdot 10^{0}$
	$1.066712948 \cdot 10^{1}$	$1.245562951 \cdot 10^{1}$	$1.439588797 \cdot 10^{1}$	$1.649215579 \cdot 10^{1}$
	$1.874922978 \cdot 10^{1}$	$2.117252653 \cdot 10^{1}$	$2.376817221 \cdot 10^{1}$	$2.654311242 \cdot 10^{1}$
	$2.950524786 \cdot 10^{1}$	$3.266360325 \cdot 10^{1}$	$3.602854026 \cdot 10^{1}$	$3.961202923 \cdot 10^{1}$
	$4.342800076 \cdot 10^{1}$	$4.749280846 \cdot 10^{1}$	$5.182584921 \cdot 10^{1}$	$5.645041308 \cdot 10^{1}$
	$6.139487752 \cdot 10^{1}$	$6.669443658 \cdot 10^{1}$	$7.239369576 \cdot 10^{1}$	$7.855074022 \cdot 10^{1}$
	$8.524387023 \cdot 10^{1}$	$9.258356301 \cdot 10^{1}$	$1.007358074 \cdot 10^{2}$	$1.099741054 \cdot 10^{2}$
	$1.208220095 \cdot 10^{2}$	$1.346277283 \cdot 10^{2}$		
39	$3.660429196 \cdot 10^{-2}$	$1.929294668 \cdot 10^{-1}$	$4.744306515 \cdot 10^{-1}$	$8.816185218 \cdot 10^{-1}$
	$1.415153403 \cdot 10^{0}$	$2.075900054 \cdot 10^{0}$	$2.864940087 \cdot 10^{0}$	$3.783582804 \cdot 10^{0}$
	$4.833377810 \cdot 10^{0}$	$6.016130156 \cdot 10^{0}$	$7.333918496 \cdot 10^{0}$	$8.789116762 \cdot 10^{0}$
	$1.038441992 \cdot 10^{1}$	$1.212287459 \cdot 10^{1}$	$1.400791538 \cdot 10^{1}$	$1.604340819 \cdot 10^{1}$
	$1.823370185 \cdot 10^{1}$	$2.058369013 \cdot 10^{1}$	$2.309888640 \cdot 10^{1}$	$2.578551437 \cdot 10^{1}$
	$2.865061891 \cdot 10^{1}$	$3.170220279 \cdot 10^{1}$	$3.494939706 \cdot 10^{1}$	$3.840267556 \cdot 10^{1}$
	$4.207412867 \cdot 10^{1}$	$4.597781756 \cdot 10^{1}$	$5.013024019 \cdot 10^{1}$	$5.455095618 \cdot 10^{1}$
	$5.926344277 \cdot 10^{1}$	$6.429629778 \cdot 10^{1}$	$6.968498128 \cdot 10^{1}$	$7.547442957 \cdot 10^{1}$
	$8.172315339 \cdot 10^{1}$	$8.851002367 \cdot 10^{1}$	$9.594632357 \cdot 10^{1}$	$1.041992613 \cdot 10^{2}$
	$1.135443740 \cdot 10^{2}$	$1.245091829 \cdot 10^{2}$	$1.384523795 \cdot 10^{2}$	
40	$3.570039431 \cdot 10^{-2}$	$1.881622832 \cdot 10^{-1}$	$4.626942813 \cdot 10^{-1}$	$8.597729640 \cdot 10^{-1}$
	$1.380010821 \cdot 10^{0}$	$2.024209136 \cdot 10^{0}$	$2.793369354 \cdot 10^{0}$	$3.688702678 \cdot 10^{0}$
	$4.711641147 \cdot 10^{0}$	$5.863850878 \cdot 10^{0}$	$7.147247908 \cdot 10^{0}$	$8.564017018 \cdot 10^{0}$
	$1.011663405 \cdot 10^{1}$	$1.180789229 \cdot 10^{1}$	$1.364093371 \cdot 10^{1}$	$1.561928589 \cdot 10^{1}$
	$1.774690595 \cdot 10^{1}$	$2.002823283 \cdot 10^{1}$	$2.246824998 \cdot 10^{1}$	$2.507256077 \cdot 10^{1}$
	$2.784748001 \cdot 10^{1}$	$3.080014574 \cdot 10^{1}$	$3.393865708 \cdot 10^{1}$	$3.727224588 \cdot 10^{1}$
	$4.081149282 \cdot 10^{1}$	$4.456860318 \cdot 10^{1}$	$4.855776353 \cdot 10^{1}$	$5.279561119 \cdot 10^{1}$
	$5.730186332 \cdot 10^{1}$	$6.210017907 \cdot 10^{1}$	$6.721937093 \cdot 10^{1}$	$7.269515885 \cdot 10^{1}$
	$7.857280291 \cdot 10^{1}$	$8.491123114 \cdot 10^{1}$	$9.178987467 \cdot 10^{1}$	$9.932080872 \cdot 10^{1}$
	$1.076724406 \cdot 10^{2}$	$1.171223095 \cdot 10^{2}$	$1.282018420 \cdot 10^{2}$	$1.422800445 \cdot 10^{2}$

Calculated roots for Laguerre polynomials of grad N. The accuracy is the last cipher.

Bibliography

[1] J. Stark. 'Observations of the effect of the electric field on spectral lines I. Transverse effect'. Annalen der Physik, **43** (1914) 965–983

[2] D. Farrelly and W. P. Reinhardt. 'Uniform semiclassical and accurate quantum calculations of complex energy eigenvalues for the hydrogen atom in a uniform electric field'. J. Phys. B, **16**(12) (1983) 2103–2117. doi:10.1088/0022-3700/16/12/008

[3] J. A. C. Gallas, H. Walther and E. Werner. 'WKB solution of the Stark effect in hydrogen'. Phys. Rev. A, **26**(3) (1982) 1775–1778

[4] M. Hehenberger, H. V. McIntosh and E. Brändas. 'Weyl's theory applied to the Stark effect in the hydrogen atom'. Phys. Rev. A, **10**(5) (1974) 1494–1506. doi:10.1103/PhysRevA.10.1494

[5] R. J. Damburg and V. V. Kolosov. 'A hydrogen atom in a uniform electric field'. J. Phys. B, **9**(18) (1976) 3149–3157. doi:10.1088/0022-3700/9/18/006

[6] R. J. Damburg and V. V. Kolosov. 'An asymptotic approach to the Stark effect for the hydrogen atom'. J. Phys. B, **11**(11) (1978) 1921–1930. doi:10.1088/0022-3700/11/11/009

[7] V. V. Kolosov. 'A hydrogen atom in a strong electric field'. J. Phys. B, **20**(11) (1987) 2359–2367. doi:10.1088/0022-3700/20/11/008

[8] C. S. Lai. 'Calculation of the Stark effect in Hydrogen atoms by using hypervirial relations'. Physics Letters, **83A**(7) (1981) 322–325

[9] V. V. Kolosov. 'Stark effect near the peak of the potential barrier'. J. Phys. B, **16**(1) (1983) 25–31. doi:10.1088/0022-3700/16/1/004

[10] C. Y. Lin and Y. K. Ho. 'Complex scaling in Lagrange-mesh calculations for Stark shifts and widths of the screened Coulomb potential'. J. Phys. B, **44**(17) (2011) 175001. doi:10.1088/0022-3700/13/9/009

[11] A. Maquet, S.-I. Chu and W. P. Reinhardt. 'Stark ionization in dc and ac fields: An L^2 complex-coordinate approach'. Phys. Rev. A, **27**(6) (1983) 2946–2970

[12] R. F. Stebbings. 'High Rydberg Atoms: Newcomers to the Atomic Physics Scene'. Science, **193** (1976) 537–542. doi:10.1126/science.193.4253.537

[13] M. G. Littman, M. L. Zimmerman and D. Kleppner. 'Tunneling Rates for Excited States of Sodium in a Static Electric Field'. Phys. Rev. Lett., **37** (1976) 486–489. doi:10.1103/PhysRevLett.37.486

[14] E. Schrödinger. 'Quantification of the eigen value problem'. Annalen der Physik, **80**(13) (1926) 437–490. doi:10.1002/andp.19263851302

[15] P. S. Epstein. 'The Stark effect from the point of view of Schroedinger's quantum theory'. Phys. Rev., **28** (1926) 695–710

[16] Y. K. Ho. 'The method of complex coordinate rotation and its application to atomic collision'. Physics Reports, **99**(1) (1983) 1–68. doi:10.1016/0370-1573(83)90112-6

[17] A. Burgess and H. P. Summers. 'The recombination and level populations of ions. I - Hydrogen and hydrogenic ions'. Mon. Not. R. Astr. Soc., **174** (1976) 345–391. ADS: http://adsabs.harvard.edu/abs/1976MNRAS.174..345B

[18] A. Dinklage, R. Reimer, R. C. Wolf, W. .-X. Team, M. Reich and A. U. Team. 'Forward Modeling of Motional Stark Effect Spectra'. Fusion Science and Technology, **59**(2) (2011) 406–417

[19] M. F. M. De Bock, N. J. Conway, M. J. Walsh, P. G. Carolan and N. C. Hawkes. 'Ab initio modeling of the motional Stark effect on MAST'. Review of Scientific Instruments, **79**(10) 10F524. doi:10.1063/1.2966459

[20] A. Boileau, M. von Hellerman, W. Mandl, H. P. Summers, H. Weisen and A. Zinoviev. 'Observations of motional Stark features in the Balmer spectrum of deuterium in the JET plasma'. J. Phys. B, **22**(7) (1989) L145–L152. doi:10.1088/0953-4075/22/7/002

[21] N. C. Hawkes, K. Blackler, B. Viaccoz, C. H. Wilson, J. B. Migozzi and B. C. Stratton. 'Design of the Joint European Torus motional stark effect diagnostic'. Review of Scientific Instruments, **70**(1) (1999) 894–897. doi:10.1063/1.1149415

[22] W. Mandl, R. C. Wolf, M. G. von Hellermann and H. P. Summers. 'Beam emission spectroscopy as a comprehensive plasma diagnostic tool'. Plasma Phys. Control. Fusion, **35**(10) (1993) 1373–1394. doi:10.1088/0741-3335/35/10/003

[23] R. Jaspers, B. S. Q. Elzendoorn, A. J. H. Donné and T. Soetens. 'Spectra polarimetry of the motional Stark effect at TEXTOR-94'. Review of Scientific Instruments, **72**(1) (2001) 1018–1022. doi:10.1063/1.1319611

[24] K. Jakubowska, M. D. Bock, R. Jaspers, M. von Hellermann and L. Shmaenok. 'Motional Stark effect diagnostic on TEXTOR'. Review of Scientific Instruments, **75**(10) (2004) 3475–3477. doi:10.1063/1.1784535

[25] K. Ida, M. Yoshinuma, K. Y. Watanabe, T. Kobuchi and K. Nagaoka. 'Measurements of rotational transform due to noninductive toroidal current using motional Stark effect spectroscopy in the Large Helical Device'. Review of Scientific Instruments, **76**(5) 053505. Available from: http://link.aip.org/link/?RSI/76/053505/1, doi:10.1063/1.1898943

[26] H. Y. Yuh, F. M. Levinton, S. D. Scott and J. Ko. 'Simulation of the motional Stark effect diagnostic gas-filled torus calibration'. Review of Scientific Instruments, **79**(10) 10F523. Available from: http://link.aip.org/link/?RSI/79/10F523/1, doi:10.1063/1.2969419

[27] A. J. H. Donné, A. E. Costley, R. Barnsley, H. Bindslev, R. Boivin, G. Conway, R. Fisher, R. Giannella, H. Hartfuss, M. G. von Hellermann, E. Hodgson, L. C. Ingesson, K. Itami, D. Johnson, Y. Kawano, T. Kondoh, A. Krasilnikov, Y. Kusama, A. Litnovsky, P. Lotte, P. Nielsen, T. Nishitani, F. Orsitto, B. Peterson, G. Razdobarin, J. Sanchez, M. Sasao, T. Sugie, G. Vayakis, V. Voitsenya, K. Vukolov, C. Walker, K. Young and the ITPA Topical Group on Diagnostics. 'Chapter 7: Diagnostics'. Nuclear Fusion, **47**(6) (2007) S337. Available from: http://stacks.iop.org/0029-5515/47/i=6/a=S07

[28] D. Ciric. 'JET Neutral Beams – Yesterday, Today and Tomorrow' (2010). EFDA–JET Science Meeting: Neutral Beams in JET, ITER and DEMO

[29] R. McAdams. 'Negative ion beams for ITER' (2010). EFDA–JET Science Meeting: Neutral Beams in JET, ITER and DEMO

[30] A. Stäbler, J. H. Feist, E. Speth, J. L. Dunne, S. Goeth, B. Heinemann, A. Krauss, R. C. Kunze, H. Lohnert, J. Sielanko, W. Szyszko, O. Vollmer and K. Wittenbecher. 'Design of the Neutral Beam Injection system for ASDEX-Upgrade'. Fusion Technology, 620

[31] A. Stäbler, J. Hobirck, F. Leuterer, F. Meo and J. M. Noterdaeme. 'Current drive in ASDEX Upgrade'. Fusion Science and Technology, 730

[32] B. Streibl, P. T. Lang, F. Leuterer, J. M. Noterdaeme and A. Stäbler. 'Chapter 2: Maschine design, fuelling, and heating in ASDEX Upgrade'. Fusion Science and Technology, 578

[33] G. Duesing, H. Altmann, H. Falter, A. Goede, R. Haange, R. S. Hemsworth, P. Kupschus, D. Stork and E. Thompson. 'Additional heating systems for JET: Neutral Beam Injection system'. Fusion Technology, **11** (1987) 163–202

[34] D. H. McNeil. 'H-alpha photon yield in fuelling of tokamaks'. J. Nucl. Mater., **162–164** (1989) 476–481. doi:10.1016/0022-3115(89)90315-2

[35] M. G. von Hellermann, G. Bertschinger, W. Biel, C. Giroud, R. Jaspers, C. Jupen, O. Marchuk, M. O'Mullane, H. P. Summers, A. Whiteford and K.-D. Zastrow. 'Complex Spectra in Fusion Plasmas'. Physica Scripta, **2005**(T120) (2005) 19. Available from: http://stacks.iop.org/1402-4896/2005/i=T120/a=003

[36] E. Källne, J. Källne, E. S. Marmor and J. E. Rice. 'High Resolution X-Ray Spectroscopy Daignotics of High Temperature Plasmas'. Physica Scripta, **31**(6) (1985) 551. doi:10.1088/0031-8949/31/6/016

[37] A. Boileau, M. von Hellermann, L. D. Horton, J. Spence and H. P. Summers. 'The deduction of low-Z ion temperature and densities in the JET tokamak using charge exchange recombination spectroscopy'. Plasma Phys. Control. Fusion, **31**(5) (1989) 779–804. doi:10.1088/0741-3335/31/5/006

[38] F. M. Levinton, R. J. Fonck, G. M. Gammel, R. Kaita, H. W. Kugel, E. T. Powell and D. W. Roberts. 'Magnetic field pitch-angle measurments in the PBX-M tokamak using the motional Stark effect'. Phys. Rev. Lett., **63**(17) (1989) 2060–2063. doi:10.1103/PhysRevLett.63.2060

[39] S. S. Henderson. 'Collisional Radiative Modelling and Population Structure of Resolved Angular Momentum States in Hydrogen and Helium'. 4th yr. dissertation, University of Strathclyde (2009)

[40] B. den Hartog, J. Ko, D. den Hartog and D. Craig. 'MSE Spectral Analysisd on the Madison Symmetric Torus'. In 'ADAS Workshop', (2009). Schloss Ringberg, Germany. 4–7 October. Available from: http://www.adas.ac.uk/2009talks/2009_ADAS_Bdenhartog.ppt

[41] R. Dux, B. Geiger, R. M. McDermott, T. Ptterich, E. Viezzer and ASDEX Upgrade team. 'Impurity density determination using charge exchange and beam emission spectroscopy at ASDEX Upgrade'. Europhysics Conference Abstracts (CD-ROM, Proc. of the 38th EPS Conference on Plasma Physics, Strasbourg, France, 2011) , (Ed.) A. Becoulet and T. Hoang and U. Stroth (European Physical Society, Geneva), **35G** (2011) 1.056. Available from: http://tinyurl.sfx.mpg.de/t4ja

[42] E. U. Condon and G. H. Shortley. *The Theory of Atomic Spectra*. Cambridge University Press (1935). ISBN 0521092094 (1991 paperback)

[43] H. A. Bethe and E. E. Salpeter. *Quantum Mechanics of One- and Two-Electron Atoms*. Dover Publications Inc. (2009). ISBN 978-0486466675 (paperback)

[44] T. F. Gallagher. *Rydberg Atoms*. Cambridge University Press (2005). ISBN 978-0521021661 (paperback)

[45] B. Thaller. *Advanced Visual Quantum Mechanics*. Springer (2005). ISBN 978-0387207773

[46] W. P. Reinhardt. 'Complex coordinates in the theory of atomic and molecular structure and dynamics'. Ann. Rev. Phys. Chem., **33** (1982) 223–255. doi:10.1146/annurev.pc.33.100182.001255

[47] D. Baye and P. H. Hennen. 'Generalised meshes for quantum mechanical problems'. J. Phys. A, **19**(11) (1986) 2041–2059. doi:10.1088/0305-4470/19/11/013

[48] M. Vincke, L. Malegat and D. Baye. 'Regularization of singularities in Lagrange-mesh calculations'. J. Phys. B, **26**(5) (1993) 3811–826. doi:10.1088/0953-4075/26/5/006

[49] M. Abramowitz and I. A. Stegun. *Handbook of Mathematical Functions*. Dover Publications Inc. (1965). ISBN 978-0486612720 (1965 paperback)

Index